Final Report

Developing a MOBY-Net instrument, suitable for a federation network for Vicarious Calibration of Ocean Color Satellites.

Kenneth Voss (UM), Mark Yarbrough (MLML/SJSU), B. Carol Johnson (NIST) and Art Gleason (UM)

NASA grant #NNX14AP63G

Grant Period: 8/18/2014 – 9/14/2018

Outline:

1) Introduction:

Vicarious calibration is required for ocean color satellite instruments. A key part of this process is having a data set of in-situ water leaving radiance of the highest possible quality. IOCCG published a white paper on the requirements for this vicarious data set, and these requirements include the possibility of multiple vicarious calibration sites, as long as these sites have common instrumentation, common data processing, and a coordinated and common calibration. This proposal was aimed at developing the capability to develop such a network of vicarious calibration sites, based on the current "gold standard" for vicarious calibration data, the MOBY system. This includes modernizing the MOBY-Heritage control system and optical system. To support additional sites beyond the current Hawaii site, it would require being able to transport the complete system to the chosen site, have a buoy hull which allows removal of the intact optical system, and a stability system to validate the calibration at each step in the process. The goal of this project was to develop this complete system.

This report will present many, but not all, of the tests and the results of these tests, which we have performed during the development of the MOBY-Net system. This system consists of the MOBY-Net instrument (optical system, buoy hull, control system) and, just as importantly for the concept, a stability system which is used to validate the state of the system calibration during

the steps of instrument deployment and recalibration. In terms of the MOBY-Net instrument, the format of the report will be to start with the back end of the system (the camera) and work forward, rather than in a chronological order. After describing the work we have done developing the instrument, we will discuss several tests we have done with the system in the field. After this discussion we will present the progress on developing and testing the stability system. Finally at the end we will describe what we feel would be the next steps in our work.

2) Camera

For the MOBY-Net system we have chosen to use the Andor iKon-M934 camera. Earlier in our development of this system we had started with a similar camera but from a different manufacturer. Through our testing of the other system, we had some strange operation that we could not understand, including large jumps in the baseline dark values. Because we could not get these resolved, we moved to the Andor camera which has worked more stably. The iKon-M934 is a mega-pixel camera (1024 x 1024), with 13 um pixels and a 100,000 electron well depth. The read noise is specified to be 2.9 electrons, and it has a selection of 4 read out speeds (5, 3, 1, 0.05 MHz). We use the same model (with the BR-DD imaging chip) in both the red and blue spectrographs. This is a back illuminated CCD, deep depletion (thicker active photosensitive area) with fringe suppression to prevent etalon effects. The various tests performed on the camera by itself will be summarized.

2a) Camera settings

The camera maybe initialized with many different base settings. Initially we performed many tests with the different possible settings, investigating issues such as dark current stability, scanning/reading speed, optimal gain settings, etc. For many of these there are tradeoffs. For example reading the array out faster would allow data to be taken more quickly, and perhaps more replicate samples. However reading the array faster also increases the noise in each image. With our measurements in the field, wave focusing effects are an important factor. One can either make a lot of short measurements and average them, or make fewer measurements but with long exposure times, to average out the light field. Because of the time involved in reading and storing the camera images, and the data storage requirements, it is more efficient to average several images with longer exposure times than many short exposure images. So this drove our settings to be optimized to longer exposures and slower reading of the images. The camera settings we decided on are shown in Table 1.

Table 1) Camera settings determined from testing

Single Scan
Read full images
Horizontal Shift Speed = 3 MHz, vertical shift speed 4.250 uS
Gain 4 x (Note at the A/D conversion this means approximately 1.2 electrons/count
Cooler at -60 C
No baseline clamp

2b) Shutter speed

We have done several calibrations of the shutter speed or integration time. The issue is that the mechanical shutter takes time to both open and close. If too short an integration time is chosen, the shutter cannot keep up, and the CCD in the camera is exposed for a longer time than expected. Figure 1 shows a typical result over several orders of magnitude of integration time. This shows the typical type of curve, where at short integration times the ratio of the measured light to the light expected for that integration time grows. Basically the shutter cannot open and close fast enough to accommodate the short integration times. We are planning to use the system with integration times from 1s to 60s or more, so we will not be using the very short integration times which cause problems.

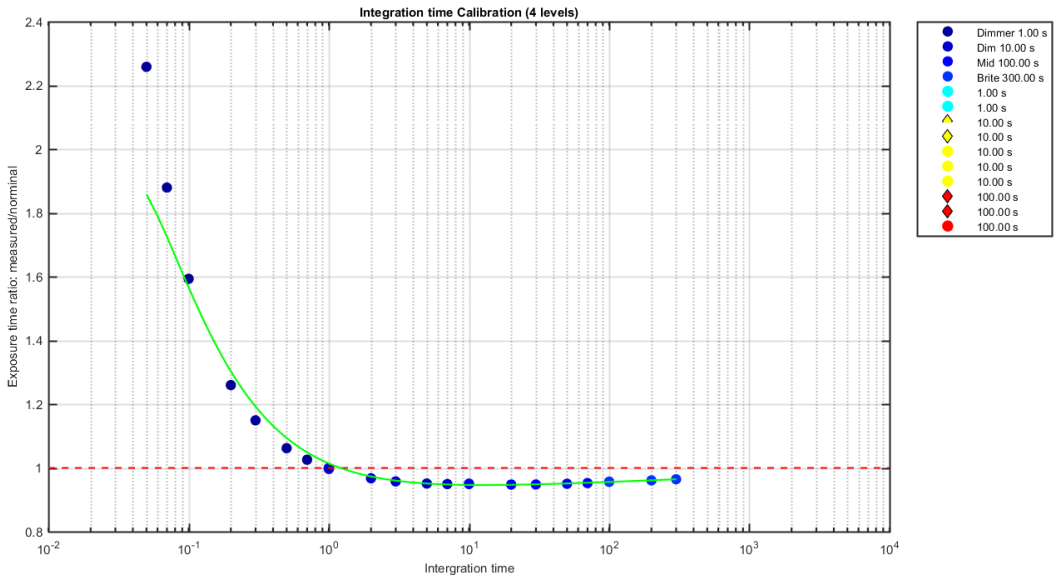

Figure 1) Ratio of measured values and values expected for a given integration time vs integration time, normalized to 1 s. If the shutter speed was very fast, this ratio would be 1. At short integration times, the ratio grows as the shutter cannot open and close fast enough.

Another look at this is shown in Figure 2, where we are displaying integration time on a linear scale. From this it can be seen that in the range of integration times we will be using (1-60 s) the values are fairly constant, and while we will be applying corrections to account for the small deviations from a constant, the accuracy of this correction will not be a significant factor in the final radiance provided.

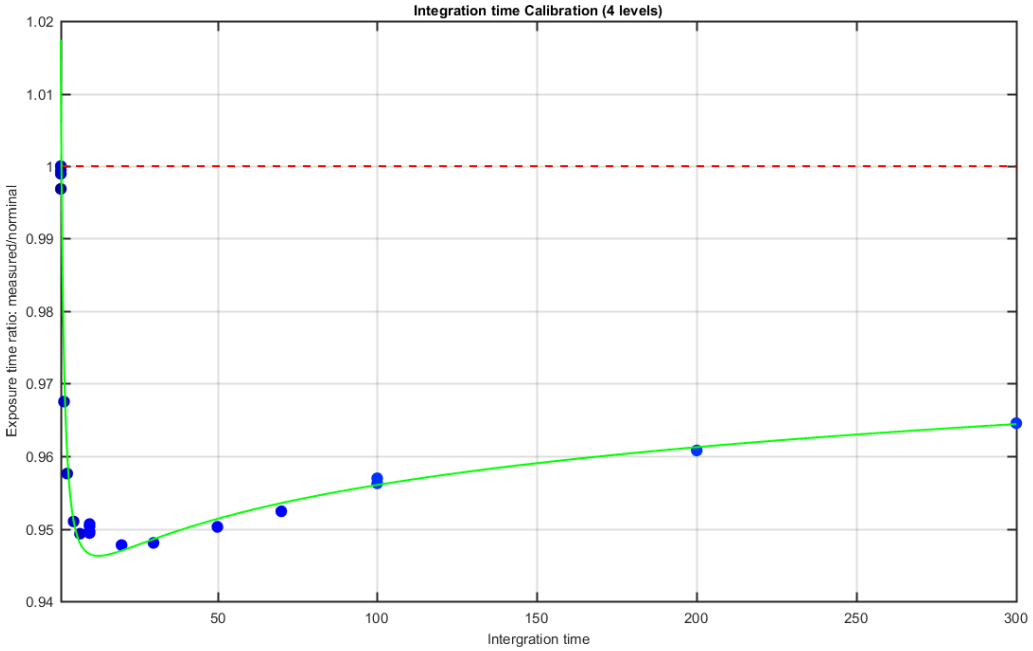

Figure 2) An expanded linear scale of the data shown in Fig. 1. This shows that in the range of integration times we are planning to use (1-60s), the ratio is very constant.

2c) Bright and dark pixels

Our preliminary work with the camera was done with the cooling systems off. We started noticing that each camera had several bad pixels (either much lower or much higher than expected, see Fig. 3). After much investigation, and discussions with the camera manufacturer about whether a higher grade CCD was required, we found that simply cooling the system to -20 C caused these bad pixels to disappear. Since our plan, to accommodate longer integration times, is to operate at -60C, these bad pixels will not be a problem.

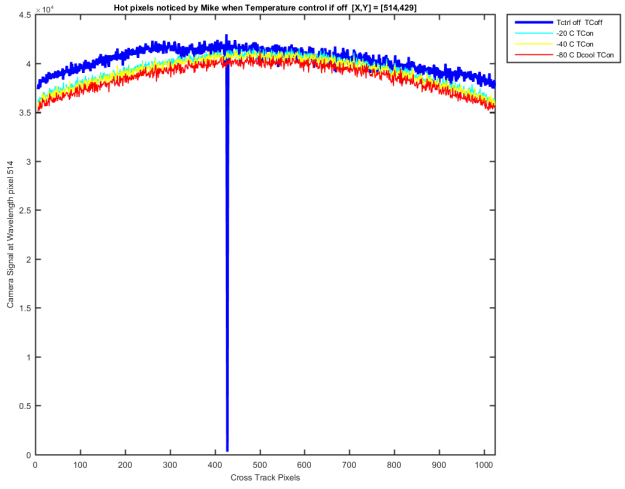

Figure 3) Example of a bad pixel. Note these only seem to show up if the cooling is not on. Since we will be operating the system at -60 C, it will not be a factor.

3) Spectrograph

The base spectrograph was built by Resonon. It has a Volume Phase Holographic grating, which has very low straylight and very good imaging. These gratings allow us the possibility to image all of the environmental optical inputs at once (downwelling sky irradiance, Es, downwelling irradiance measurements from the three arms (EdTop, EdMid, and EdBot) and upwelling irradiance from the three arms (LuTop, LuMid, LuBot) An example image from the spectrograph camera operating in the field is shown in Fig. 4.

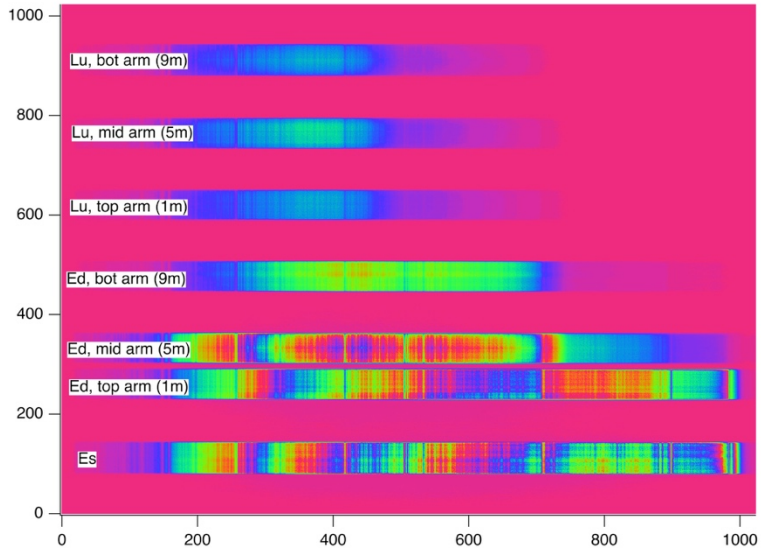

Figure 4) sample image from blue spectrograph in the field. Across the horizontal axis is wavelength, running from approximately 340 nm to 700 nm. The different measurements, or tracks are shown vertically starting with Es at the bottom, then EdTop, EdMid, EdBot, followed by LuTop, LuMid, LuBot. All measurements were taken simultaneously.

The spectrographs went through several iterations as issues were found that required different solutions. In our application we may have situations where a bright source (for example Es) must be imaged at the same time as a darker source (for example LuBot). During this project we have been very careful to look for artifacts in our test systems and implement corrections to the system to eliminate any of the artifacts we find. It is better to eliminate the artifacts at this stage, rather than devise correction schemes for the data at a later time. Some of the artifacts may not have been significant in the final product, but the more we can eliminate the better. It is important to note that these artifacts are typically too small to see in the initial modeling of the system, as they are generally due to higher order (less likely) reflections. So they are only discovered as we test and characterize the built system and require this iteration process to eliminate each one. As we go through the process, we also make it possible for any follow-on systems to be built more reliably.

The discussion on the spectrograph development will follow the chronological order of what we discovered and how we addressed any issues that were found. The process began in April 2015 when we received our first Blue spectrometer. Note that the order for the MOBY-Net spectrometers took until Jan 2015 to be processed, but since the spectrometers in MOBY-Net

were the same as the ones for the NOAA supported effort (MOBY-Refresh), we were able to start our testing when the MOBY-Refresh spectrometers, which had been ordered earlier, arrived.

3a) Refocusing and asymmetric flair

The first Blue spectrometer that we received was not imaging as well as we expected. Figure 5 shows an example of the cross track (the vertical direction in Fig. 4) cut through the data, at the maximum spectral value for the wavelengths indicated in the legend.

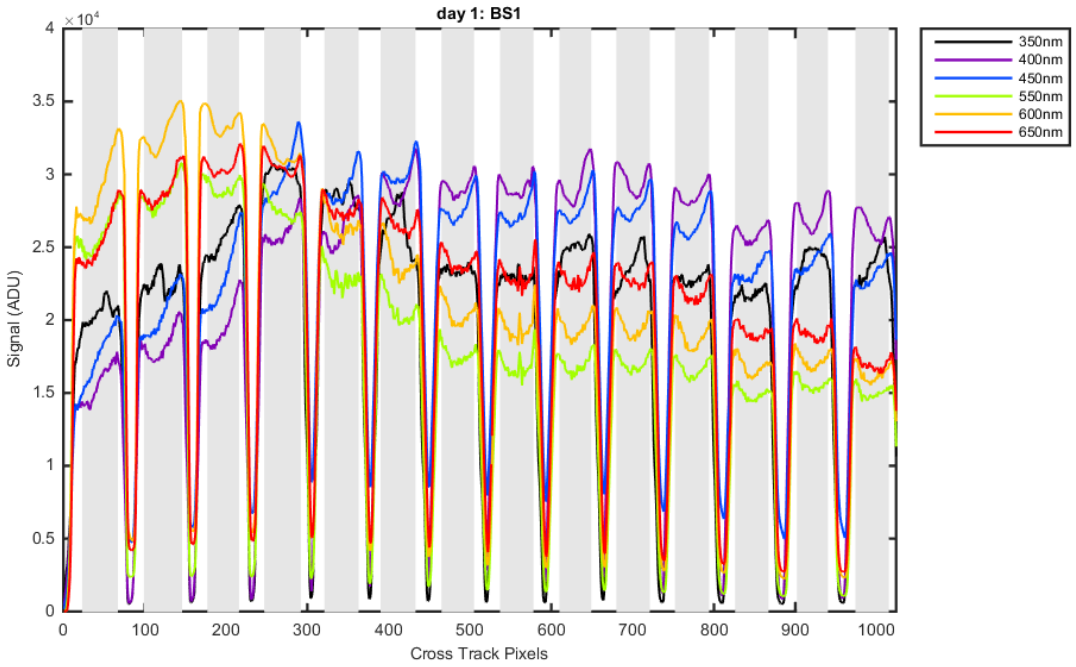

Figure 5) cross track data at several wavelengths. Of note is the amount of signal that is still on the array in between the tracks. In the image the central in-track region is shown as the grey areas, while the area in-between tracks is part of the area shown in white.

We expected to see much lower signals in this region between the tracks. While the system had been focused at Resonon, we felt we needed to have the system focused better, so sent the system back to Resonon. For contrast, in Figure 6, we show an image from the same spectrograph, after it had been refocused at Resonon. Note how much better the region looks between the tracks.

While Resonon was working with the system they discovered an asymmetric flair in the images. The Andor cameras can come with either wedged or parallel faced windows. The original thought on the source of the asymmetric flair was that this was caused by the wedged window that was on that specific camera. After further work it was discovered that this flair was actually caused by a camera software setting in the software that Resonon was using to read the camera data. However a decision at this time was made to use only parallel windows in the systems, rather than wedged windows, so all cameras bought after this time were purchased with flat windows. The reasoning was that it would be easier to include the effect of this window in the optical modeling of the whole spectrometer. This decision has come back to haunt us

recently. But at the time, correcting the software fixed the flair problem, and Resonon was able to improve the imaging through refocusing.

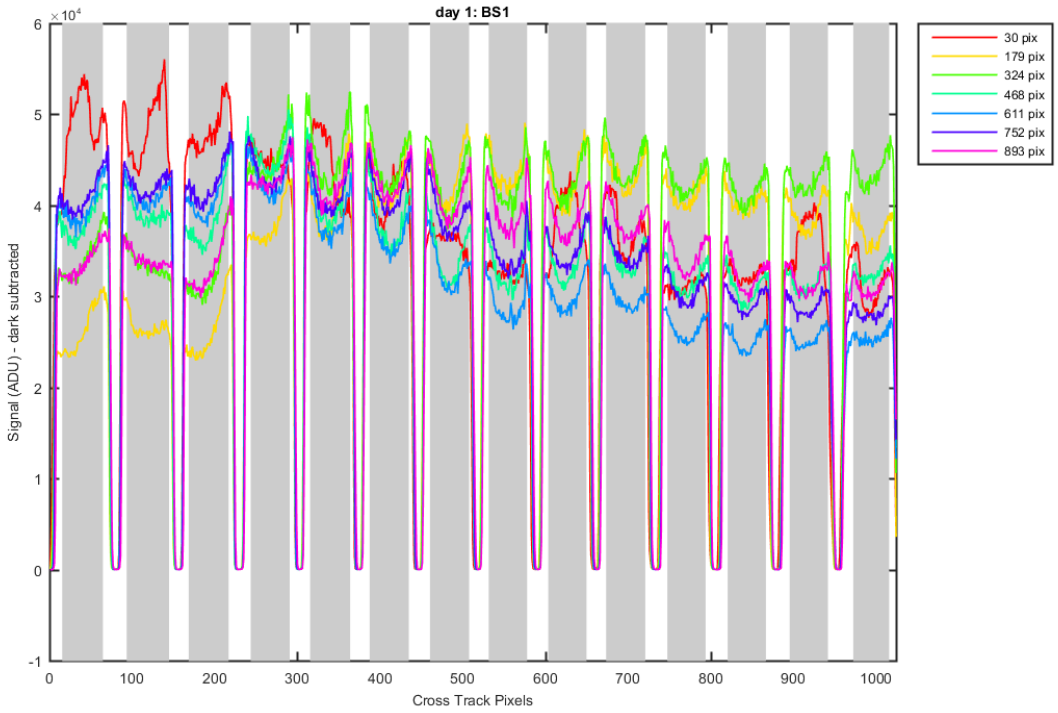

Figure 6) A cross track image from the refocused blue spectrograph, showing much improved imaging, as evidenced by the very low values between tracks.

3b) Blue spectrograph infrared artifact

While continuing to test the spectrometers in May 2015, Resonon discovered an infrared artifact in the images. Figure 7 shows an image of this artifact. By placing spectral filters in front of the system, it was traced down to being caused by radiation between 900 and 1100 nm (May 2015, Mike Kehoe, Resonson). The system has a filter to eliminate light above 700 nm, which while not significant when used in the water, can be a large signal in the lab when using red-rich lamps for calibration. It took several days to determine the origin of the artifact with optical modeling software. In the end it appears to be caused by a double bounce ghost reflection in the optical system; bouncing first off of the filter coating on the front of the prism, then off of a doublet lens that is right before the prism, as shown in Fig. 8. Whereas the original specification for this red filter was between 700 and 900 nm, the solution to this problem was to modify the filter used in the system to eliminate all light between 700 and 1100 nm from the system. In Fig. 9 we show the original filter that was installed, in a later discussion below (Fig. 12) we will show the new filter that has been installed to eliminate light between 900 and 1100 nm.

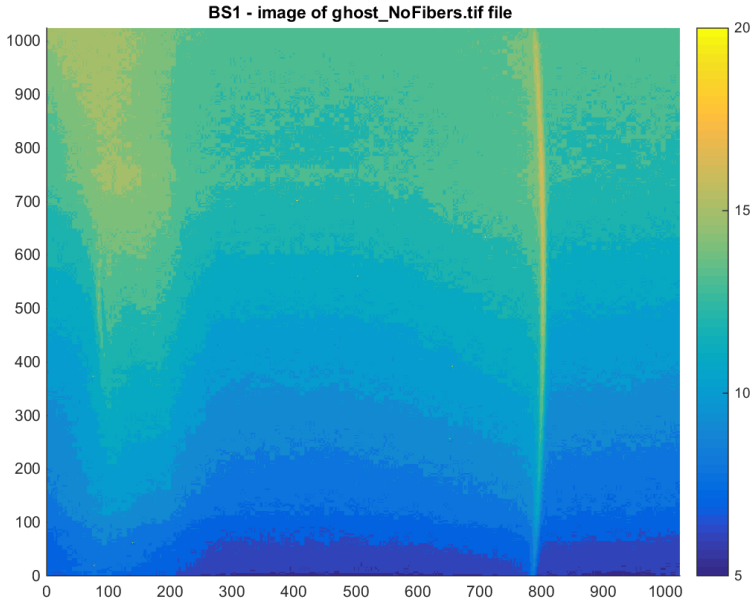

Figure 7) Infrared artifact, shown as the yellow band going through the data at around pixel 800.

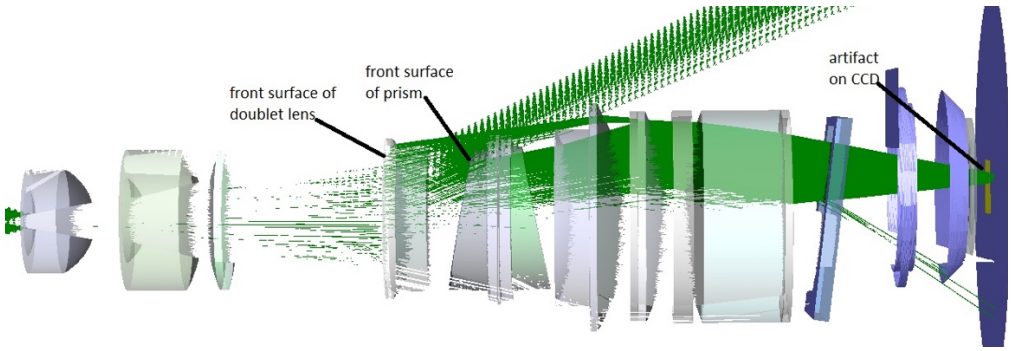

Figure 8) Model of blue spectrograph signal, showing the suspected cause of the infrared artifact. Infrared light coming through the system reflects backwards off of the front surface of the prism, then reflects again off the front surface of the double lens, returning through the system. While the double reflection is a low order effect, it still caused a noticeable signal on the CCD.

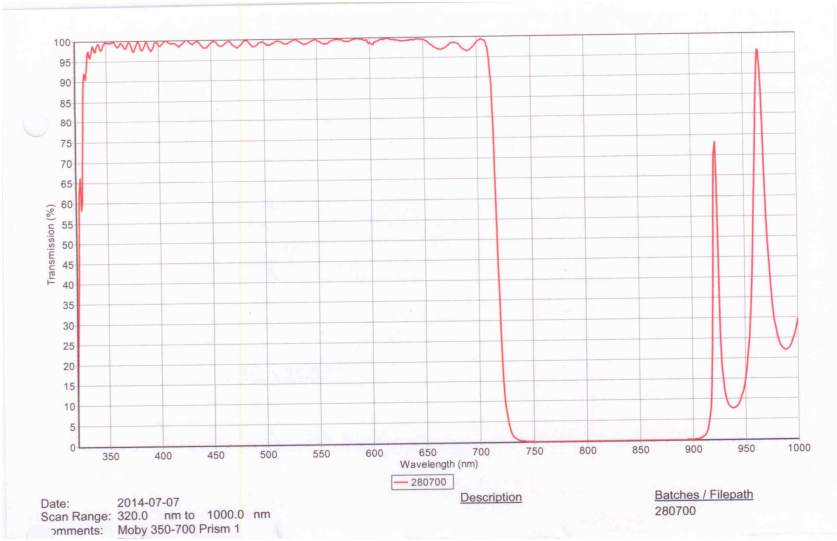

Figure 9) Transmission of the filter originally installed in the blue spectrographs to eliminate light above 700 nm. Note the transmission of light between 900 and 1100 nm, which was allowing light in this spectral region to enter the system.

3c) Shoulder on edge of track

In May 2015 BS01 was shipped back to Hawaii for further testing, with the knowledge that it would have to be retrofitted with the new filter to block the infrared artifact. While testing the system we found that each track was exhibiting a shoulder towards higher track number.

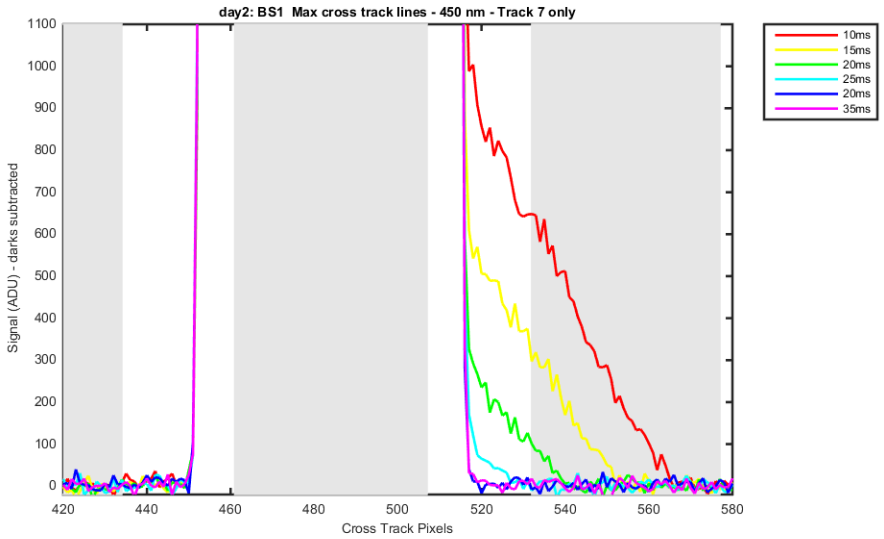

Figure 10) Variation of shoulder on side of track with shutter delay setting in camera software.

After much discussion with Resonon, and trying various optical tests, it was discovered that this effect was being caused by having too short a "shutter delay" setting in the camera software. We had been using a shutter delay of 10 ms, but if a longer shutter delay was specified (greater than 30ms), the problem went away. Effectively the shutter delay tells the camera how long to wait after telling the shutter to close, before it is safe to start reading the camera. Part of the

process of reading a CCD array involves moving the columns on the array to the left at which point the values in each pixel are read. With the short shutter delay time, the shutter was not quite closed when the camera started moving the columns of data, so extra charge would accumulate if these columns overlapped with the illuminated tracks. The solution was to use a shutter delay that was at least 30ms.

3d) Blue filter for blue spec

At this point we started illuminating the system with lasers to look at spectral bandpass, rough wavelength calibration, and straylight. Figure 11 shows an example for Track 7, of illuminating the system with various laser wavelengths.

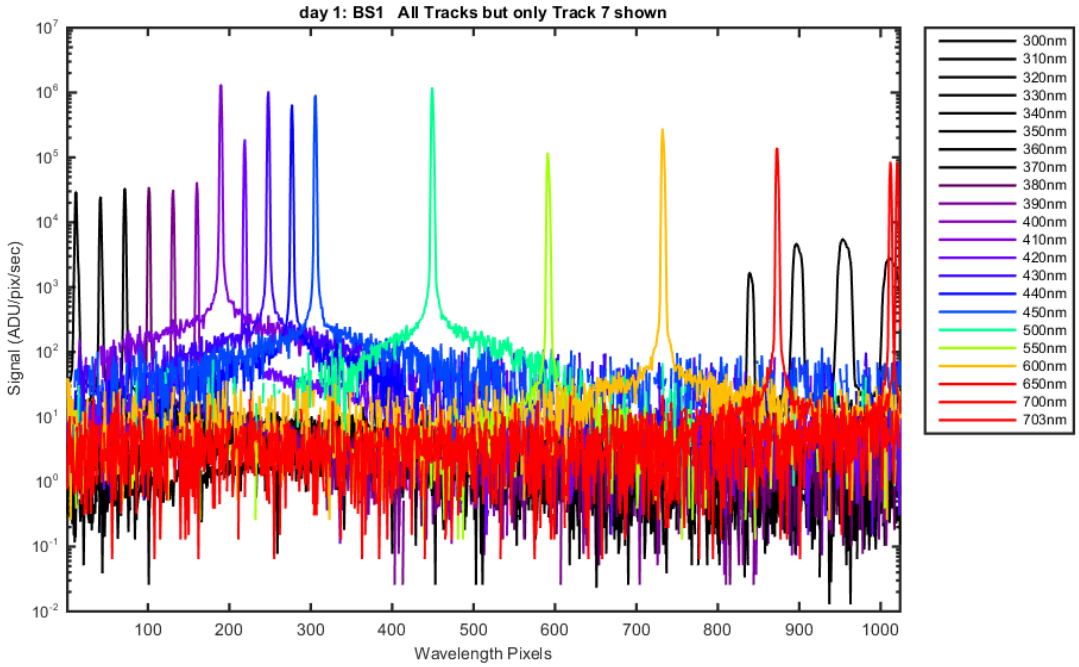

Figure 11) Track 7 illuminated with a laser at several wavelengths.

This spectrometer is designed to work from 350 nm to 700 nm. In reality it starts at 340 nm. However wavelengths below 340 nm can show up in the 2nd order of the spectragraph. For example the first black peak at around pixel 850 is really due to light at 330 nm, rather than 650 nm light that one would expect (and is shown as the red peak just ot the right of the black peak). The system is also not linear for this second order light, so 330 nm does not show up where 660 nm would appear, it actually moves to lower wavelengths. While we can correct for the 2nd order light between 340 and 360 nm, because we have a masurement of the first order at these wavelengths, below 340 nm is referred to as "off CCD", we do not have a measure of this light, and it would be difficult to impossible to correct for 2nd order below 340 nm. To correct for this the filter that was going to be specified to eliminate the infrared artifact was modified to include a cut on near 340 nm. The filter resulting from these specifications, and that is currently beign used in the blue spectrographs, is shown in Fig. 12. Noting that the y axis is a log scale, one can see that this filter sharply cuts on between 340 and 350 nm, and starts to cut off at 690 nm. It has significantly less out of band response at wavelengths greater than 700 nm, as compared ot the original filter used in the system.

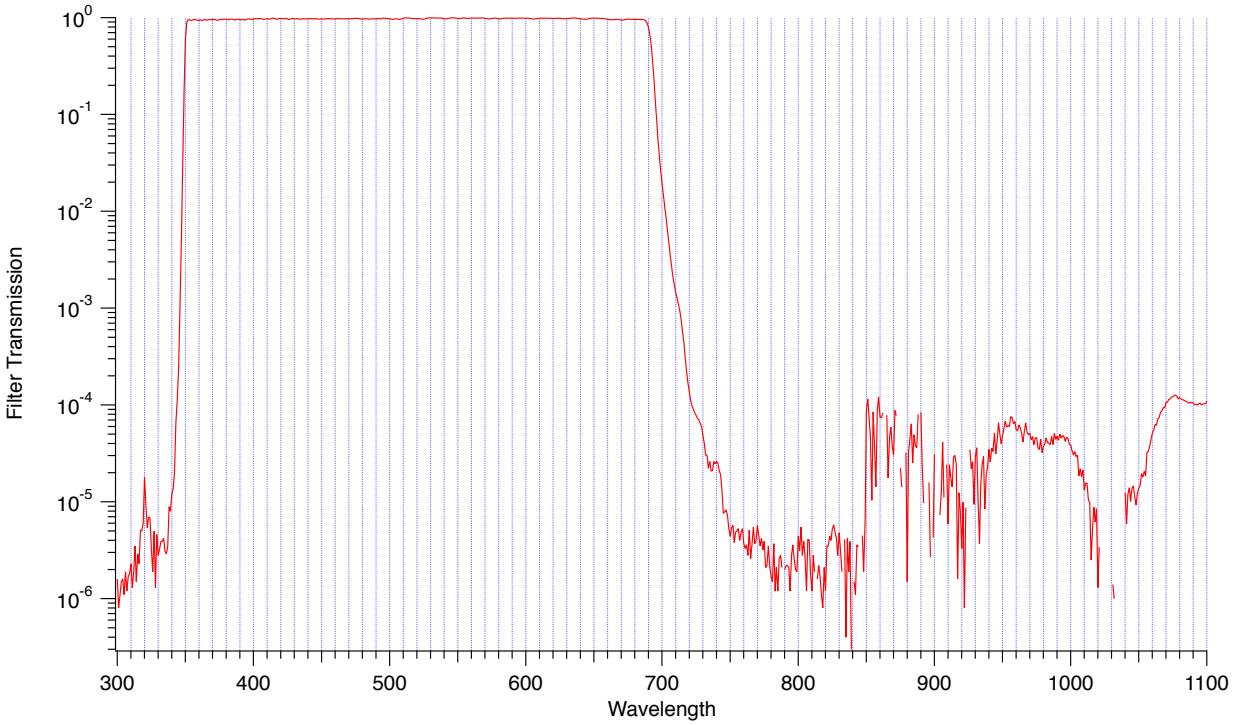

Figure 12) Filter transmission (in log scale) vs wavelength for the filter that gets rid of both the infrared artifact and 2nd order light below 340 nm.

With this new filter the response to many laser lines is as shown in Figure 13.

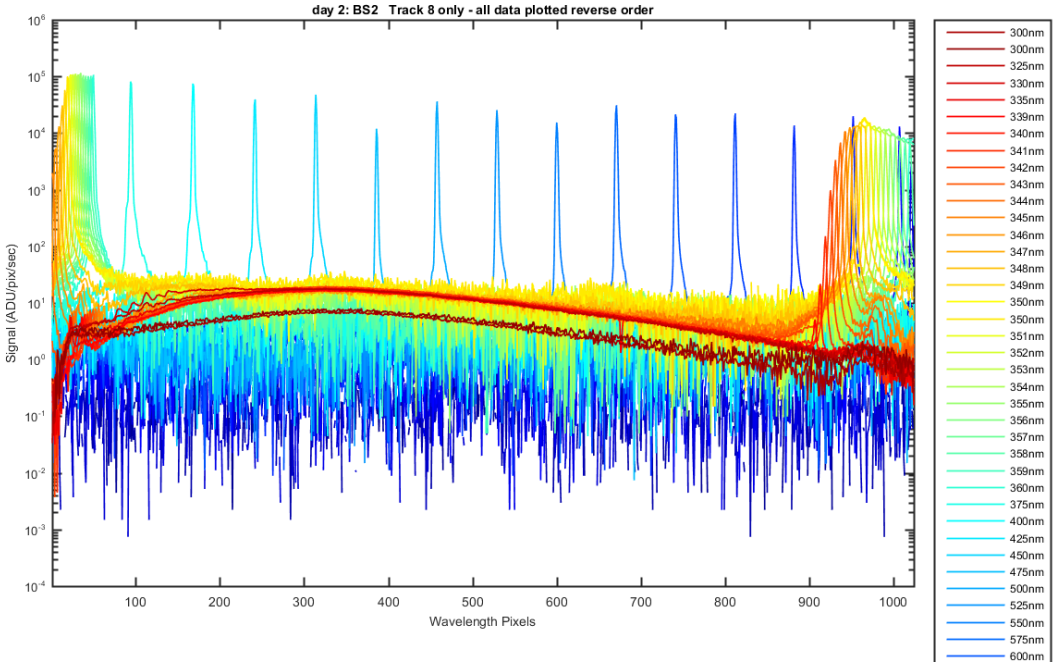

Figure 13) System response, with new filter, to many laser lines.

3e) Red spectrometer image fitting on array

During the initial build of the new red spectrometers at Resonon it was discovered that the image of the first and 14th tracks did not fit onto the CCD array (shown in Fig. 14). After many measurements of the optical system and modeling the system, it was decided that the best solution was to have 2 (out of 7) custom lenses in the system rebuilt. These new lenses were ordered, and received and the first red spectrometer was assembled in December 2015. Issues were also found with the fiber optic bundle that provides the input to the spectrometer. These issues were all corrected and the first red spectometer was shipped to Hawaii and arrived in April 2016.

Figure 14) Fiber 1 and Fiber 14 (tracks 1 and 14)are not imaged totally on the array.

3f) Red spectrometer performance

With these changes the red spectometer response is shown in Figure 15. This verified that we were getting a bandpass for each channel of approximately 1.2 nm, and spectral sampling at 0.4 nm/pixel as desired.

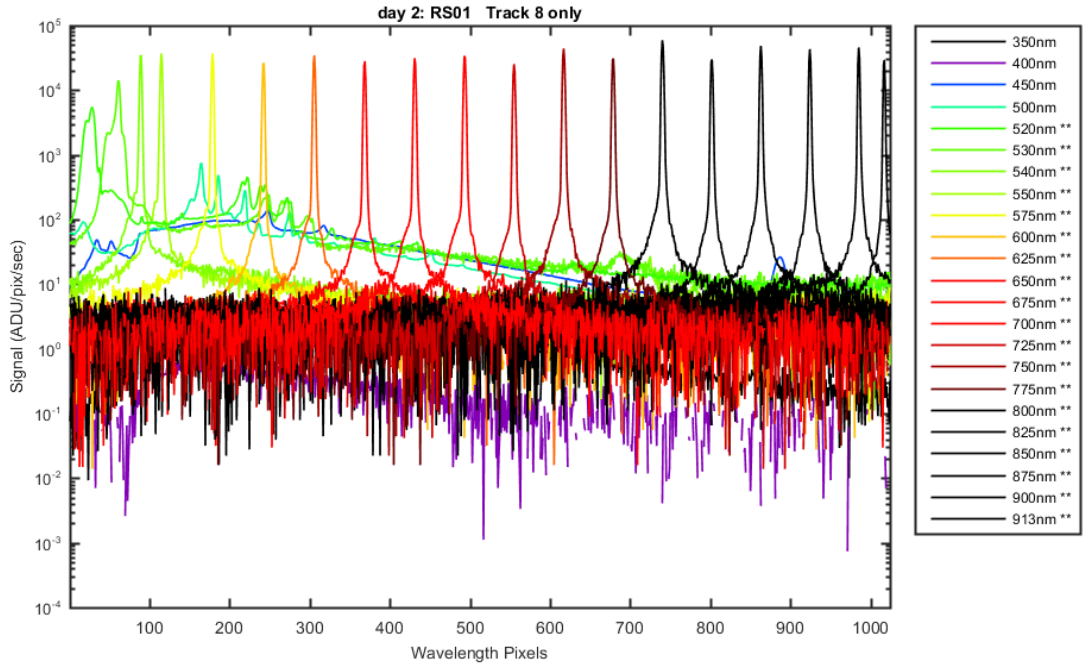

Figure 15) Red spectrometer response to many laser lines.

The funny wiggles in the data at 500, 520, 530 nm are due to the spectral filter that is installed in this system to eliminate the blue light below 500 nm from the system. This filter is shown in Figure 16. Note that the y -axis in this figure is optical density, which is – log transmission.

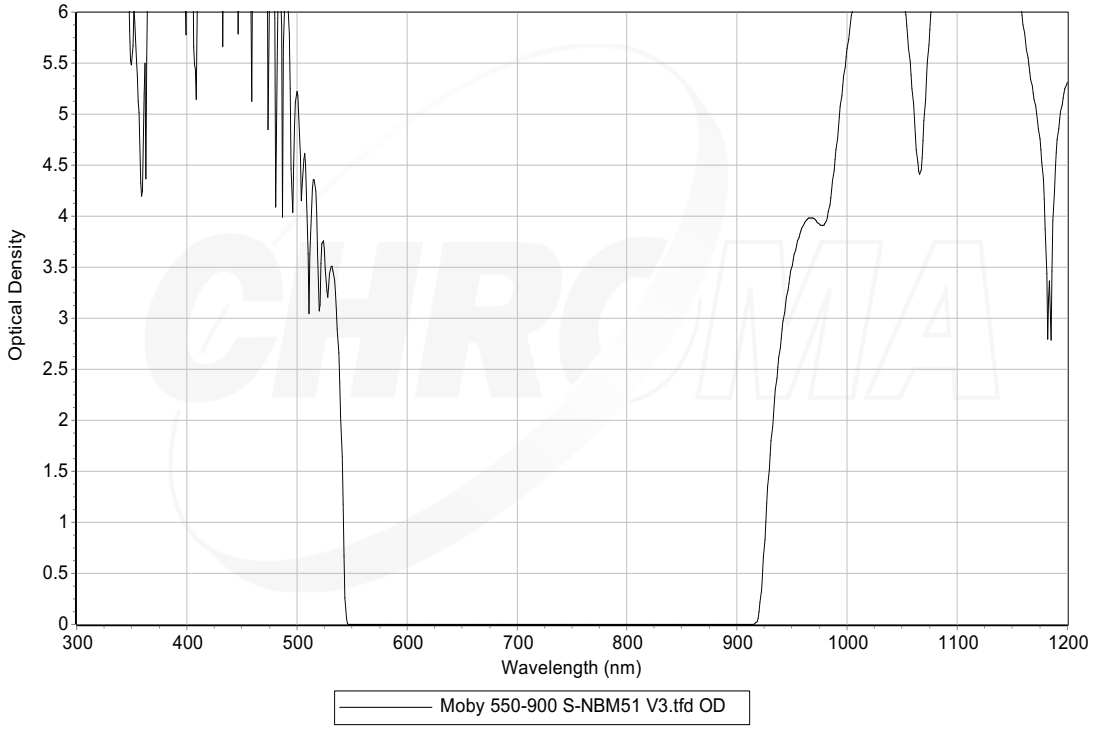

Figure 16) Filter installed on red spectrograph to eliminate light outside the desired operating range of 550-900 nm.

3f) Final issue: UV ghosting

As discussed earlier (*3a*) in initial testing of the blue spectrograph, flare was discovered that was hypothesized to be due to the wedged windows, so at that point a decision was made to only use parallel windows in the camera systems. On further testing this flare was found even with flat windows, but we had already specified parallel windows for the cameras. During field testing we recently discovered a low level reflection which sent light from one track to the symmetric position in the image, for example track 2 onto track 13 (Fig. 17) . Unfortunately it is not just one wavelength sending light to the same wavelength on a different track, but more complicated. The name given to this was "UV ghosting" because it is most evident in the UV where there is less light, not because the light comes from the UV or that it is only UV light that is being reflected. Looking through the test data that we had on all of our systems, we discovered that this effect only occurred with the cameras that had parallel windows, never with the systems with wedged windows. It also was evident in both the red systems and in the blue systems. So at this point we have sent all of our cameras with parallel windows (8 out of the 12 total we have) back to Andor to be retrofitted with wedged windows. We are currently waiting for the return of these cameras.

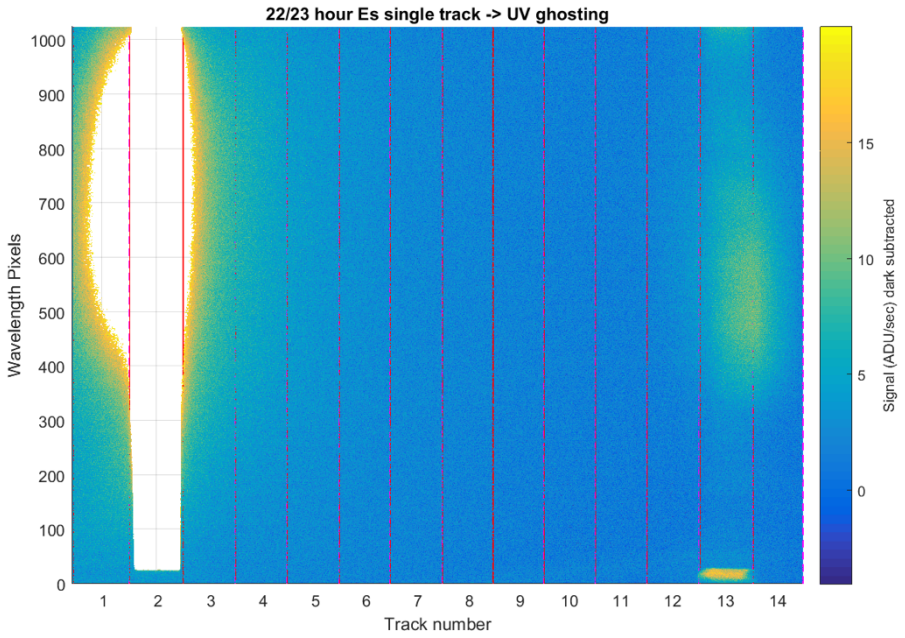

Figure 17) "UV-Ghosting" illustrates the small reflection of light from track 2 onto track 13.

3g) Fiber bundle

The spectrometers can take up to 14 different fibered inputs, so a fiber bundle is required to take these different fibers and align them on the entrance slit of the spectrometer. The fiber bundle we are using was built by Leoni. A diagram of the bundle is shown in Fig. 18.

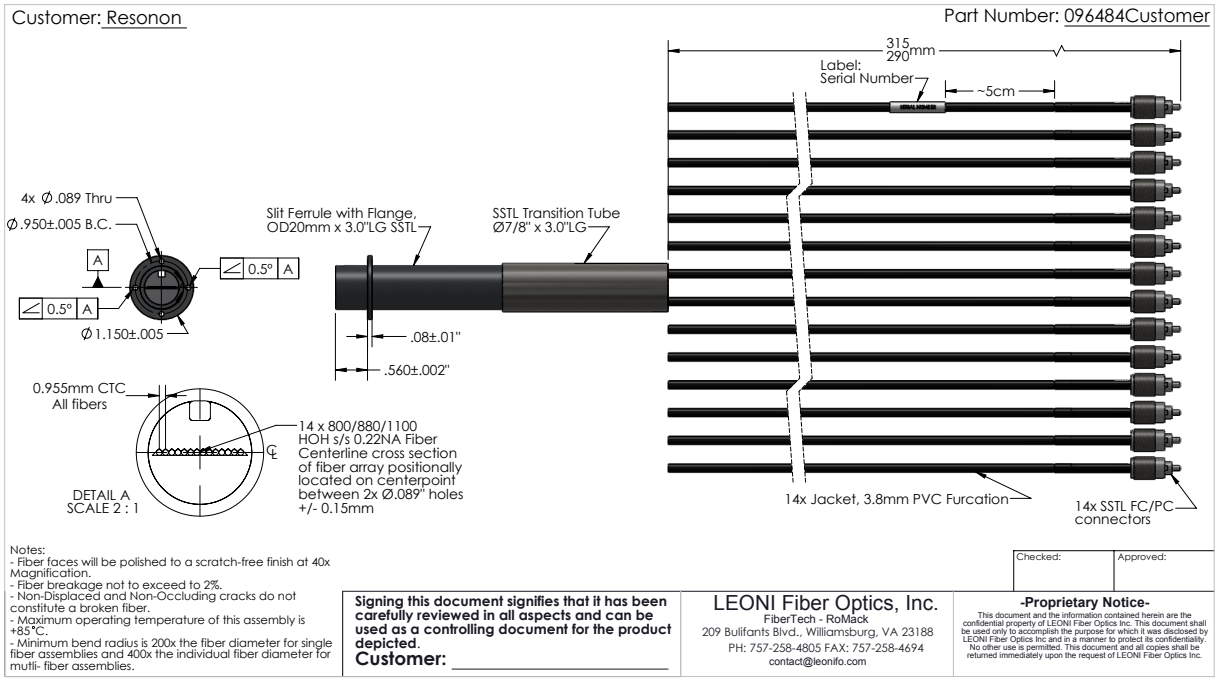

Figure 18) fiber bundle used to illuminate the spectrometer entrance slit.

We needed one of these bundles for each spectrometer, and in 2016 delivery of these began to be an issue. We started hearing from Leoni that they were having trouble making them, and many were breaking in the process so their yield was very low. We did not get more information until May 2017 when they asked if they could change the design slightly, effectively increasing the length by 5cm, which apparently made them easier to build. We agreed, the main impact was to make the spectrometer housing longer by this distance, which was not optimal but not a huge problem, and this apparently helped their process and allows us to get our complete set of input fiber bundles.

4) Fiber Splitter

In MOBY-Net (as in the other systems) light from the collector is brought down through a fiber and at some point split between the red spectrometer and the blue spectrometer. In MOBY-Heritage this is done with a dichroic beam splitter which splits the blue light from the red light. In MOBY-Net, because the 14 channels are simultaneous, splitting in this way would require 14 different dichroic mirrors. Each of these mirrors would have their own specific characteristics in terms of fine detail, hence could be very complicated to maintain and characterize. These dichroic mirrors typically have fine spectral features near the cutoff wavelength that are temperature sensitive.

In our original MOBY-Net design, we were planning to use in-line fiber optic splitters to split the light between the two spectrometers. In these light comes in on one fiber and is split internally into the two channels. Fig. 19 is a picture of one of these splitters.

Figure 19) Picture of fiber optic splitter

The splitting ratio of the fiber is known to be dependent on the mode structure of the light field inside the input fiber, so in July and August 2015 we did many tests of a pre-delivery splitter to make sure that, in our application, the splitting ratio was stable for the differences in illumination that we would expect with our collector designs. The splitter passed these tests without a problem so a set of these splitters was ordered for MOBY-Net.

In September 2016 we received the splitters and started a thermal test of their stability . We found that in the range from 23-43 C the splitting ratio varied in a regular fashion between 0.7353 and 0.7315, so it appeared the splitters were working. Unfortunately the splitter we were working with failed completely for some reason and we decided we needed to find more ruggedized versions of the splitters. We began at this point working with Fibersense on an extended temperature range device. At the time we were concerned not just with operation, but also with what would happen if, during shipment, the splitters were exposed to very high temperatures in the shipping containers.

While working through the extra costs involved with these ruggedized filters Carol Johnson tested some of the other Fibersense splitters we had received in her environmental chamber at NIST. During these tests we discovered some very troubling aspects of the splitters. During several days of testing, the temperature was varied between 22 and 30 C. The result on the

splitting ratio is shown in Figure 20. While the splitting ratio varied in somewhat of a controlled way during each day of testing, the overall ratio was different from day to day.

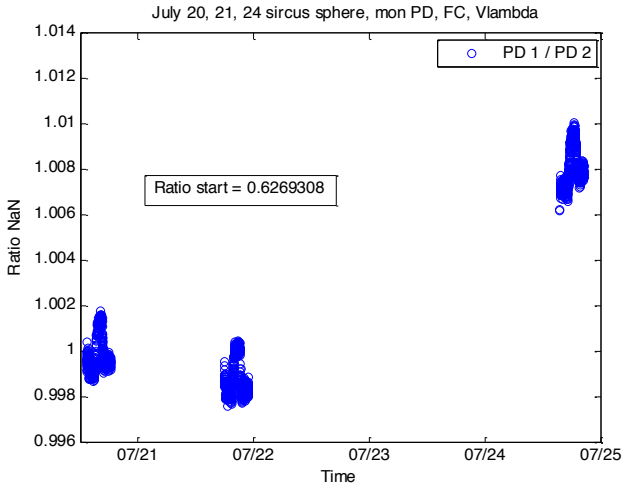

Figure 20) Splitting ratio for three days of tests. Temperature ranged from 22-30C

Even more concerning was that there was a larger change in total throughput of the system (Fig. 21), and these changes were not consistent from day to day. Thus we felt that the splitters would introduce unknown variations in the system that would not be acceptable.

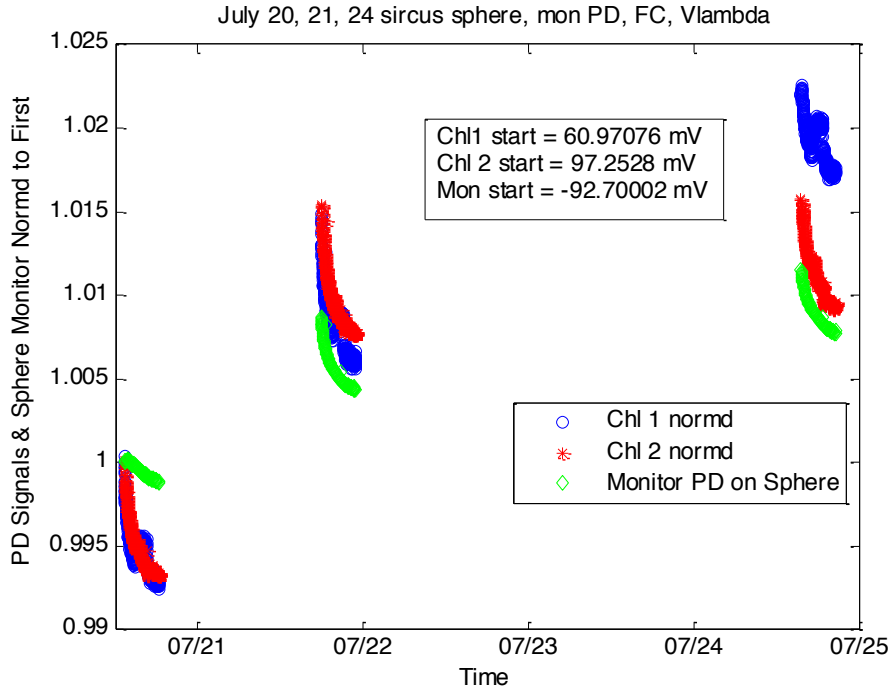

Figure 21) Overall throughput of the system during the temperature tests.

At this point we decided we needed a new method to do the splitting between the two spectrometers and settled on a design using polka-dot mirrors in an optical beam splitter. Polka-dot mirrors are as they sound, the surface of the mirror has dots of mirror over the glass substrate, and the splitting ratio is determined by the fraction of mirror vs clear space. Figure 22

shows a schematic of the system, while Fig. 23 shows a picture of part of the system. In this system light comes in from the right side, where the fiber from each collector (irradiance or radiance) enters the system. There is a pair of lenses to collimate the light, at which point the light goes through a sealed window barrier. The light then can strike the polka-dot mirror and be directed upwards to the fold mirror and then focused down onto a fiber again, or go straight through where it is focused onto another fiber. One of these fibers then goes to the blue spectrometer, while the other goes to the red spectrometer.

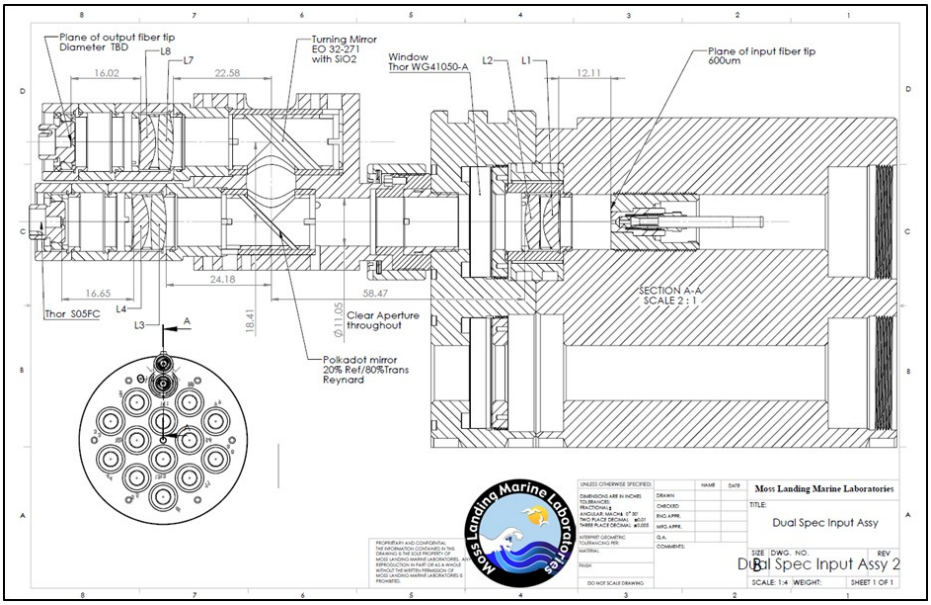

Figure 22) Schematic of polka-dot mirror beam splitter

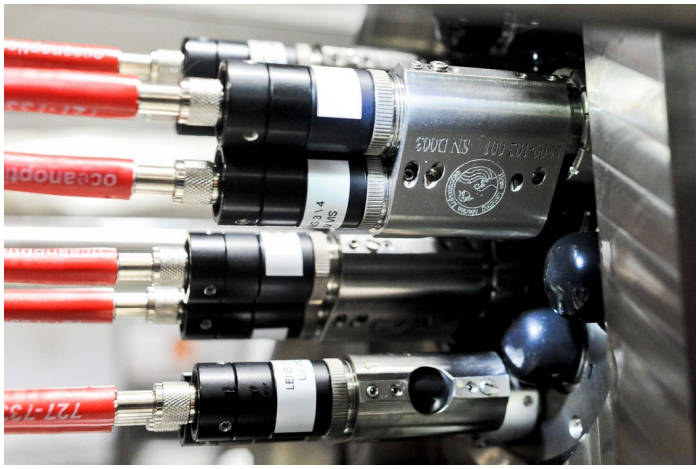

Figure 23) Picture of inside beam splitter housing showing each polka-dot mirror housing.

We have done several tests of these beam splitters to look at the temperature sensitivity. In Figs. 24 and 25 we show the temperature sensitivity of the fold and thru channels of these devices. This is a compilation of several days of testing. The results show a small, but consistent temperature variation. The fold channel has a temperature coefficient on the order of 0.013%/C, while the thru channel is higher, 0.044%/C. But each of these variations are consistent from day to day, so are correctable. It makes sense that one goes up when the other

goes down, as light is transferred from one channel to the other (almost like the polka-dots are growing). The extra losses in the thru channel must be from some other factor, perhaps alignment.

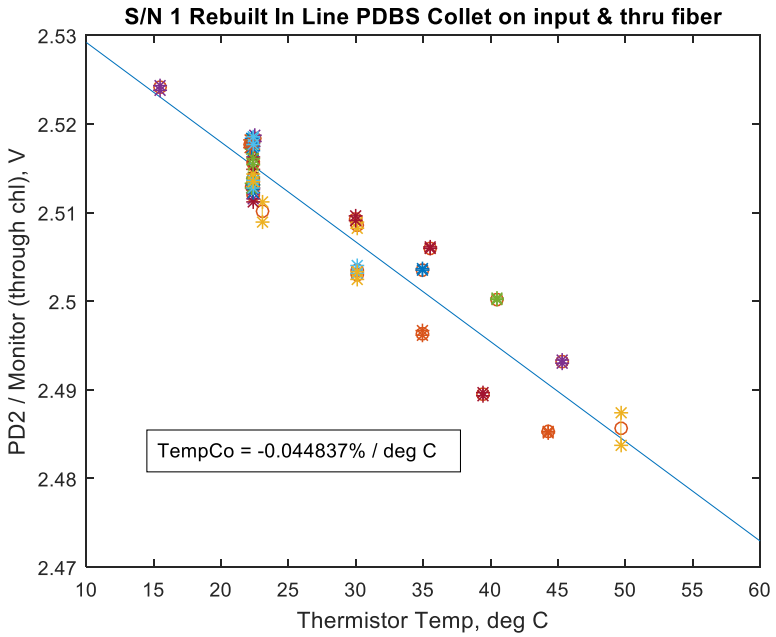

Figure 24) Thru channel of polka-dot beam splitter versus temperature.

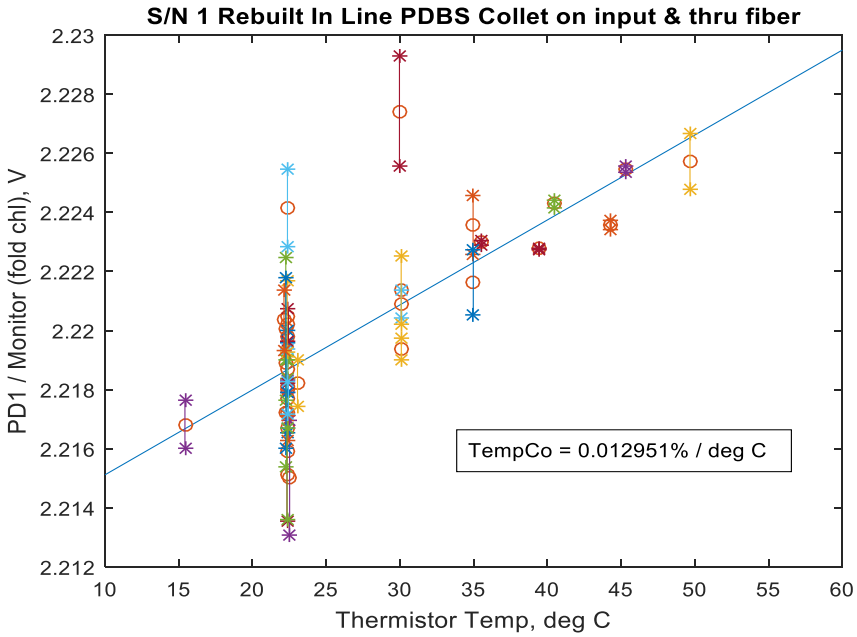

Figure 25) Fold channel of polka-dot beam splitter versus temperature.

5) MOBY Hull

With MOBY-Net we maintained the 3 arm configuration of MOBY-Heritage. While some may complain about the lack of profiling, there are many advantages to this configuration:

- Arms allow us to get farther from the main instrument hull (reducing self-shadowing).
- 3 arms over 2 arms offers redundancy:
  - We have had the top arm damaged during deployments, the extra arm allows continued operation.
  - Occasionally a calibration will drift in one or other arm, with three arms we can see this by comparing the derived KL from different arm pairs, and can eliminate the bad arm measurement.
- Arms at fixed depths allows long integration times (30-60 seconds) and repetitive measurements to eliminate wave focusing variations.
- Fixed arms are more reliable than a mechanical profiling system.
- (not as important for Vicarious calibration but) simultaneous measurements with the three depths will allow measurement in less optimal broken cloud situations.

Our design criteria for MOBY-Net included having a method for the optical system to be removed intact, without disconnecting the fibers, for calibration in another location. Figure 26 shows the arm assembly on the main spar, in the Hall Spars manufacturing location. The opening at the bottom of the arm attachment point is shown, and it is through this opening that the collectors can be removed, with the fibers attached.

Figure 26) MOBY-Net carbon fiber spar and arm assembly.

The other requirement for the MOBY-Net Buoy assembly was that it could be shipped from place to place in a standard 40' shipping container. Figure 26 shows the main MOBY-Net buoy spar and floatation at Mooring Systems Incorporated, the manufacturer of the system. Figure 27 shows the inside of the container after shipment to our site in Hawaii. The big black pieces are the floatation for each of the buoys.

Figure 27) Flotation buoys for the two MOBY-Net systems.

The MOBY-Net hulls have been delivered to our Hawaii site, but have not been assembled. We plan on doing some testing of the buoys at sea to make sure that they work as expected, but they are very similar to our existing buoys, other than the carbon fiber pieces, so we are not expecting any significant problems.

6) System tests at sea and in lab

We have had four deployments of the blue spectrometer and one short deployment of the combined blue/red spectrometer. Figure 28 is a picture of the blue spectrometer installed alongside the MOBY-Heritage Buoy, Fig. 29 shows the dual collectors (one for MOBY-Heritage, one for the Blue spectrometer, while Figure 30 is a picture of the combined blue/red spectrometer in the field attached to the MOBY-Heritage Buoy.

Figure 28) New blue spectrometer installed on side of MOBY Heritage buoy. To operate in this manner we have additional collectors installed alongside the normal MOBY collectors as shown in Fig. 29.

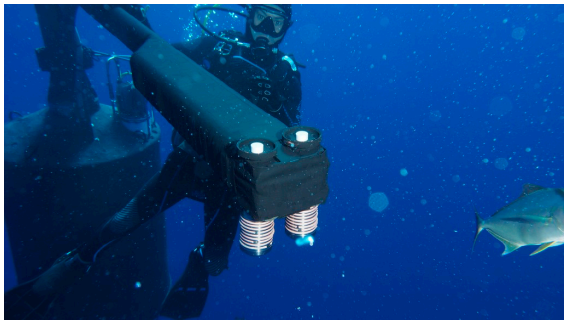

Figure 29) Dual upwelling radiance and downwelling irradiance collectors installed on MOBY to allow both Blue spectrometer and MOBY-Heritage to collect data.

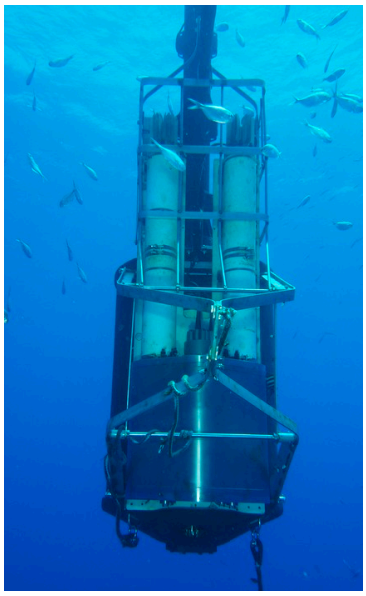

Figure 30) The new dual Blue and Red spectrometer package installed on MOBY during the short M265 deployment.

These four deployments for the blue spectrometer were:

M261: August 2016- February 2017 (top arm was sheared off by a boat strike during this deployment),

M262: February 2017 – August 2017 (mooring broke free during deployment, so deployment was interrupted for a month in the middle),

M263: August 2017- December 2017,

M264: December 2017- May 2018.

The combined deployment of the red/blue spec was a deployment on M265, which was cut short because a boat broke the tether between MOBY and the mooring buoy.

These deployments were used to test different stability aspects of the operation of the buoy. We will discuss each of the type of stability separately.

6a) Spectral Stability

The first type of stability is the spectral stability of the system during deployment. Because we have very high spectral resolution we can accurately use the solar Fraunhofer lines, and some

additional atmospheric lines, to perform spectral calibrations while in the field. For each deployment of the blue spectrometer we have watched the apparent locations of the Fraunhofer lines in our spectra throughout the deployment. Figure 31 shows two of these during deployment M264.

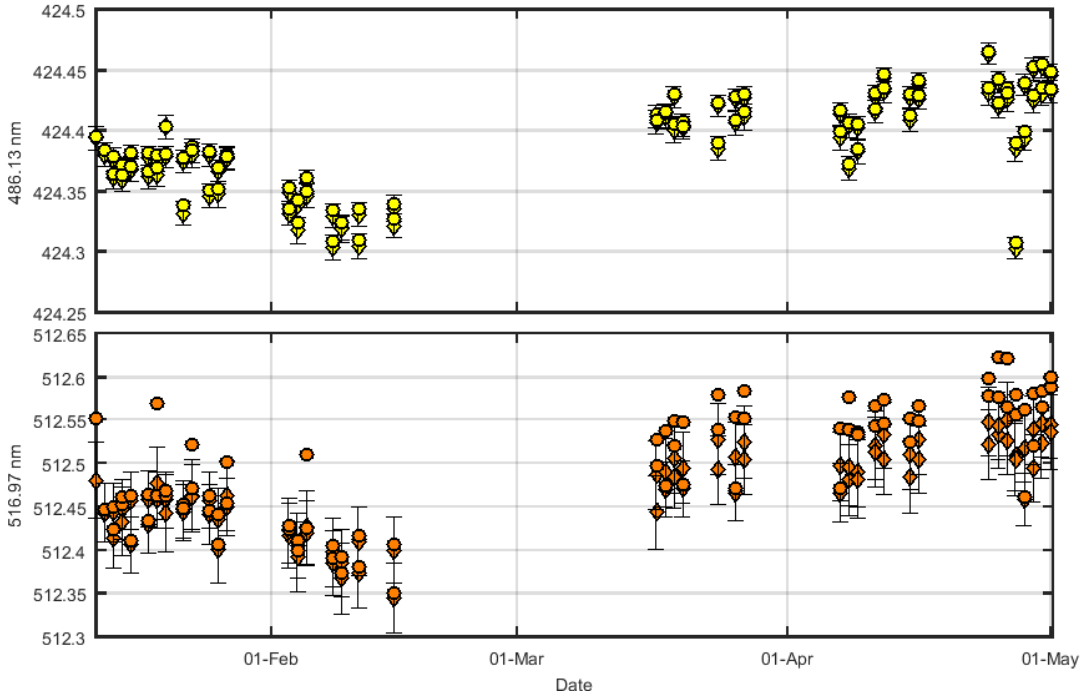

Figure 31) Position of two solar Fraunhofer lines on the CCD array. The x-axis is time during the 4 month deployment, the y axis is pixel location. Note each pixel represents approximately 0.3 nm. The exact position of the Fraunhofer line is determined by fitting a gaussian curve to the spectra in the vicinity of the Fraunhofer line.

This result is typical of 3 out of 4 of the deployments (M261, M263, and M264). Note each of these deployments had a different spectrometer installed. In these deployments the drift was within 0.2 pixels over the 4 month deployments, or approximately 0.07 nm. This is probably close to the accuracy of our gaussian fit technique, as we are looking at very small fractions of a pixel difference. The one bad deployment seemed to have something loose in the spectrometer, as there was a spectral drift of 1 nm over the 6 month deployment (and the tracks were moving, as will be discussed later). This spectrometer also had had problems earlier, when it had been shipped to Miami and arrived with several pieces loose. At the time we found that several of the screws holding it together were too short, and barely had any threads engaged. We thought this had been fixed, but this spectrometer was still acting anomalously.

The general result (0.07 nm shift over the deployment) is easily within our goal of 0.1 nm for spectral stability.

6b) Track stability

The track, or position, of each input signal is also an important factor that must be stable. If the track moves around it may affect the calibration, as each pixel in the CCD will have slightly different response characteristic.

Once again, as with spectral stability, the same 3 out of the 4 deployments worked very well, an example is shown in Fig. 32. This was the worst case track for a good deployment (M264), i.e. the track showing most movement, but even then the movement was less than 0.5 pixels, which is negligible as we will be oversampling the track when we average the data. During the one anomalous case (M262) tracks moved around 6 pixels during the deployment, but not in a regular progression. M262 was also the deployment that was basically two deployments as it had to be recovered in the middle when the mooring broke free. But in general, the three good deployments have definitely met our goals for track position stability.

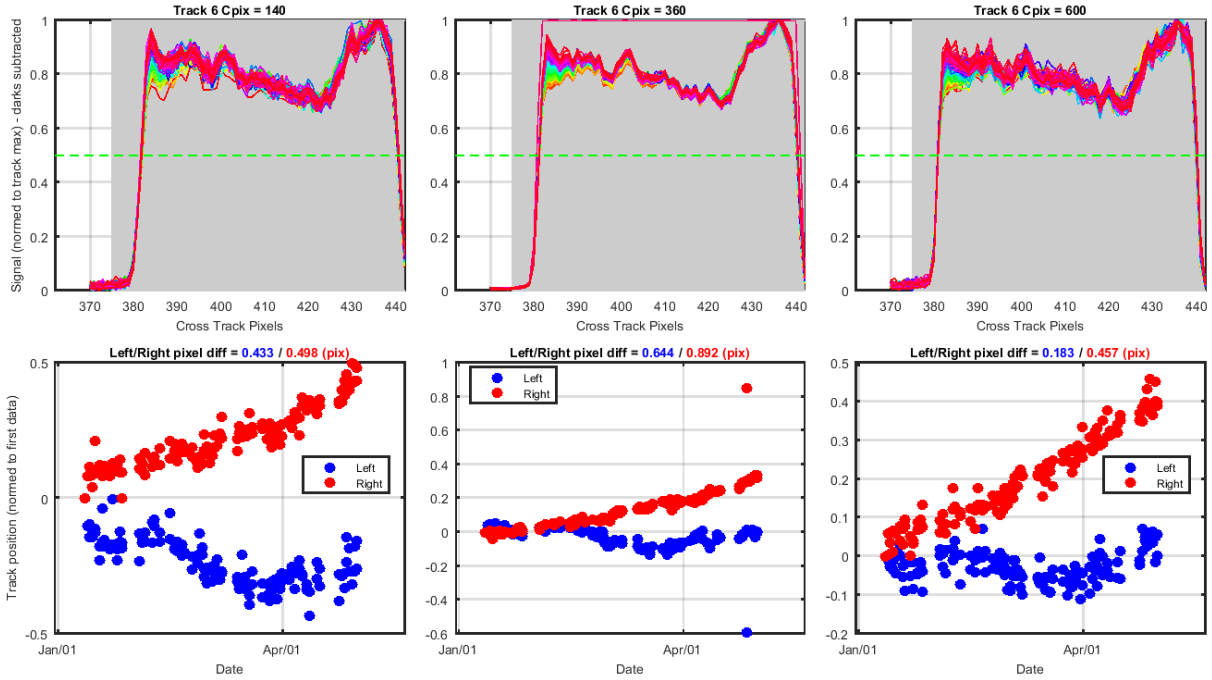

Figure 32) Track location during deployment for M264. Shows that the track position was also stable, similar to the spectral calibration stability.

6c) Radiometric stability

This is the one area that is causing us problems. I am not going to discuss the M265 dual spec deployment, as for many issues there was not enough data acquired during that shortened deployment. I will also ignore deployment M261, as the camera installed on this deployment was not working properly, and would not allow us to collect data at gain 4 (our desired gain). It did allow us to collect data at another gain, which was useful for track and spectral stability, but not useful for radiometric stability. I will focus on deployments M262-M264.

There are three ways to look at the radiometric stability. The first would be to look at a comparison between pre/post deployment calibration. The second way, which looks at inter arm stability, is by comparing diffuse upwelling attenuation measurements, KL. The third method, since we are taking data close to the same time as the MOBY-Heritage data collection times, is

to use MOBY-Heritage to vicariously calibrate the blue spectrometer. We will present the data for these types of comparisons separately.

6c-1) Radiometric stability by pre/post calibration.

I will go through the pre and post calibration stability in the system response for each deployment separately, starting with M262. Note that the system response definition has units of (ADU/pix/sec)/(uW/cm^2/sr/nm) for radiance and (ADU/pix/sec)/(uW/cm^2/ nm) for irradiance.

We would not expect the pre/post calibration for M262 to be very good, given that it experienced large spectral and track shifting during the deployment. And as such, in general it meets these low expectations.

Figure 33 shows the post/pre calibration responses for Es, while Fig. 34 shows the similar factor for the 3 Lu channels. There are several interesting features here. First there is a large difference between these factors for each sensor, and Es shows a large spectral variation that is not evident in the Lu pre/post response calibrations. LuTop actually shows very good stability for the pre/post calibration. LuMid, while greater than 5%, is spectrally flat from 450 to 600 nm. LuBot, while not as good as the others in terms of pre/post calibration does not have the spectral variation that Es had. One thing to note about the Es response is that on this deployment Es was placed on track 1, and track 1 had problems. It was barely on the array, and was slightly misaligned with the CCD array in such a way that the "blue" side was barely on the array while there was more space (2-3 pixels) between the track and the edge on the red side of the array. This is probably the cause of this large spectral variation between pre/post calibration in Es. After this deployment we moved Es from track 1 to track 2 to avoid this issue.

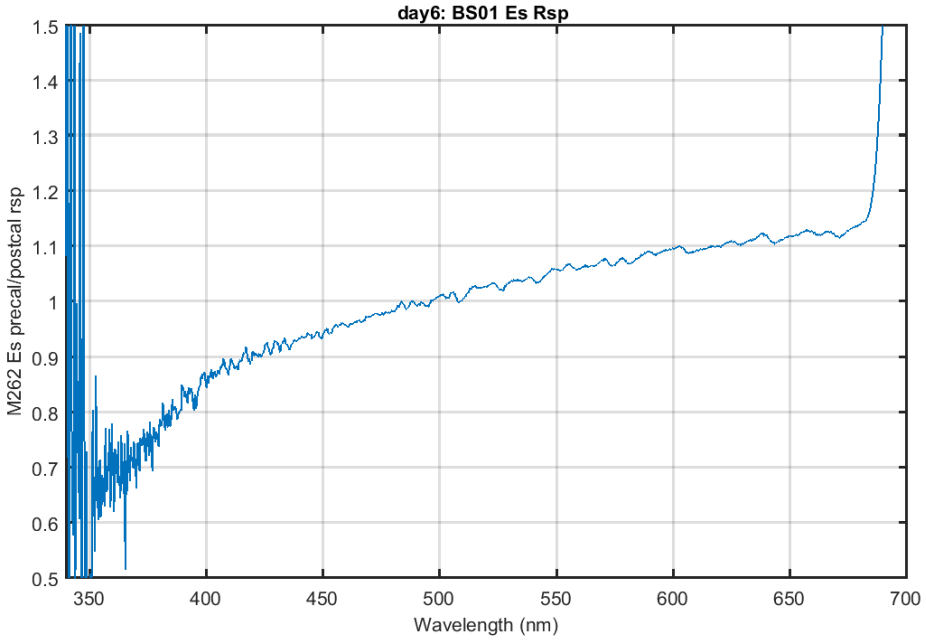

Figure 33) Pre/post calibration response for Es during deployment M262.

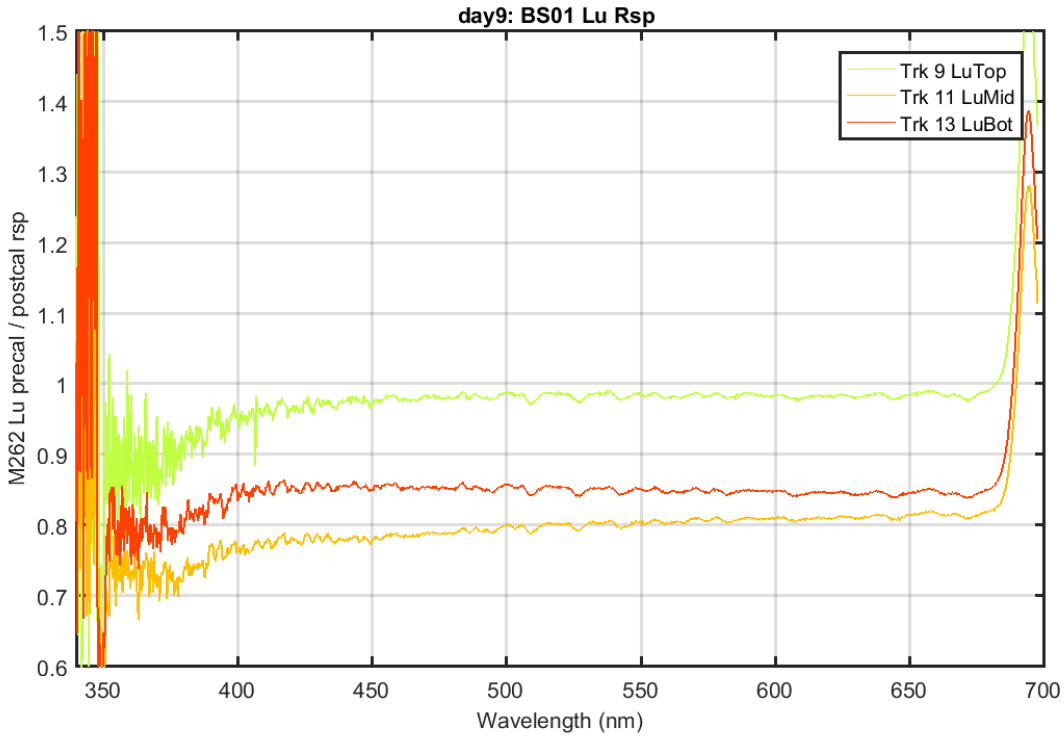

Figure 34) Pre/Post calibration responses for the three Lu channels, for deployment M262.

Moving to deployment M263, the pre/post calibration responses for Es (Fig 35) and Lu's (Fig 36) are shown below. For Es, LuBot, and LuMid the pre/post calibration responses are reasonably good between 400 and 650 nm. Near and below 400 nm, the calibration lamp flux is very low, which causes problems with the calibrations. The net ADU's can be down 3 orders of magnitude at 350 nm when compared to 650 nm, and the signal-to-noise can be 1.

LuTop had a large change, 25%, between pre/post calibration. While I am not showing the Ed calibrations here, EdTop on both MOBY-heritage and the BS also showed a big decrease in response between pre and post calibration. So something might have affected the fibers carrying the MOBY and BS EdTop and the BS LuTop during recovery. Fortunately for MOBY operations, LuTop on MOBY-Heritage was fine.

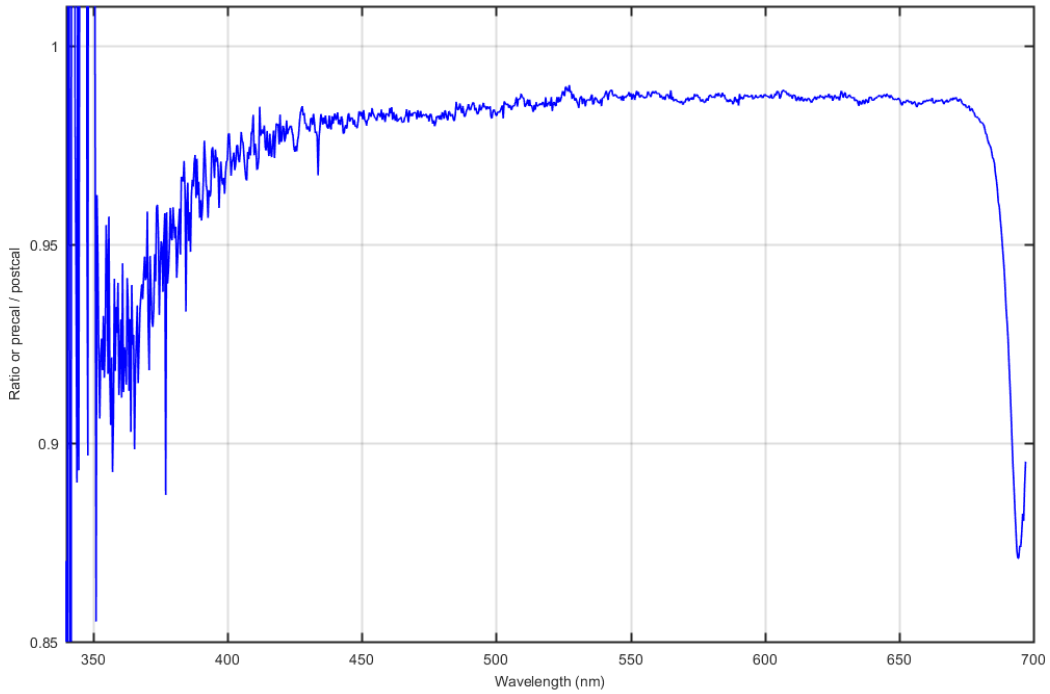

Figure 35) Pre/post calibration for M263 Es system response.

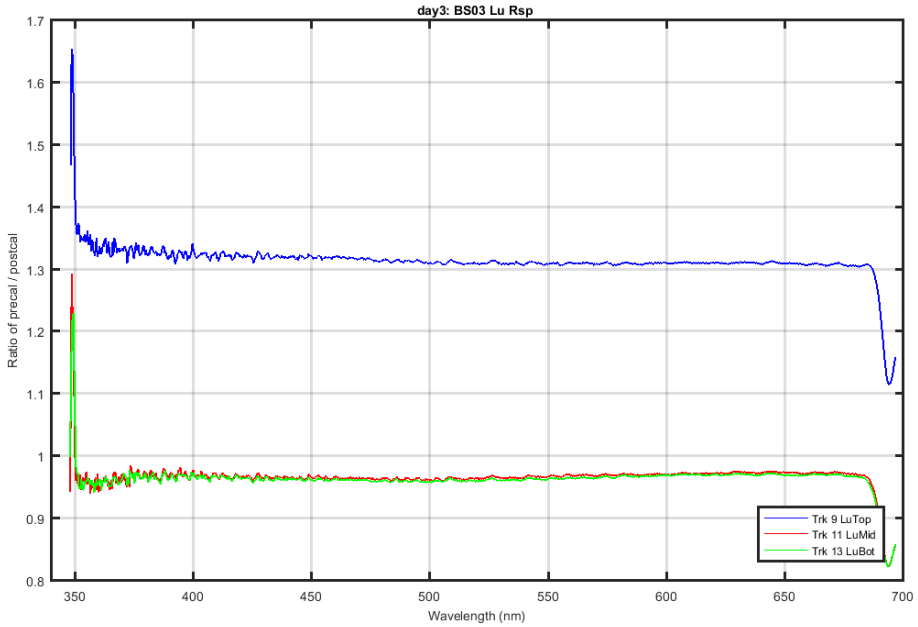

Figure 36) Pre/Post calibration responses for M263 Lu system response.

In Figure 37 and 38 we show the pre/post calibration responses for M264. Once again, Es, LuMid, and LuBot are reasonable between 400 and 650 nm, but LuTop is out of family however only by 10%, not 25 % as during M263.

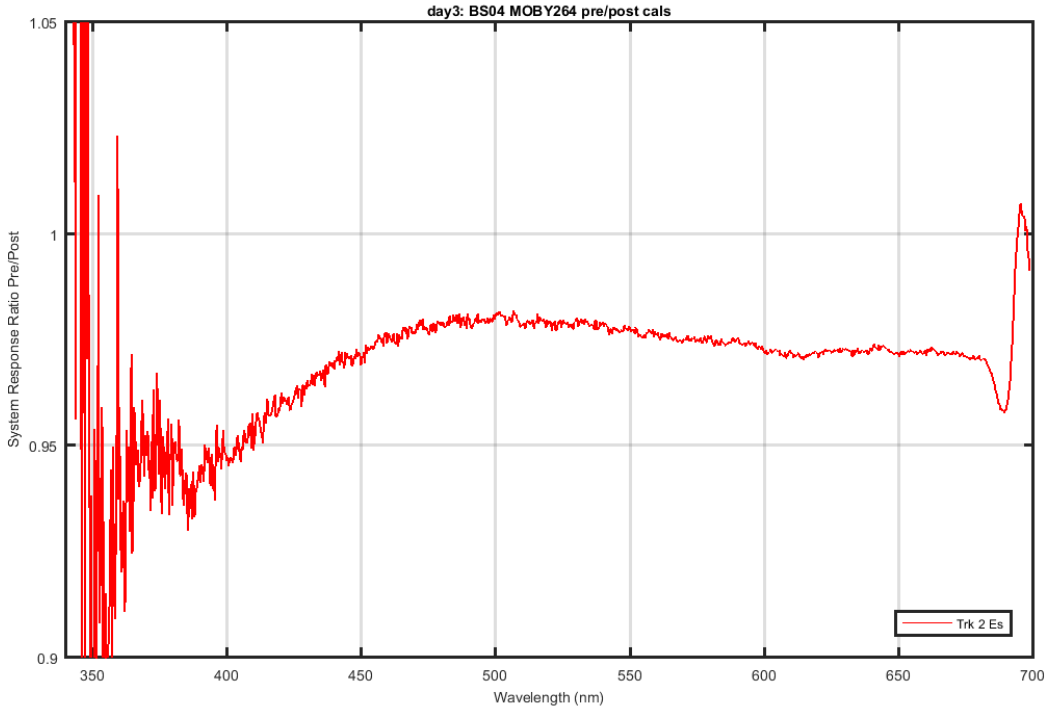

Figure 37) pre/post calibration responses for M264 Es system response

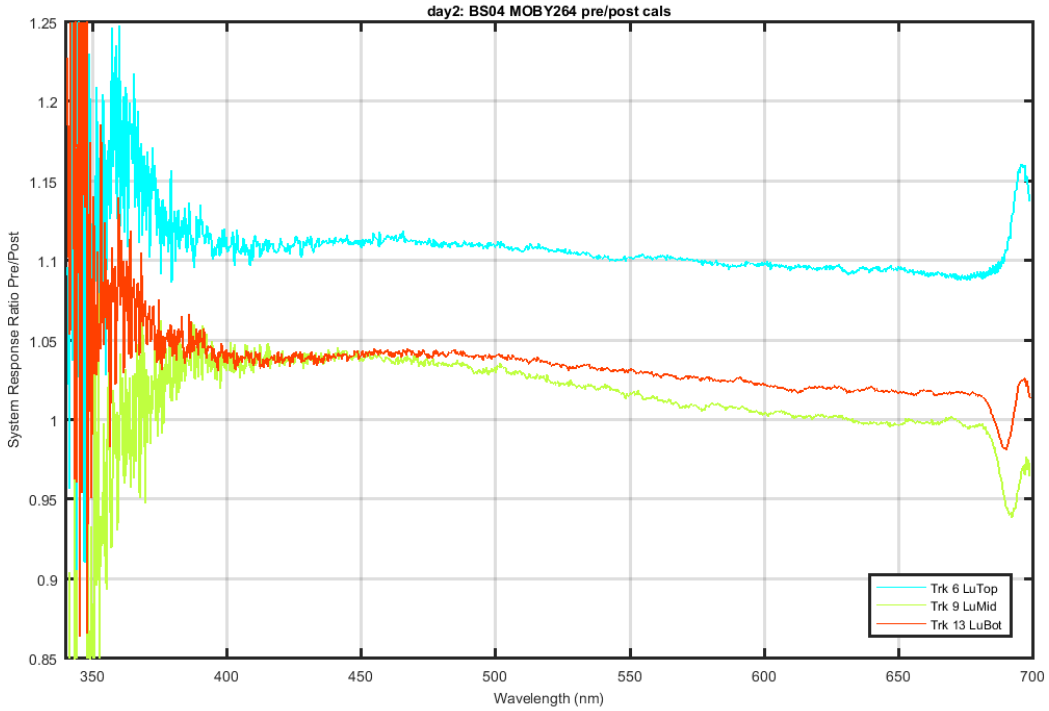

Figure 38) Pre/post calibration responses for M264 Lu's system response.

The conclusions from this method of showing system stability is that moving Es from track 1 to track 2 greatly improved its stability in terms of pre/post calibration. Ignoring M262, which we expect to have problems because of the movement in track position and spectral shifting, M263 and M264 generally had reasonable stability over the 4 month deployments with less than 5% change in the pre/post calibration response. For some reason the LuTop calibration was an outlier in this statement for both M263 and M264. In general though, work needs to be done to get to the 1% stability requirement as stated in the vicarious calibration white papers.

6c-2) Radiometric stability during deployment by following KL calculated with arm pairs.

An interesting way to track inter-arm stability during deployments is by looking at the variation in the KL calculated with different arm pairs. There are three different sets that can be used. KL1 uses the top and middle arm, KL2 uses the top and bottom arm, while KL3 uses the middle and bottom arm. By looking at the differences between these products one can track the inter-arm stability, taking out the natural variability in any individual KL measurement. This assumes, of course, that on average there is no surface layer in the top 10 m. Note that this only works for wavelengths below 575 nm as above this wavelength Raman and Chl Fluorescence become significant.

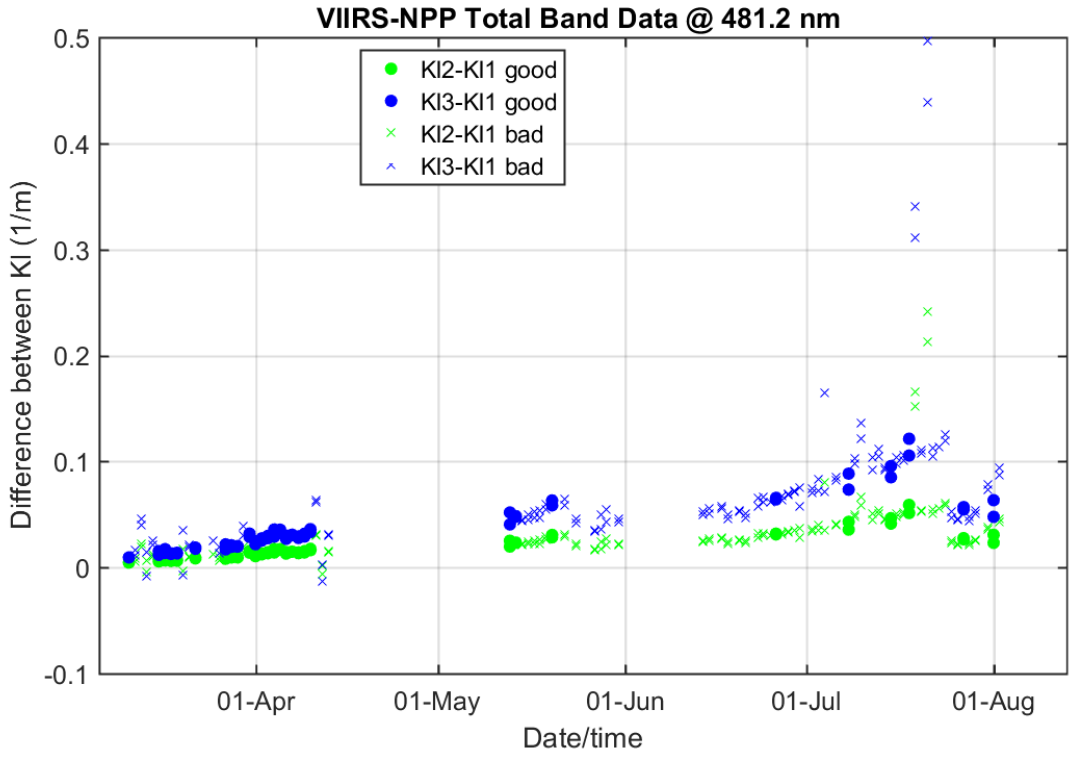

Figure 39) Differences in KL calculated with different arm pairs during deployment M262. KL1 is top and middle arm, KL2 is top and bottom arm, and KL3 is middle and bottom arm.

Figure 39 shows these differences for M262. Unfortunately by itself this does not tell you which arm is having trouble, looking at the individual KL's can help with this, as often one KL might go negative in this clear water. However even this can be misleading. During this

deployment KL1 appeared very low, indicating that either LuTop was low, or LuMid was high. KL3 appeared reasonable, which would indicate that LuMid and LuBot were fine. However, as seen in the post-calibration, LuTop was good, and both LuMid and LuBot changed. If the post-calibration data is considered, the predicted differences in these KL would be 0.04 for KL2-KL1, and 0.08 for KL3-KL1, a reasonable agreement with the values calculated below. So looking at this graph would indicate that the variation in calibration for the arms was probably a gradual process through the deployment.

A similar analysis for M263 can be done using these KL differences. Figure 40 shows this (note that there is a scale difference between M263 and M262) the variation was much smaller during this deployment when compared to M262.

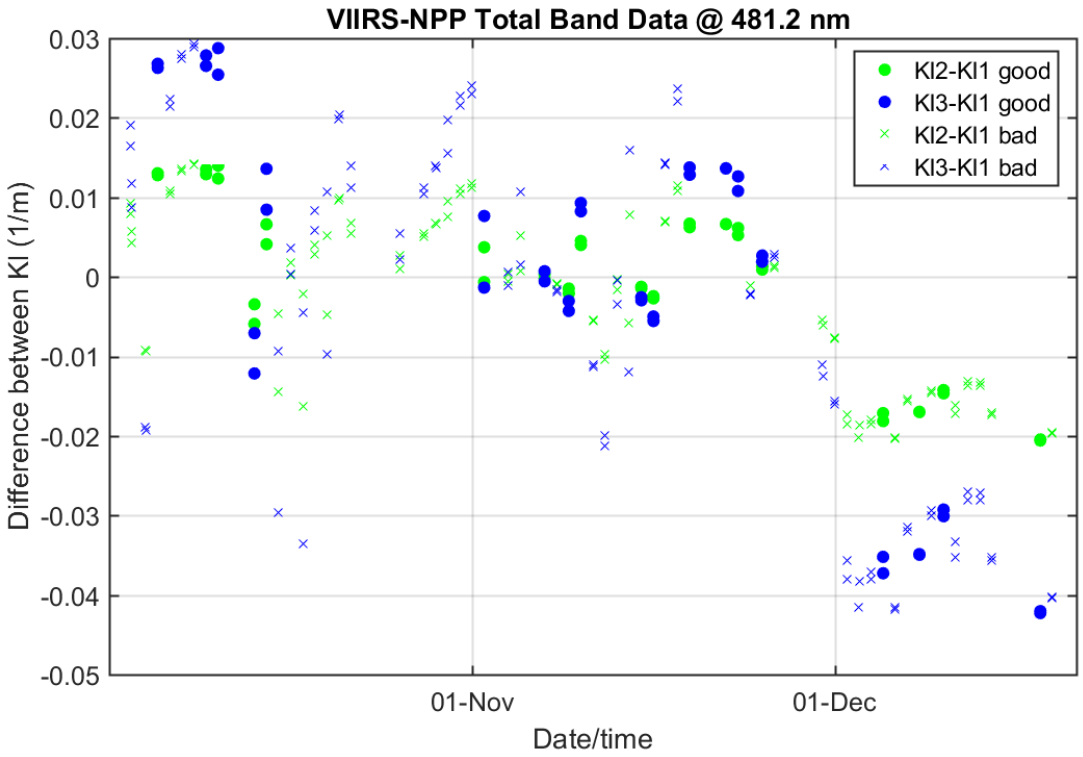

Figure 40) M263 KL differences, as in Fig. 39.

Obviously the difference between the KL's follow the same pattern. The KL3-KL1 will always be bigger in magnitude than KL2-Kl1, because KL3-KL1 uses 4 m arm separation for both factors, while KL2-KL1 has an 8 m arm separation for KL2 and a 4 m arm separation for KL1. In the calculation of KL, the 8 m arm separation reduces the effect of calibration by half. In any case, with both pairs decreasing, a common cause might be suspected, and as the post calibration showed, the top arm varied strongly between the pre/post calibration. Using a factor of 1.3 for the error in the top arm, the prediction for these differences would be KL2-KL1 = -0.04, and KL3-KL1 = -0.07. this is close to the value one would get if you looked at the overall change from the beginning of the deployment to the end of the deployment.

The final deployment to look at is M264, shown in Figure 41. Here if one looks at only the good days, the differences are stable between the KL pairs, indicating that the relative arm calibrations were stable. Applying the calibration difference found in the post calibration (1.12

for LuTop, 1.04 for LuMid and LuBot) results in the KL2-KL1 = -0.01, and KL3-KL1 = -0.02, about half of what was seen. So the post cal didn't capture the in-water differences. Actually if LuMid is increased by 8%, with LuTop and LuBot held stable, KL2-Kl1 and KL3-Kl1 go to approximately zero.

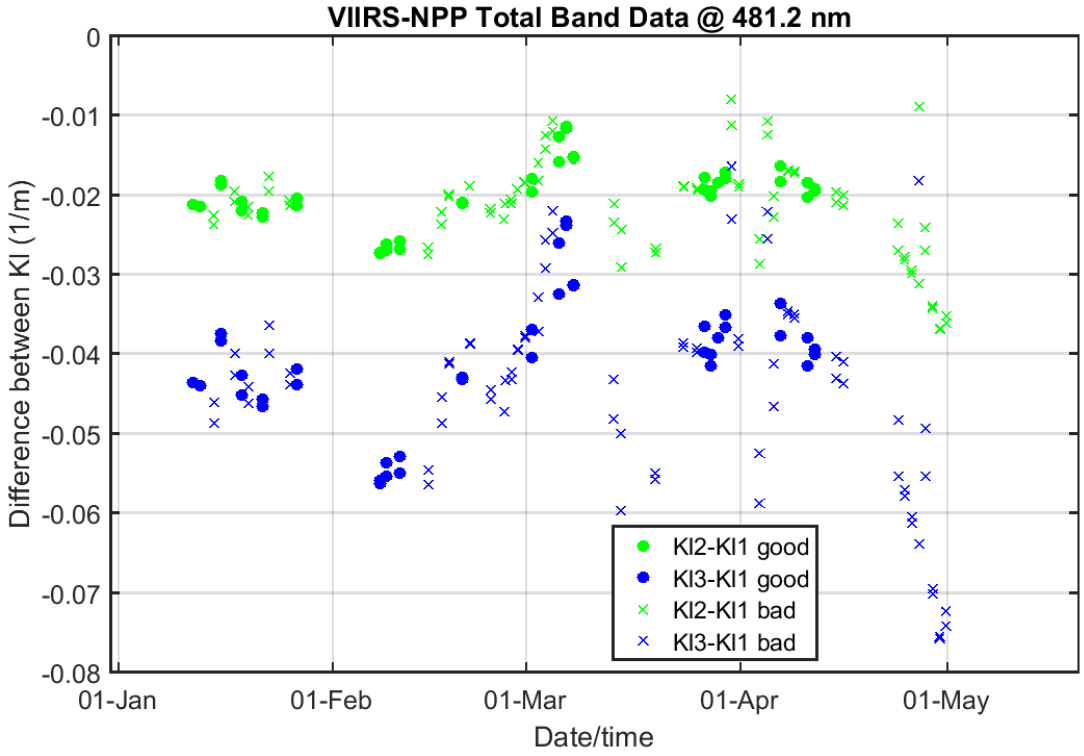

Figure 41) KL differences for M264, similar to Figures 39-40.

6c-3) Radiometric stability during deployment by vicarious calibration with MOBY-Heritage.

The next way that radiometric stability can be checked during deployment, in this time when we are running both instruments, is by doing a vicarious calibration of the blue spectrograph (BSG) sensors using the closest in time MOBY-Heritage measurement. This can then be tracked during the deployment, and also compared to the pre/post calibration responses. There will obviously be additional sources of variation due to the time differences in collection, combined instrument noise in MOBY and the BSG, and other environmental factors. However it is another way to get a handle on how the BSG performed during these three deployments.

So starting with M262 we calculated the system responses that would be obtained, through the deployment, on the "good days", best quality MOBY data. Figure 42 shows these for Es, while Figure 43 shows them for LuTop, Fig. 44 for LuMid, and Fig. 45 for LuBot. These figures provide some very interesting information.

The technique does not work as well for Es; there is greater scatter in the deployed responsivities vs the Lu results. While many of the vicariously calibrated system responses agreed well with the pre/post calibration there was much more spread in these values then the pre/post calibration had shown.

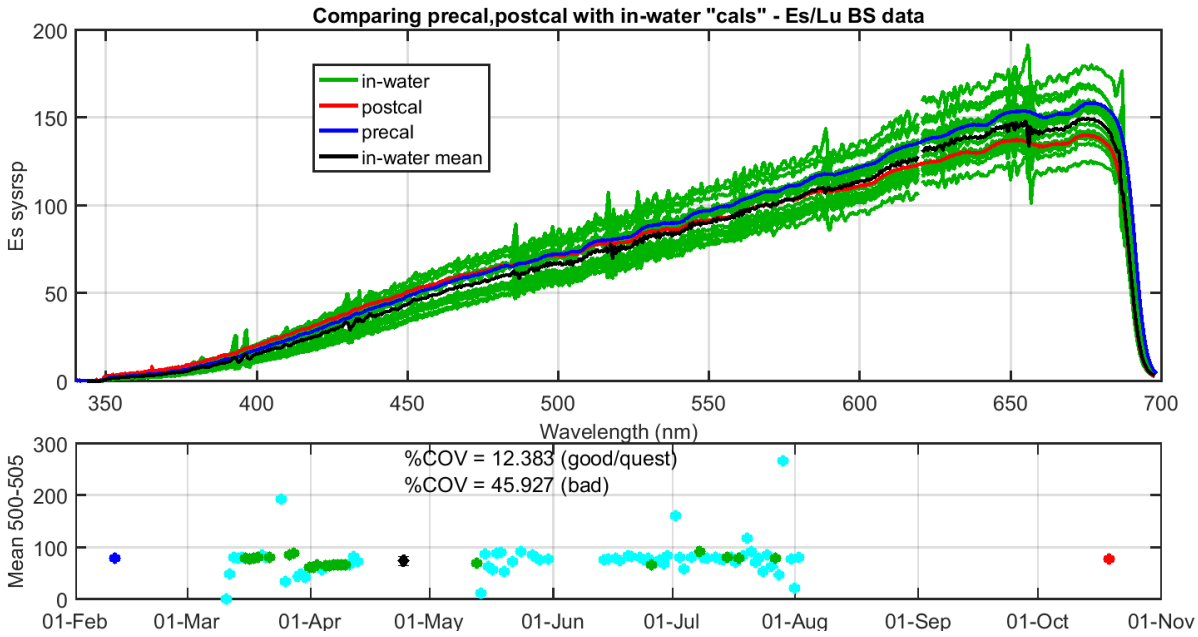

Figure 42) System response for Es during M262, along with the pre-post calibration derived system responses. The top figure shows the individual "good" days, the bottom graph shows the mean for wavelengths from 500 to 505 nm of the values shown above. The bottom graph includes both "good" days and questionable days (our next quality below good).

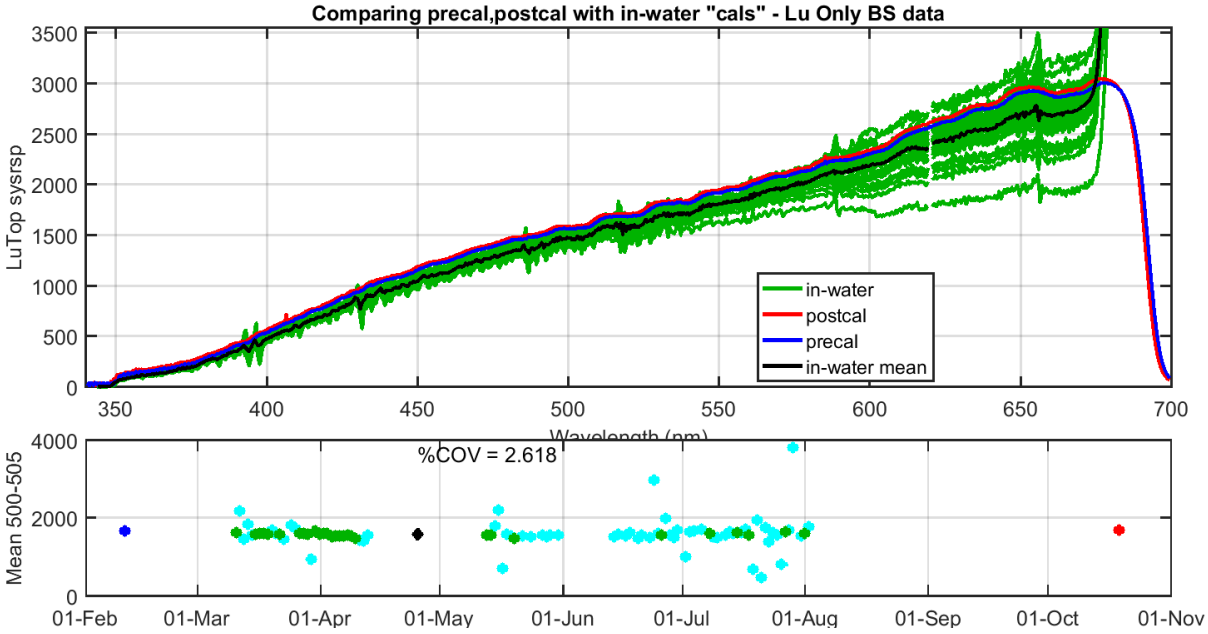

Figure 43) System responses vicariously determined by comparison with MOBY-Heritage during M262 for LuTop. The top graph shows the "good" days, the bottom graph shows these good days as green dots, while the blue dots are from "questionable" days. The bottom graph is for the average from 500-505 nm. The %COV is given for the "good" days.

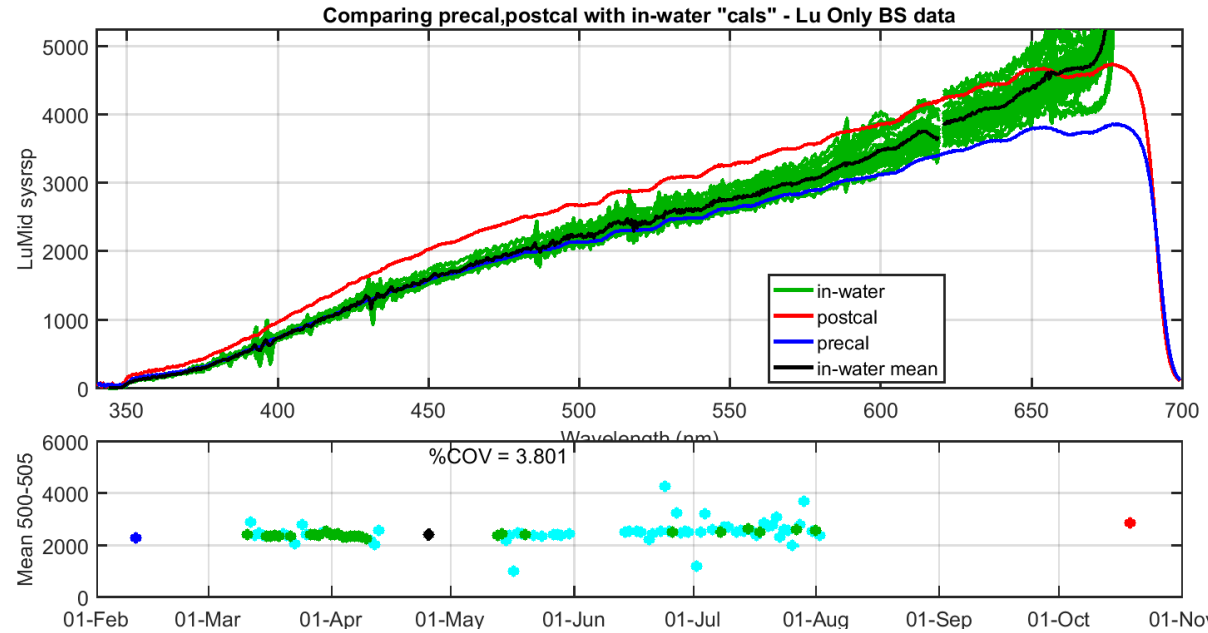

Figure 44) System responses vicariously determined by comparison with MOBY-Heritage during M262 for LuMid, otherwise similar to Fig. 43.

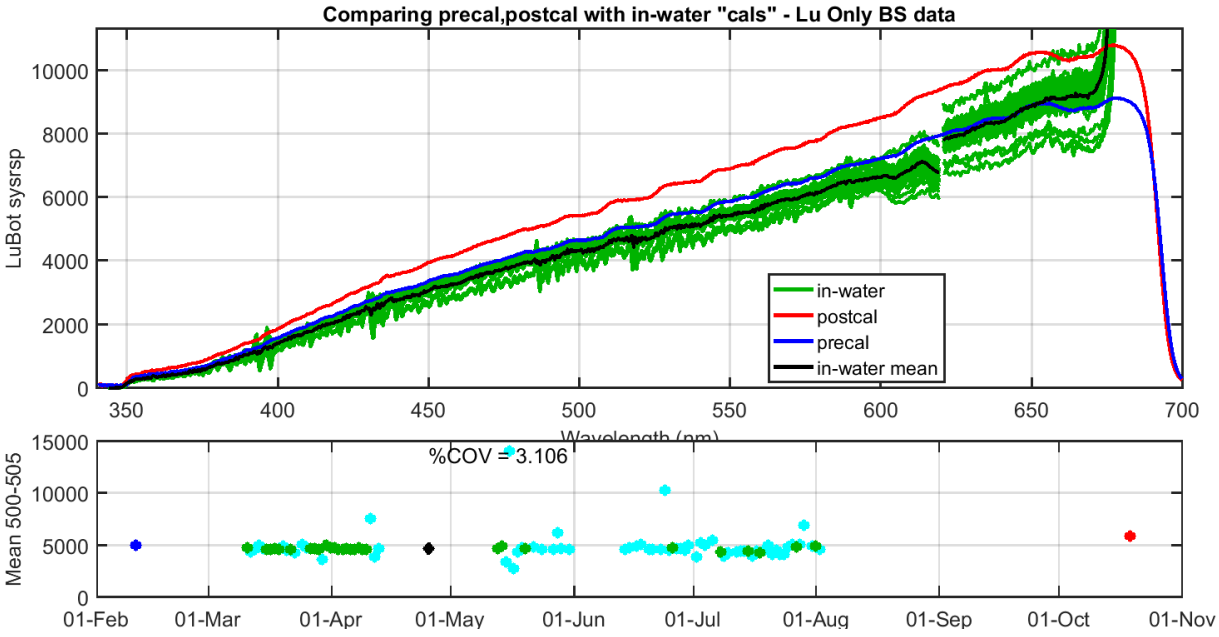

Figure 44) System responses vicariously determined by comparison with MOBY-Heritage during M262 for LuBot, otherwise similar to Fig. 43.

For the Lu measurements, the variation in these vicariously derived system responses is much smaller than for Es. For LuTop the derived system responses are almost exactly the same as the pre/post calibrations. The %COV for the average system response at 500-505 nm over the deployment is very small (2.6%), particularly considering that there will be environmental noise factors introduced in this average. In this example it validates the pre/post calibrations and their stability. LuMid and LuBot are interesting in that the %COV of the vicarious responses are

small, 3.8 and 3.1 respectively, but also the derived responses are much closer to the pre-calibration than the post calibration. M262 was taken out of the water in August, so there was a long period while the instrument was on shore, before the Lu post cal data was taken on October 19. Using the average vicarious calibration response at 500 nm, the correction of the KL differences can be calculated and they are KL2-KL1 = 0.02, and KL3-KL1 = 0.03. The first is close to the average seen during the deployment (Fig. 39), the second of these is smaller than might be expected, but it is important to note that the majority of the "good" points occurred early in the deployment, where the KL differences were smaller. So the two methods would agree with each other. This also shows the difficulty in figuring out which arm calibration is in error by just the KL differences alone. The pre/post calibration data and the vicarious system responses indicate quite different changes during the deployment, yet both can predict KL differences that agree with the data. The KL differences are very good at tracking stability, but not as useful to point out what the calibration error is.

The same 4 graphs but for deployment M263 are shown in Figures 45-48. Once again the Es vicarious calibration is very noisy, while the Lu responses are much closer to each other.

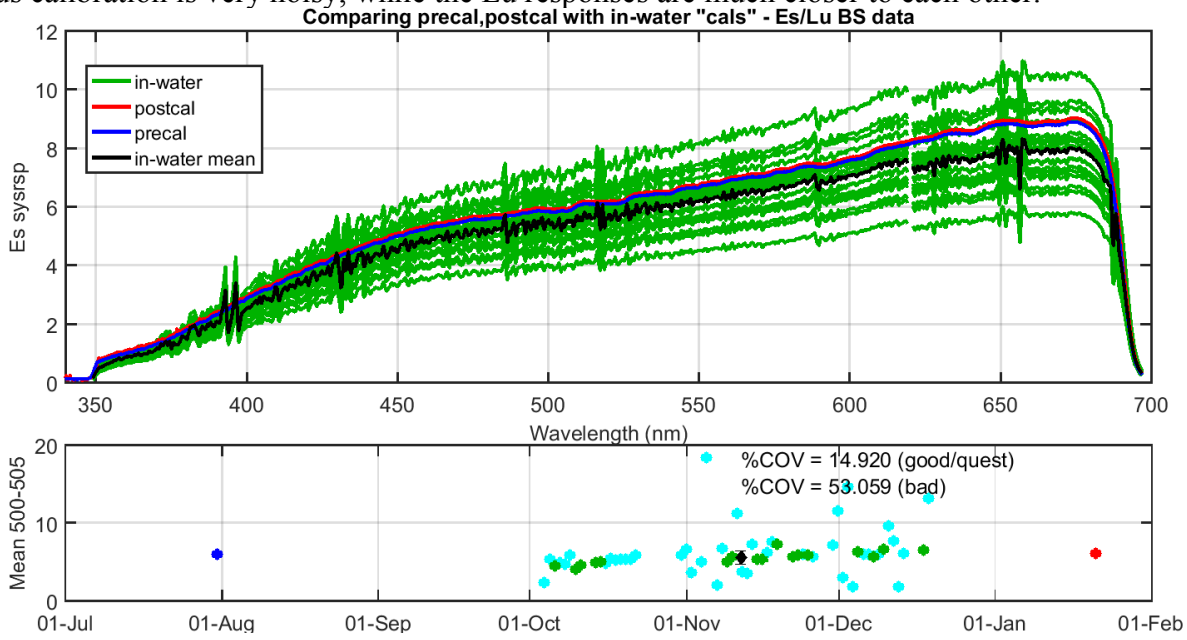

Figure 45) System responses vicariously determined by comparison with MOBY-Heritage during M263 for Es, otherwise similar to Fig. 43.

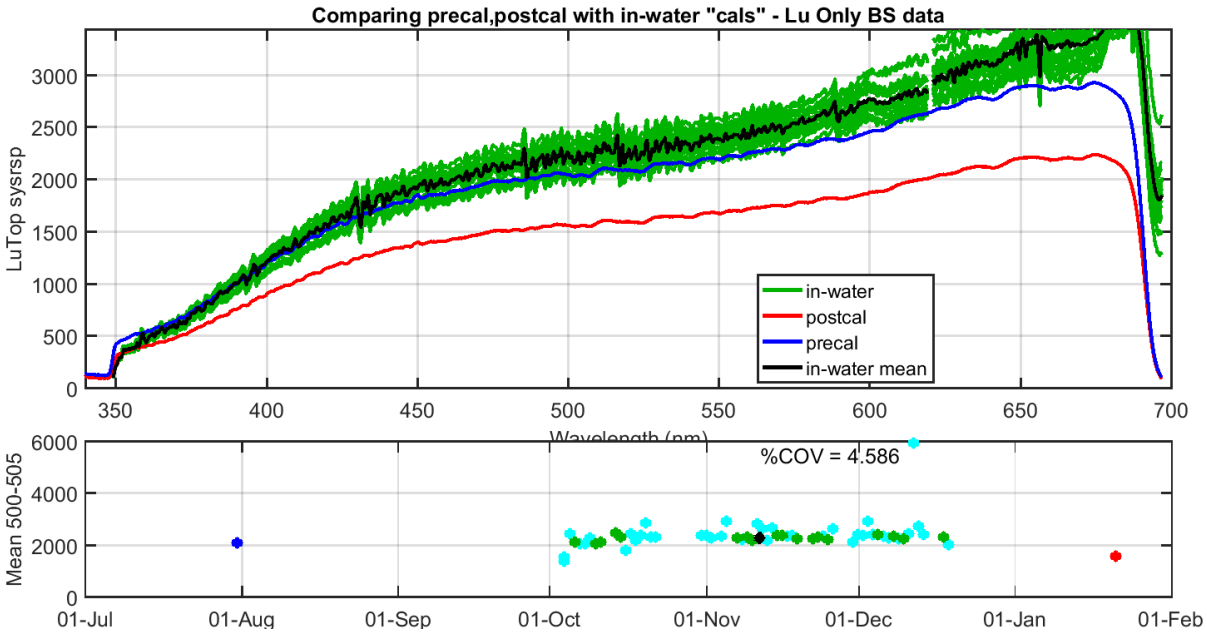

Figure 46) System responses vicariously determined by comparison with MOBY-Heritage during M263 for LuTop, otherwise similar to Fig. 43.

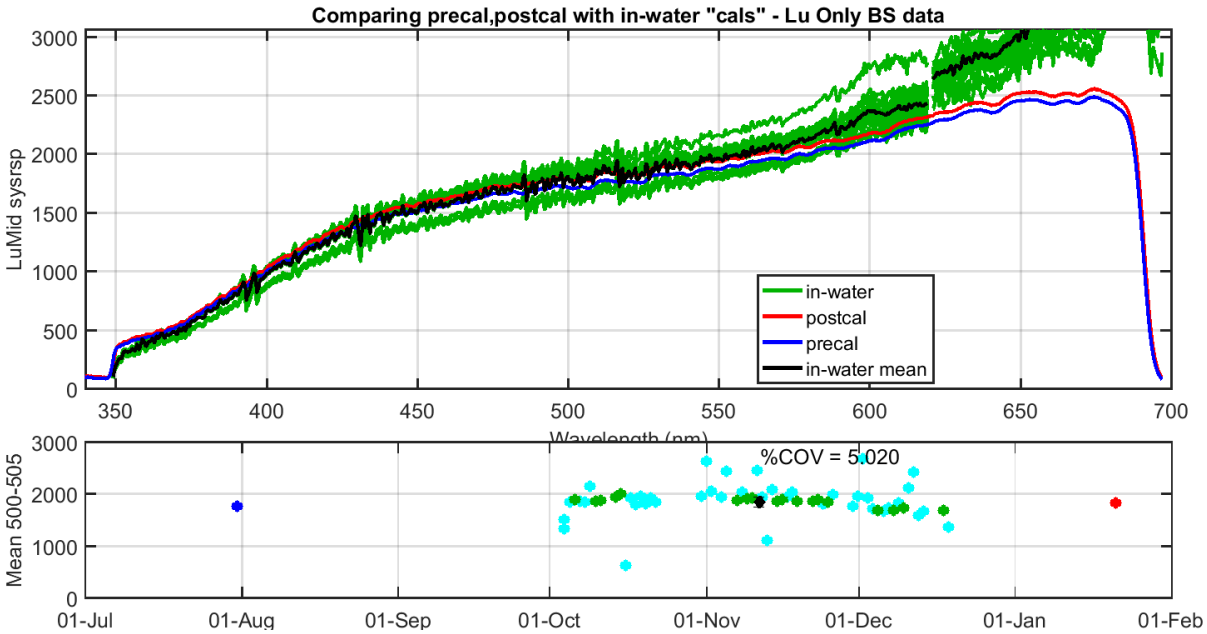

Figure 47) System responses vicariously determined by comparison with MOBY-Heritage during M263 for LuMid, otherwise similar to Fig. 43.

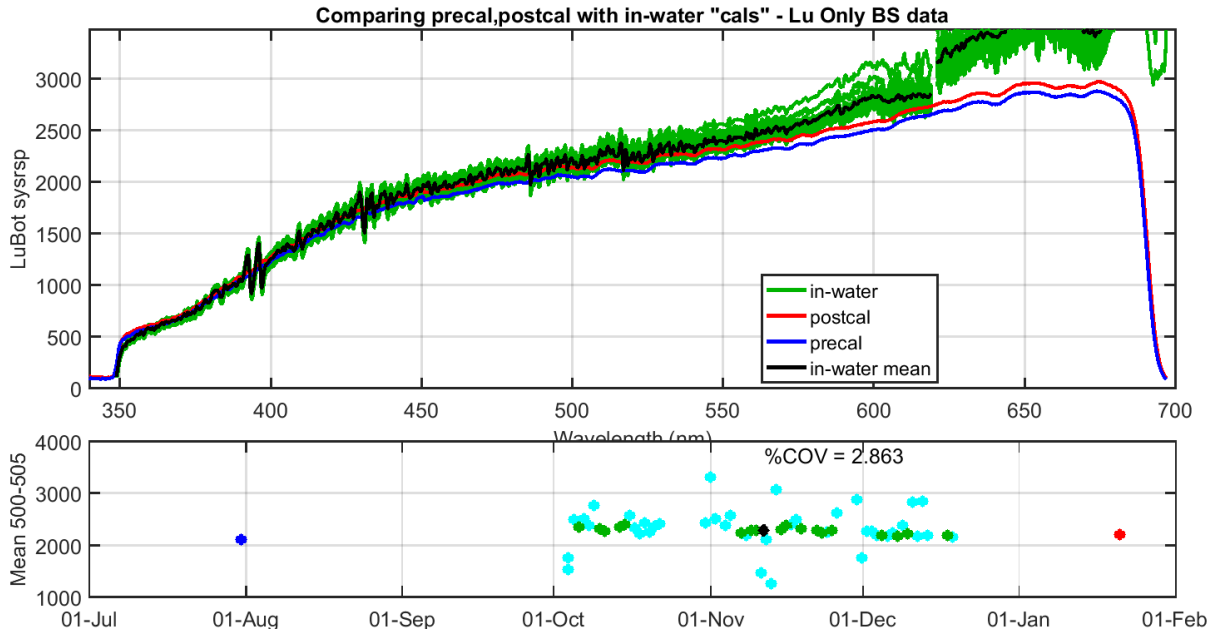

Figure 48) System responses vicariously determined by comparison with MOBY-Heritage during M263 for LuBot, otherwise similar to Fig. 43.

For LuTop, the in-situ data is fairly close to the pre-calibration response and the %COV was 4.5%, larger than the other cases, but still not as large as the difference between the pre and post calibration. The post calibration is definitely the system response that is out of family with the rest. This would reinforce the idea that whatever happened to the top arm to cause the large variation in system responses pre/post happened during recovery and not during the deployment.

The average LuMid vicarious system response was very close to the pre calibration system responses, while LuBot was closer to the post-calibration system response. But both of these were within 5% or so at 500 nm. Note that the discontinuity between 600 and 650 nm for LuMid and LuBot vicarious system responses is caused by a discontinuity in the MOBY LuMid and LuBot at the blue/red overlap region where the data is switching from the blue spectrometer to the red spectrometer in MOBY.

For this deployment, these results agree with the KL difference test, as on average the KL differences were very small, and these average vicarious system responses agree with the pre-calibration data reasonably well.

The last deployment to look at in this fashion is M264, shown in Figures 49-52. Es is the most interesting case here. While the pre/post calibration agreed very well, the agreement between these system responses and the vicarious one done in the field is very bad, almost a factor of 2. The suspicion is that the very small iris, installed in the Es channel to decrease its signal to be closer to the Lu signals, caused the system to be very sensitive to alignment, and movement. Using the instrument horizontally (as it is calibrated) versus vertical, while in the field may have caused this problem. We should note that this did not happen with any of the other systems, as shown above, so maybe it is just a loose part in the system.

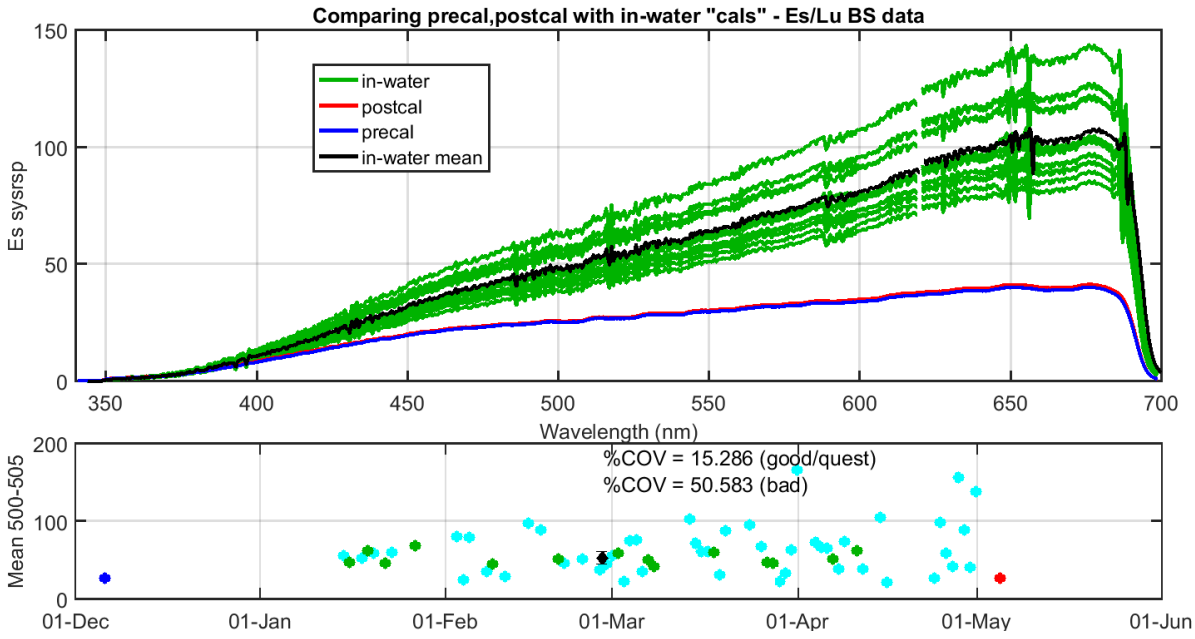

Figure 49) System responses vicariously determined by comparison with MOBY-Heritage during M264 for Es, otherwise similar to Fig. 43.

For LuTop the pre-calibration system response agreed with the vicarious calibration response much better than with the post calibration system response. Thus the 10% difference between pre/post calibrations is probably in the post calibration or something that happened after the deployment, rather than while in the field. Note that in all of these cases the %COV is much larger than in deployments M262 and M263, and maybe driven in part by the one very different system response derived on a "good" day.

LuMid looks almost perfect between the Pre/post calibration and the vicarious calibration system response, at least up to 575 nm. Note that we have not done an SLC and this data has not been corrected for cross-track error, both of which may start getting important above 575nm. For that matter we have also not corrected for 2nd order light, but that probably is not a problem until 600 nm or higher.

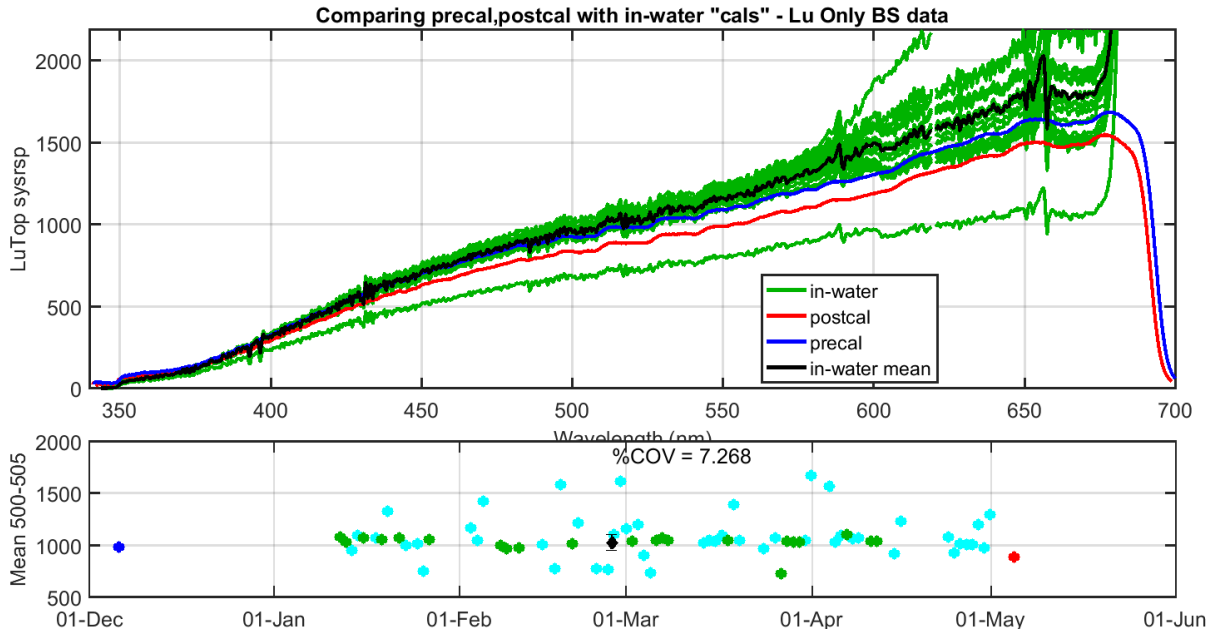

Figure 50) System responses vicariously determined by comparison with MOBY-Heritage during M264 for LuTop, otherwise similar to Fig. 43.

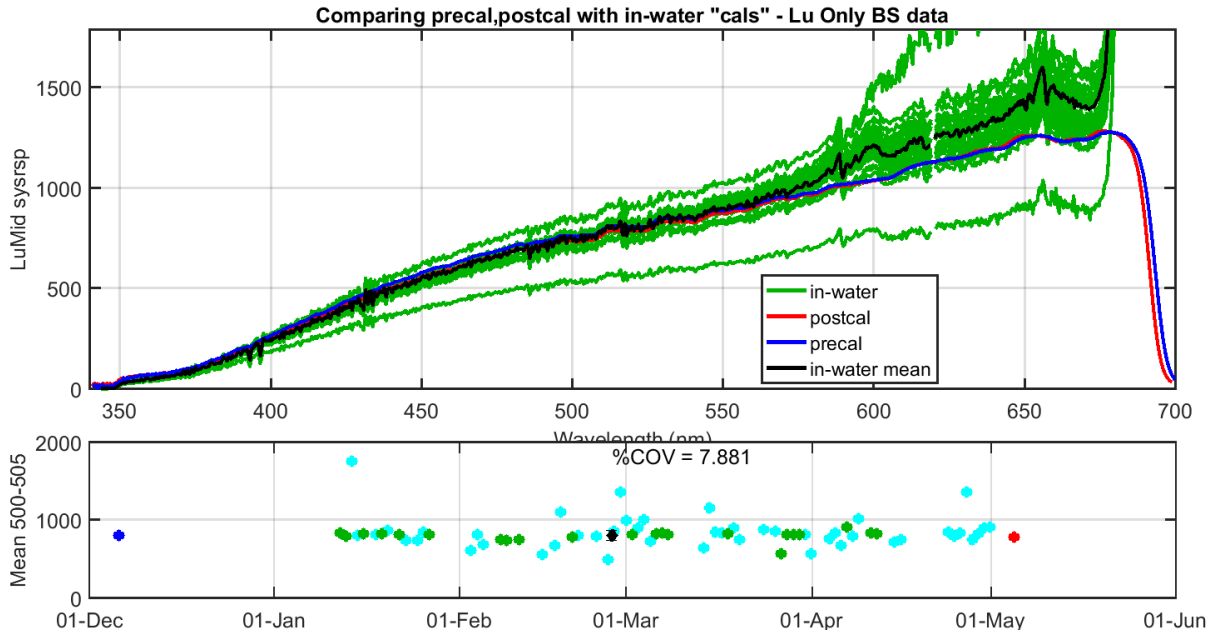

Figure 51) System responses vicariously determined by comparison with MOBY-Heritage during M264 for LuMid, otherwise similar to Fig. 43.

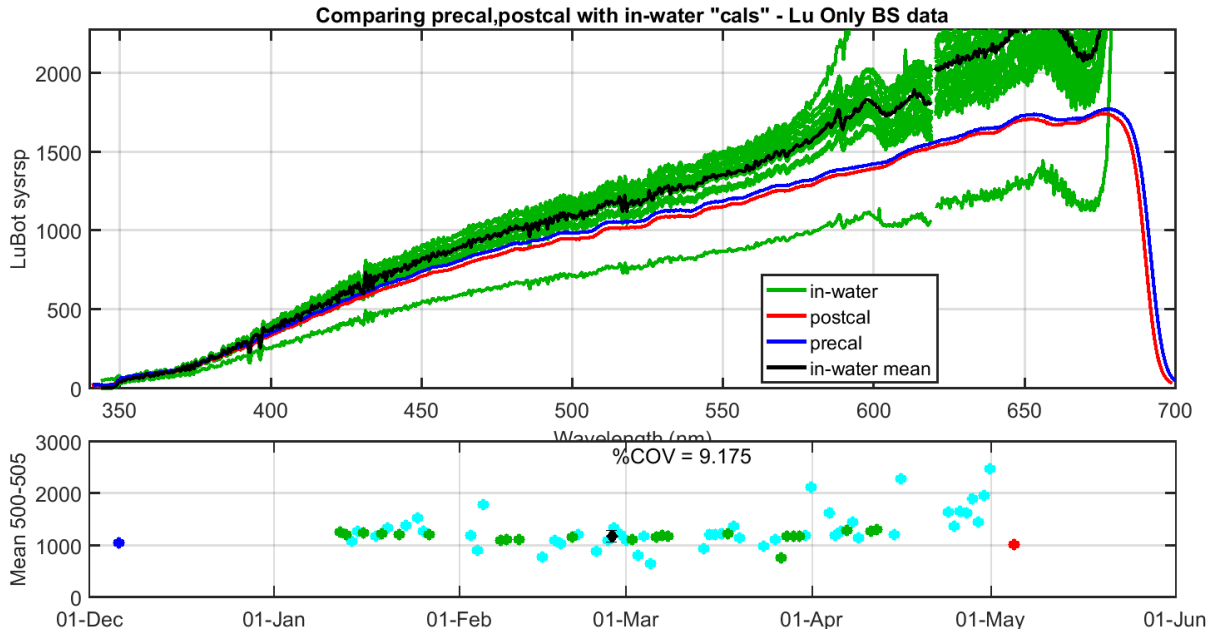

Figure 52) System responses vicariously determined by comparison with MOBY-Heritage during M264 for LuBot, otherwise similar to Fig. 43.

7) Data acquisition tests

While the system has been in the field we have done many different tests on how to optimize the acquisition strategy, the best way to reduce the data, and other issues that affect data quality. Since this system allows simultaneous acquisition of the different environmental channels we have been testing acquiring Es and Lu's simultaneously vs the Lu's without Es. While we can get higher signal levels for the Lu's if done without Es because we can have longer integration times, we have not found a significant difference between Lu's acquired in either manner.

Because we can get Es and Lu's simultaneously, it opens the door to much more averaging of individual data sets then with MOBY which takes much longer to acquire a data set. To determine the best averaging technique, a 100 pt. test was performed and will be described below. While we did several other experiments on data acquisition, in this report I will focus on this example.

We also looked at how we may be able to correct for cross track contamination, meaning light from one track interfering with a neighboring track. This test will also be described.

7a) 100 point acquisition tests

For approximately 60 days we did a test where we took 100 data samples, each with 2 second integration time, as quickly as possible. The time between the acquisitions was 5 seconds, so the whole test took approximately 500 seconds, or around 10 minutes, with dark acquisitions. The results can be divided into two categories, high wind and low wind data sets. In the following, the wind in the high wind case was 11 m/s, while it was 1.7 m/s in the low wind case. The first parameter to look at is the % standard deviation for these data sets, shown in Fig. 53 and Fig. 54.

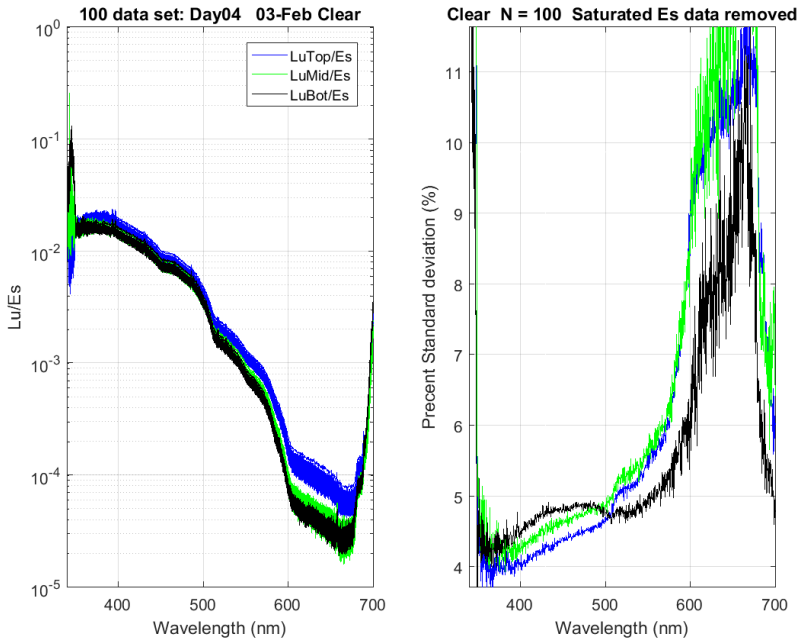

Figure 53) Low wind case (1.7 m/s) with upwelling radiance spectra shown on the left, and standard deviation of these shown on the right.

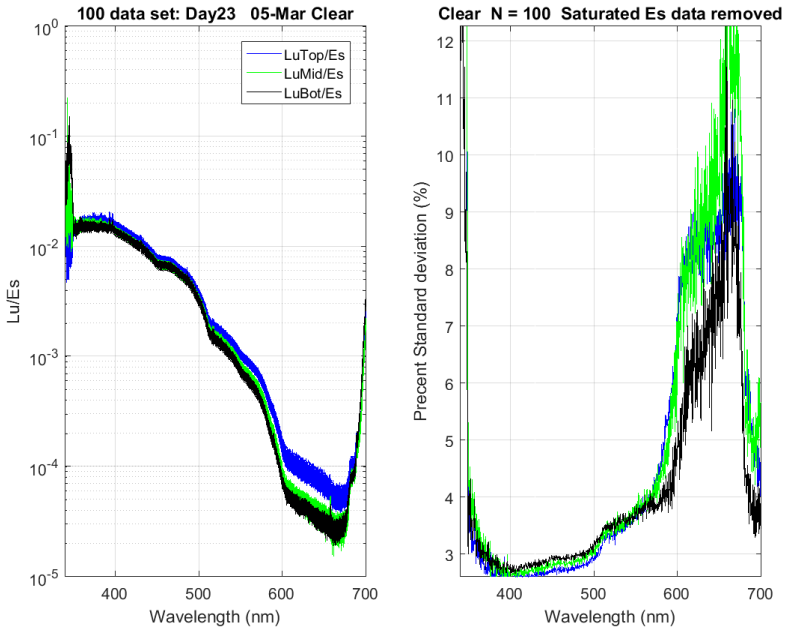

Figure 54) High wind case (11 m/s) with upwelling radiance spectra shown on the left, and standard deviation of these shown on the right.

The differences between these two cases is typical of the overall data set. When there is low wind, the % standard deviation is larger than the high wind case. This is probably caused by the wave field being much more disturbed in the high wind case, so the light field is more homogenized and there is less wave focusing. We have seen the same thing in our radiance

distribution measurements; wave focusing is much more intense when the wind is light. The impact here is that in light wind measurements, it is important that a significant number of samples are acquired to average for an accurate mean.

The next thing to look at is how normally distributed the samples are. We look at that by looking at the difference between the median and the mean (shown in Figure 55).

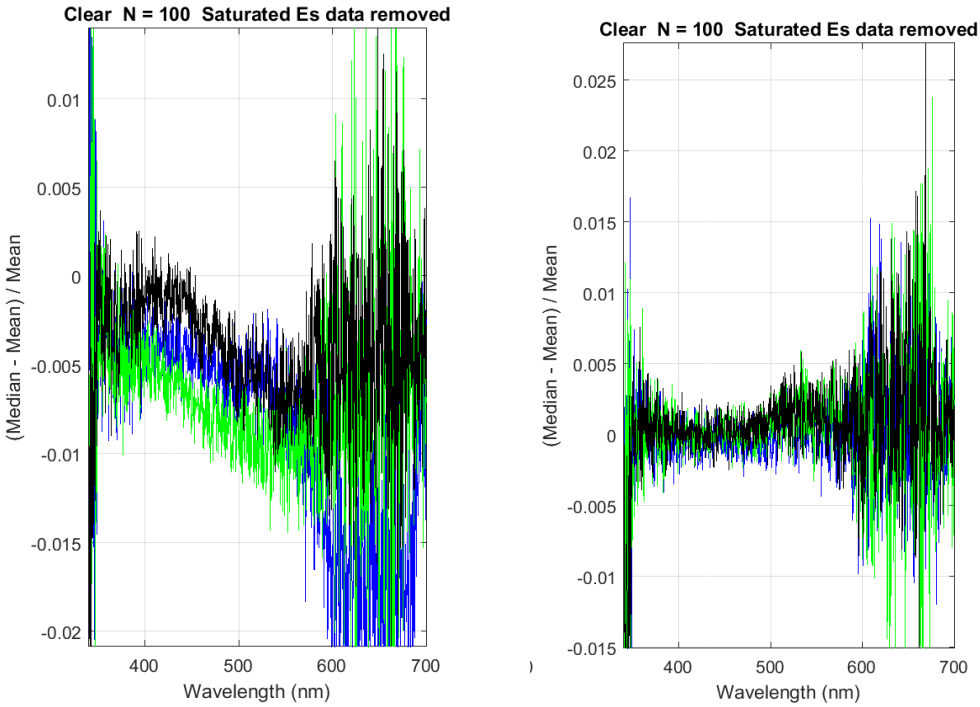

Figure 55) the normalized difference between the median and the mean for low wind (left panel) and high wind (right panel).

As can be seen in Fig. 55, while there is no difference between the median and the main in high wind cases, in low wind cases there is a slight difference, with the mean slightly higher than the median. Given that the application is to replicate what a satellite might see by averaging over a large area of the surface, the mean is probably still the quantity that should be used.

When averaging it is important to make sure that the average is being taken over a long enough period truly capture the average value. In Fig 56 we show the autocorrelation of the data sets at one wavelength (near 500 nm). As was typical for the low wind cases, there are peaks in the profile at lags corresponding to 90 s, while in high wind cases these peaks did not exist. These peaks are probably due to a combination of the wave surface and the motion the MOBY buoy is moving through. This would indicate that when averaging data, the data should be averaged over a time greater than 90s, so that whole cycles are captured.

To do the averaging either many samples can be averaged or longer integration times can be used. In the highwind case, it should be equivalent, in the low wind case one has to make sure that the samples are over a long enough time to cover several periods of these oscillations. The 100 point, 2 second samples are roughly equivalent to sampling for a 3 minute integration time, or 5 samples at 40 second integration times. Historically MOBY has averaged 5 samples at 30-60 s integration time; with the new system we should be trying to average at least this long,

either thorugh many samples at shorter integration times or fewer samples with longer integration times. But the goal should be equivalent exposures of, on the order, 3-5 minutes.

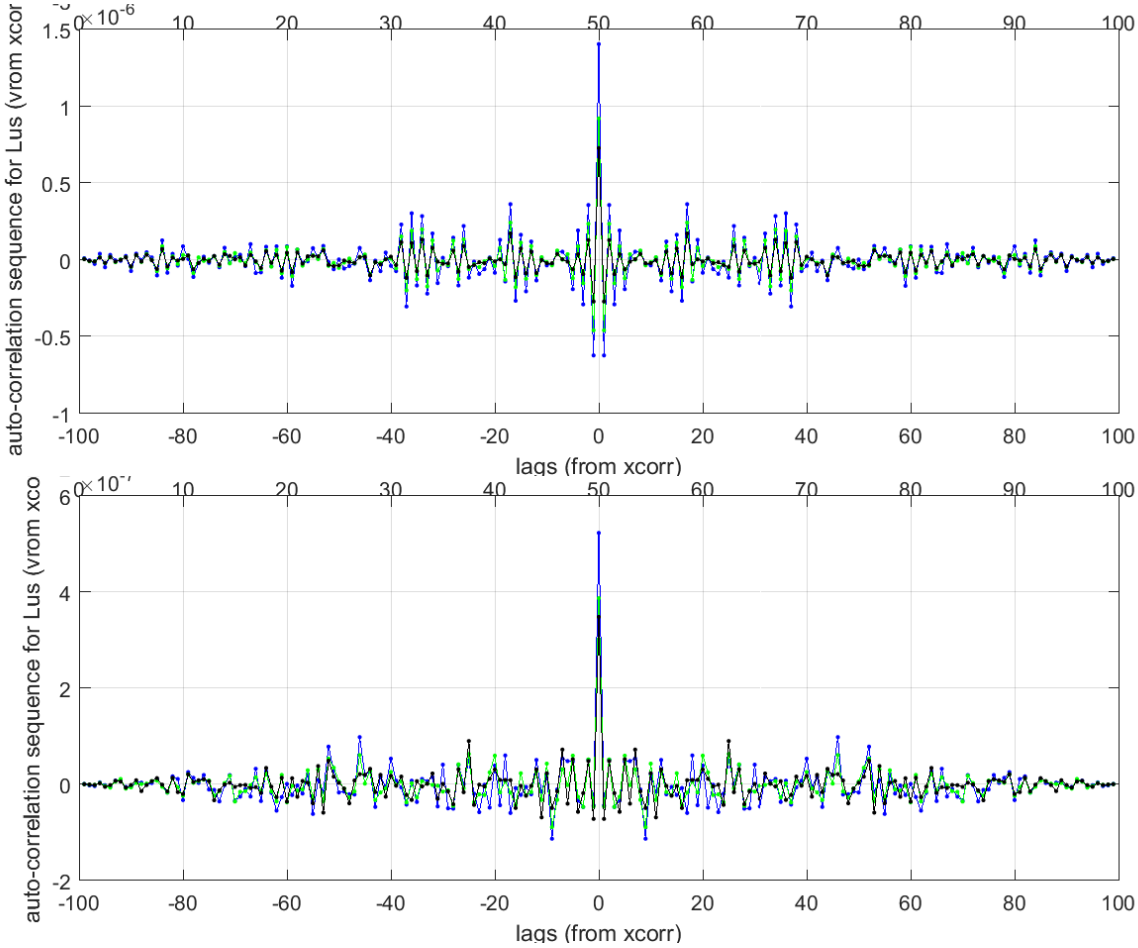

Figure 56) Top figure is autocorrelation for low wind case, lower is autocorrelation for high wind case.

7b) Cross track correction test

As previously stated, the volume phase holographic gratings in our system have very good imaging qualities, so low spectral straylight and low scattering in the track direction. But the dynamic range of the radiance field in the water is very large, the difference between the Es and Lu spectra is large (particularly in the red wavelengths), and the intensity, even after some pre-leveling, of the signal between Es and Lu's can be large. So we will probably have to do some sort of straylight correction, following our work on MOBY, and also a cross track correction.

To give an example of the straylight in the system, in Fig. 57 we show an example where laser light is captured with the system. To really capture the straylight above the noise, it is necessary to take several images starting with the central laser line and ending where the central laser line has been saturated, but the extent of the straylight away from the central line is captured correctly. In Fig. 57, the blue is the case where the central line has been captured but away from this line is just background noise, the orange line represents the true straylight

situation, when the center line has been saturated. As can be seen the spectral straylight is very low.

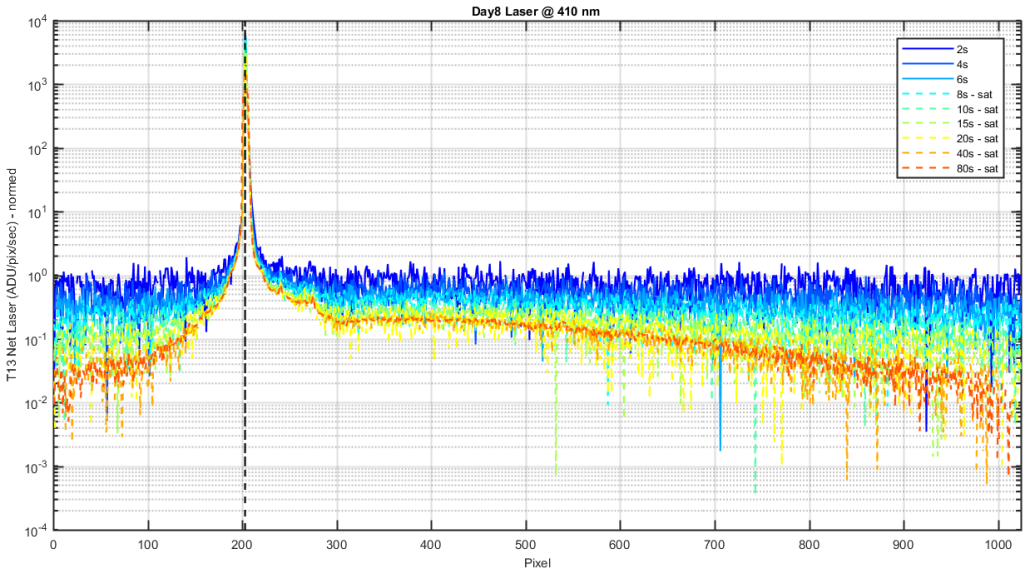

Figure 57) a laser straylight characterization.

To look at cross track contamination, we did an experiment in the field, where one track at a time was exposed at a time and we found how much signal was scattered into the other measurement tracks. The data can be made into the matrix shown in Fig. 58. In this matrix, each column is a different track that has been exposed, column 1 is exposing track 2, Es. Each row represents the light that has gone into a different track. For example the 3rd column, 2nd row is light that has gotten into the 2nd measurement track (track 6 in this case) when the 3rd measurement track is exposed (track 9 in this case). Each element is normalized by the signal in the exposed track, so the diagonal elements are all 1. The horizontal axis in each matrix element graph is pixel location from low wavelengths to high wavelengths. This system had a camera with parallel windows, as it was put into the field before we knew of the problem, hence the UV-ghosting, discussed earlier, is evident at low pixel numbers.

We effectively inverted this matrix. Multiplying an input data file, a column vector where the elements are track 2, track 6, track 9, and track 13, by this inverted matrix effectively gives us the corrected data. An example of using this technique on a sample data set is shown in Fig. 59. The correction barely changes the Es channel, as this is the brightest channel. However there are significant differences towards the red side of the data in the Lu tracks (Track 6, 9, and 13), where the upwelling light is small, but large in Es. The blue line gives an indication of how much correction has been made, and in general it is small, but still important in the red wavelengths. Fortunately the accuracy of this correction can be monitored using the red spectrograph, which will overlap this part of the spectrum.

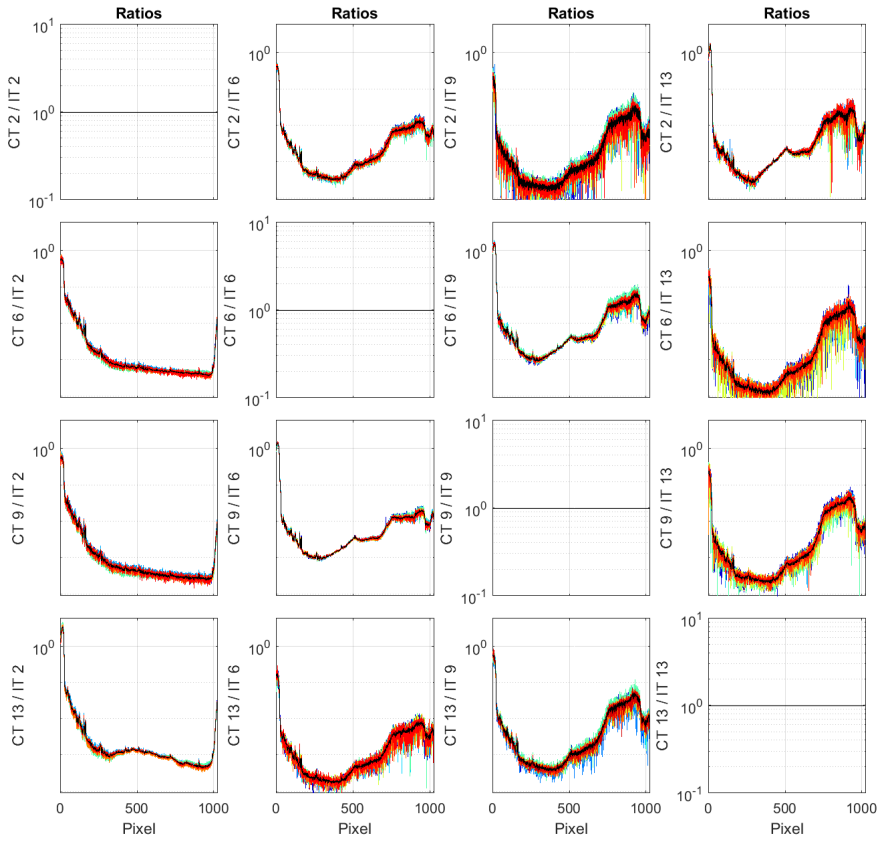

Figure 58) Example data matrix for cross track

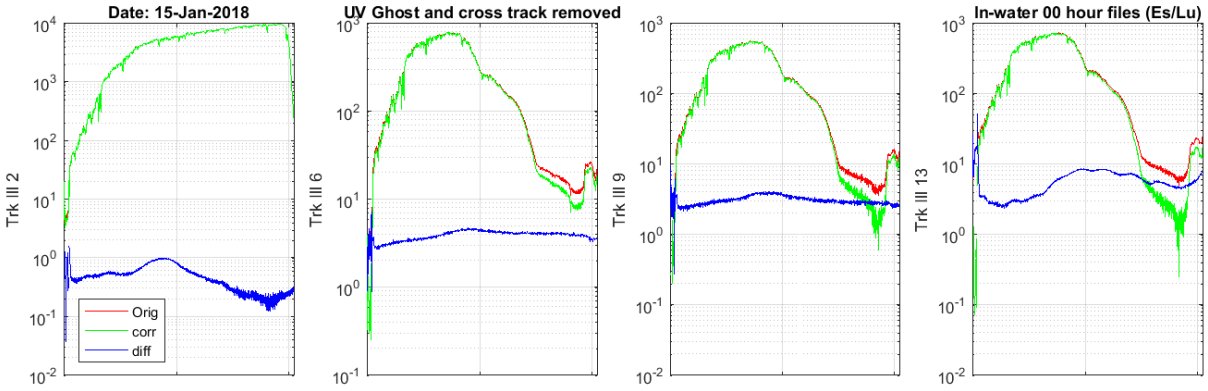

Figure 59) corrected data set, showing the original data (red), corrected data (green) and difference (blue).

7c) Coiling test

We also did an experiment, relevant to MOBY-Net, where we coiled and uncoiled a fiber to see how the fiber throughput changed. This is important as the fibers in the MOBY-Net system will have to be coiled to be transported back to the calibration facility for recalibration. Figure 60 shows the result of this test. In this test the fiber was coiled onto a spool and 10 measurements were made of the thru-put. Then the fiber was uncoiled, coiled, uncoiled, coiled,

and uncoiled. The data points near 1:10, 1:35, and 2:00 are the uncoiled points, and the signal measured was constant to within 2%. This would indicate that we will need to uncoil the fiber to do the calibration, but with care to set up on a jig similar to the MOBY structure, we should be able to uncoil the shipped fiber and get a repeatable calibration. Note that there was no special care taken with the uncoiled fiber in this case, yet the measurement was repeatable within 2%.

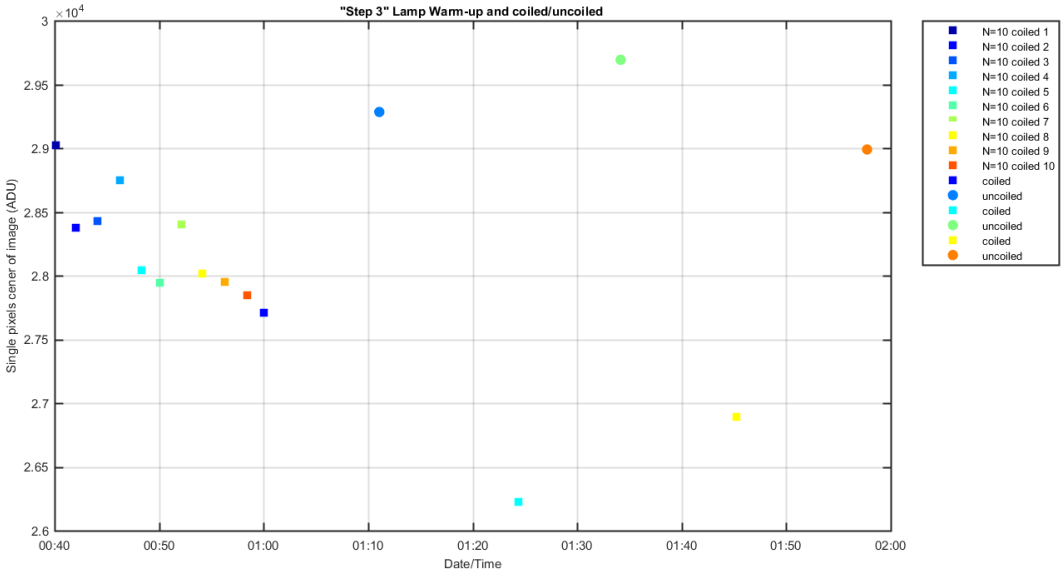

Figure 60) Coiling and uncoiling test on thru-put of the fiber.

8) Stability source system

The unique feature in MOBY-NET is the optical system is removed intact from the supporting buoy and shipped back to a central calibration facility (CCF), refurbished and recalibrated, and shipped back to the host site. The Stability System is a source and radiometer that is transported with the MOBY-NET optical system to verify its radiometric performance during these operations. The objective is to quantify changes in the irradiance and radiance system level responsivities during all phases, except for the in situ, in water deployment of MOBY-NET. The goal is to identify changes at the 1% level so that the stability of the MOBY-NET responsivities does not dominate the overall uncertainty budget for the in situ Lw and Es values. The method we selected was to adapt a commercial stability source and fiber-coupled hyperspectral spectrograph and characterize them separately and as a system. The source is the Satellite Quality Monitor (SQM = OCS-5002 S/N 103) from Yankee Environmental Systems, Inc. (YES) and the spectroradiometer is a CAS140CT-156 ("MOBY CAS") from Instrument Systems, Konica Minolta Group. The SQM has three internal monitor photodiodes for tracking radiometric stability, and the CAS provides redundancy by repeat measurements viewing the SQM output in the same manner as the MOBY-NET optical heads would.

With the host site in operation, the proposed sequence of events is:

1. Retrieve MOBY-NET buoy from host site in water location;
2. At the host site, measure the SQM with MOBY-NET and the CAS;

3. Remove the MOBY-NET optical system from the buoy and measure the SQM with MOBY-NET optical system (option to take additional data with the CAS);
4. Ship the MOBY-NET optical system and the Stability System to the CCF;
5. Measure the SQM with MOBY-NET optical system and the CAS;
6. Perform all post-deployment activities as are currently done with MOBY (post calibration, selected characterizations, necessary refurbishments);
7. Option: CAS measure the MOBY radiometric reference standards and/or MOBY (if available) measures SQM;
8. Perform pre-deployment calibration on MOBY-NET optical system,
9. Measure the SQM with MOBY-NET optical system and the CAS;
10. Ship the MOBY-NET optical system and the Stability System to the host facility;
11. At the host site, measure the SQM with MOBY-NET optical system and the CAS;
12. Install the MOBY-NET optical system on the buoy;
13. Deploy the new MOBY-NET buoy.

SQM

The SQM is a commercialization of the SeaWiFS Quality Monitor (Johnson, Shaw et al. 1998) that was used after minor modifications at SIRREX-5 and on the Atlantic Meridional Transect cruises 3 to 7 where it quantified the short term repeatability of ocean radiometers within 1% (Hooker and Aiken 1998). NASA's supported commercial development, resulting in the SQM-II (Satlantic) and the OCS-5002 aka SQM (YES). They were used in SIRREX-7 and the SIMBIOS project. Meister reported the time series of the YES SQM over a six year interval for the internal monitor photodiodes and external measurements using the SXR-II and observed the short term trending (several months) showed agreement in the trends at the 0.5% level, which increased to 2% over the six year study (Meister, Fargion et al. 2009).

We selected the YES SQM for this study. There are two lamp sets, 8 lamps in each set, for three different flux levels. Three internal, temperature-regulated, monitor detectors record the flux levels. Two have filters for the blue and red spectral region and the third is unfiltered ("blue," "red," "white"). A 23.8 cm diameter transmitting acrylic diffuser forms the exit aperture of the SQM. The source chamber is cylindrical in shape, with the diffuser on one end and the internally-mounted lamps and monitor photodiodes on the other end, facing the diffuser, see Fig. SS1. The walls are bead blasted aluminum. The two lamp rings are at the outer circumference and the three monitor photodiodes are centrally located and view the center of the back side of the diffuser. An adaptor plate with a 10.48 cm diameter hole and alignment pins forms the interface to the Device Under Test (DUT). The lamps are operated in constant current with a thermally stabilized regulation circuit. The thermal control systems can be operated prior to turning on the lamps to minimize warm up time. The control of the lamp currents, the pre-heater, and the cooling are automated using the internal 6812 microprocessor running FORTH. The SQM can be operated stand alone; in this case the operator observes the output data on a display panel. Or, these data are logged using the RS232 interface. A rotary knob selects the mode (off, pre-heat, LO, MED, HI) where LO is the 1A lamp set, MED is the 3A lamp set, and HI is both lamp sets. There is no AC off switch; when the SQM is connected to AC power, data can be recorded in the "off" position. The overall dimensions, including the handles, are 41 cm diameter by 76 cm length, and it weighs 46 kg. The stated operational temperatures are -30°C to +34°C

with input power of 115/230 VAC at 50/60 Hz. There are three supports mounted to the SQM cylinder housing with ¼-20 clearance holes for mounting to a standard (English) 1" bolt pattern.

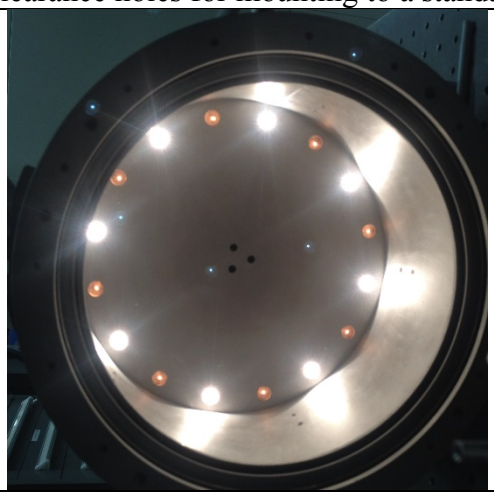

Figure SS1. SQM light chamber with the window and diffuser removed. One lamp set is fully on and the other is warming up. The three holes in the center of the back plate correspond to the monitor photodiodes.

SQM Software

The software delivered with the SQM was inoperable. It was compatible with Win 95 or NT operating systems, which were obsolete and no longer available on NIST computers. YES supplied the LABVIEW logging software as an executable, which functioned in "strip chart recorder" mode but this was also an obsolete version. NIST then acquired the original software from YES and converted the obsolete version in LabVIEW, tested the updated YES version and reformulated the YES logging software into an analogous YES version in LabVIEW 2015, so we could begin testing. Minor changes were made, such as updating the parsing VI, reworking the serial VISA, and using a USB to serial interface. During this initial phase, we performed tests, such as to identify which of the output signals corresponded to the red monitor. The YES manual was inadequate in this regard and fails to identify one of the four temperature readings.

Operations with the SQM and CAS will be performed by personnel with differing degrees of familiarity and training. Anticipating this, and the generation of many data files, we designed and implemented a protocol that accounts for, as much as possible, human engineering and automated processing. The elements are log sheets, a master bound lab notebook, an event log Excel workbook, LabVIEW 2017 data acquisition (DAQ) software, and MATLAB codes for implementing automated analysis in the MLML data base structure (MLdbase) that is used for MOBY.

- The logsheets allow for a manual record of metadata and operating parameters, as well as a place for experimental diagrams. Times of SQM status changes and DUT observations are recorded. The DUT filename and its parameters (e.g. integration time, OD filter, etc.) are recorded. Comments are recorded as appropriate, for example, noting any corrections needed for the data file.
- The master bound lab notebook is an index to all SQM operations, filename, date, location, times of SQM status changes, and any relevant notes. If more convenient, it can be filled in after the day's activities are complete.

- The event log workbook is a history of every SQM type activity, taking note of shipments, lamp changes, and so forth. It should be updated frequently.
- The LabVIEW DAQ software had to address several functions. Obviously, a key function was to record the SQM housekeeping data. We wanted to allow for investigation into the length of the warm up interval and to remind the operator to turn on and off the AC power strip in the absence of a power switch. We needed to insert comments in the header section of the file after acquisition had begun. And, we had to write the header data to be compatible with the MLdbase structure and variable definitions.
- The MATLAB MLdbase codes needed to be fully automated given the SQM output file and a pdf of the logsheet. The desired analyses steps and graphics had to be designed, and an overall organization structure defined. The web site for displaying the results needed to be designed, so that the entire team could view the results.

Given the DAQ and analysis requirements and range of expertise, three team members developed the SQM software – Tom Larason for the DAQ in LabVIEW, Stephanie Flora for the MLdbase in MATLAB, Carol Johnson for project definition and coordination. The ascii DAQ file has two sections, header data followed by the SQM output values and a code for which DUT was viewing the SQM as a function of time. For each SQM data file, the MLdbase processing generates a ascii configuration file that is executable by MATLAB and a MATLAB (*.mat) binary file with defined variables. The configuration file archives processing steps and assigns the metadata according to the header in the data file. These variables in the *.mat file correspond to a matrix of time-stamped data (with time as rows and quantity as columns), a matrix that both is a numeric pointer into the data columns and the metadata in numeric format, and associated other variables (such as the filename, ascii description of the data column quantities, etc.). There are two types of metadata: a value or a code. (Data file comments are in the configuration file.) Examples of a value would be the ambient temperature or relative humidity. A code is needed when describing a condition, such as the DUT in place, the version of the DAQ software being used, etc. Before any code is written, the desired metadata must be defined, and the possible codes assigned. There is also an instrument configuration file to describe the SQM (e.g., details on the diffuser); a new instrument configuration file is made when there are major changes to the SQM hardware. Figures SS2 to SS9 illustrate selected components of the DAQ and analysis software.

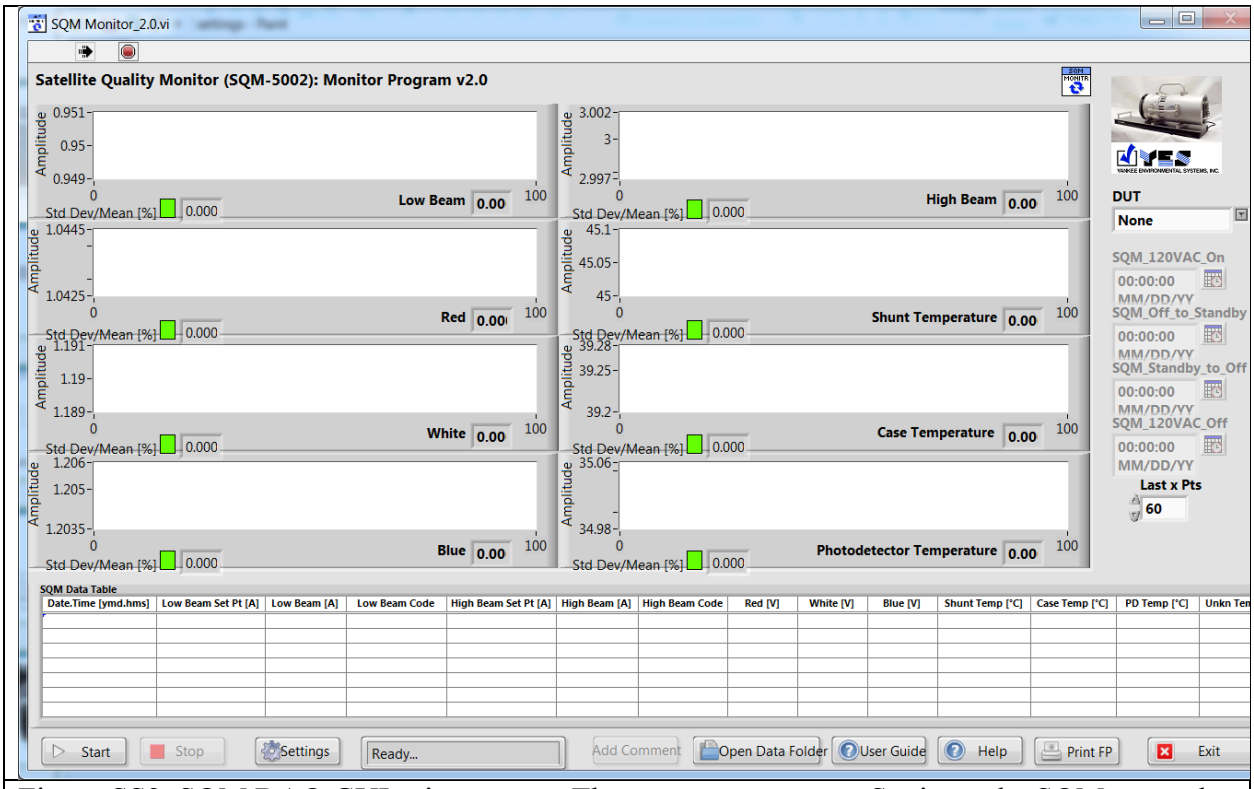

Figure SS2. SQM DAQ GUI prior to start. The operator can go to Settings, the SQM manual, a Help file, or Start the program.

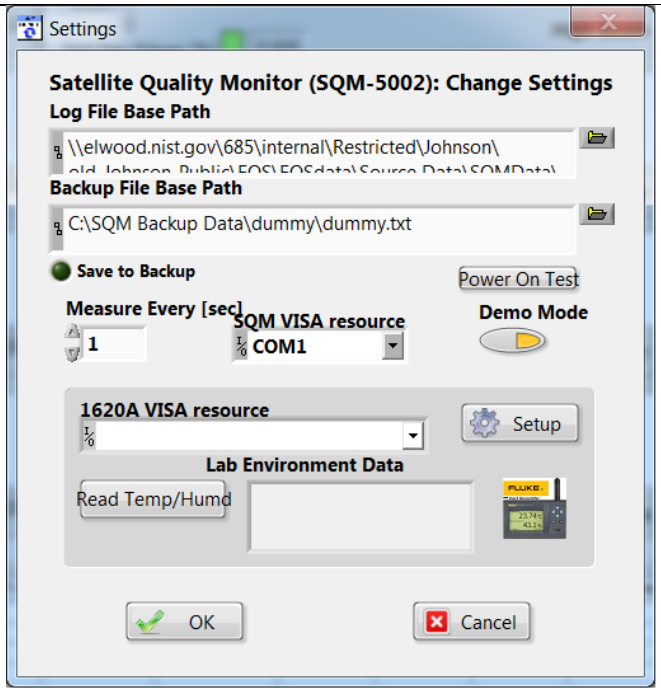

Figure SS3. The Settings tab allows the operator to change the primary and backup file paths, the measurement interval, the communications port, check the communications with a Fluke 1620A temperature and humidity sensor, or go to Demo mode. The Fluke is optional, if it is not present the operator is prompted to enter the ambient temperature and relative humidity.

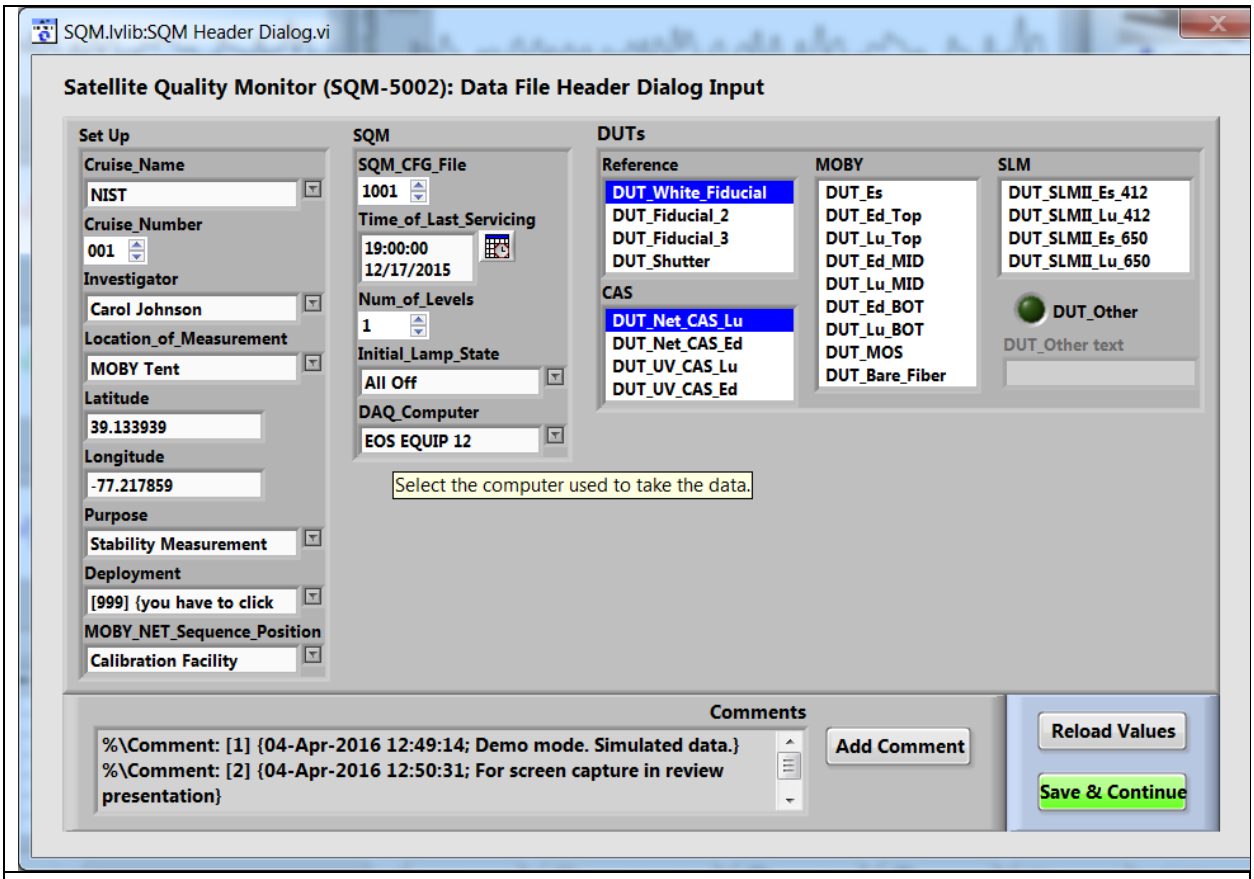

Figure SS4. This window appears after the Start tab is activated. Parameters are set according to the experiment, and all the DUTs expected to be operated for this run must be selected. Logging began when the Start button was activated, but “Save & Continue” or “Add Comment” updates the header portion of the file without interrupting the data acquisition.

Figure SS5. During execution, the lamp currents, internal temperatures, and photodiode signals are graphed, and the data is displayed in tabular form. The operator would have selected the current DUT from the pull down menu and set the time the AC power was activated and the rotary knob was switched from "off" to "standby". In real time, the operator can change the number of points being averaged, which is used to determine the relative percent standard deviation for each data stream. The colors of the green squares go from red to yellow to green depending on the relative percent standard deviation.

```
%\Begin_Header:
%\Filename: [SQM_20180720_001]
%\---------- Set Up Info ----------
%\DAQ_Program_Name: [2] {SQM Monitor_2.1.vi}
%\DAQ_Program_Version: [19]
%\File_Format_Version: [2] %Ver 2 NIST DAQ designed by Tom Larason
%\Cruise_Name: [1] {NIST} %MOBYNET Cruise ID
%\Cruise_Number: [2018-001] %MOBYNET Cruise Number
%\Investigator: [1] {Carol Johnson}
%\Location_of_Measurement: [2] {NIST B019_221}
%\Latitude: [39.133935] %Degrees (+/- 90, N+ and S-) [DD.dddddd]
%\Longitude: [-77.217356] %Degrees (+/- 180, E+ and W-) [DDD.dddddd]
%\Purpose: [1] {Stability Measurement}
%\Deployment: [999] {unknown} %MOBYNET Deployment
%\MOBY_NET_Sequence_Position: [1] {Calibration Facility}
%\Ambient_Air_Temp: [22.9] %deg C
%\Relative_Humidity: [53.3] %percent
%\---------- Comments Info ----------
%\Comment: [1] {20-Jul-2018 13:44:03; running labview 15 version today, think it is the same as 17}
%\Comment: [2] {20-Jul-2018 13:44:24; and that we did not make any changes}
%\Comment: [3] {15-Oct-2018 19:57:00; bcj changed initial row codes from 0 to 1}
%\---------- Device Under Test (DUT) Info ----------
%\DUT_White_Fiducial: [1]
%\DUT_Black_Fiducial: [2]
%\DUT_Net_CAS_Lu: [5]
%\DUT_VXR: [401]
%\DUT_SEI: [402]
%\---------- SQM Info ----------
%\Source_ID: [350] {SQM} %Satellite Quality Monitor (SQM-5002)
%\SQM_Instrument_CFG_File: [1001] {SQM1001.txt} %Current hardware attributes
%\Time_of_Last_Servicing: [20151218.000000] %Date format GMT YYYYMMDD.HHMMSS
%\#_of_Levels: [3] %Approx # of lamp levels in data file: off, low, medium, high
%\Initial_Lamp_State: [0] {All Off}
%\Time_Step: [10] %sec
%\DAQ_Computer: [15] {EOS EQUIP 13}
%\SQM_120VAC_On: [20180720.133800] %Date format GMT YYYYMMDD.HHMMSS
%\SQM_Off_to_Standby: [20180720.133900] %Date format GMT YYYYMMDD.HHMMSS
%\SQM_Standby_to_Off: [20180720.155324] %Date format GMT YYYYMMDD.HHMMSS
%\SQM_120VAC_Off: [20180720.155600] %Date format GMT YYYYMMDD.HHMMSS
%\---------- Misc Info ----------
%\Time_adjustment_to_GMT: [00.00.00] {Adjust file times to GMT (HH.MM.SS)} %Manual edit of SQM_yyyymmdd_xxx.txt file during processing.
%\VR_Number: [15] %number of data columns
%\Column_Headers: %Date.Time [ymd.hms], Low Beam Set Pt [A], Low Beam [A], Low Beam Code, High Beam Set Pt [A], High Beam [A], High Beam Code, Red [V], White [V], Blue [V]
%\End_Header@
20180720.134354 0.000000    0.006008    10.000000   0.000000    0.004479    10.000000   0.002443    0.003370    0.045528    39.847411   23.670684   35.134125   25.676635
20180720.134404 0.000000    0.006008    10.000000   0.000000    0.004482    10.000000   0.002784    0.003317    0.044958    40.358184   23.710448   35.055908   25.809600
20180720.134415 0.000000    0.006008    10.000000   0.000000    0.004438    10.000000   0.002214    0.003392    0.046409    40.813720   23.756927   34.913390   25.961150
```

Figure SS6. Initial section of an example SQM data file. The header convention is quantity descriptors are bracketed by "%\" and ":", e.g. "%\Filename:". The square brackets […] contain either a code or a value. If it is a code, then the curly brackets {…} are the identification of that code. For example, "[22.9] %deg C" indicates the ambient temperature was 22.9°C while "[1] {Carol Johnson}" indicates the investigator was Carol Johnson. The MLdbase processing does not require the curly brackets to be present, but it is helpful to have this information in the header for quality control purposes. Any comments are formatted with the time stamp. This is useful for documenting when something of note happened during the SQM operation. The header starts with "%\Begin_Header:" and ends with "%\End_Header@". The last line before End Header identifies the quantities in the columns.

The data are organized in separate folders for each day, with a date-type naming convention. Each daily folder contains a pdf of the logsheets and all the SQM data files that were taken. An example path is SQM\data\2018-08-02\. This path is mirrored on a server at MLML and ftp protocol used to transfer the files to the remote site. Then the automated processing is performed, generating results in graphical and tabular form on the MOBY web site. The web site is organized with a Stability System page that summarizes the tests we have done, with the SQM time series as one of the available links.

Figure SS7 is a screen shot of a portion of the SQM time series page. In this section of the web page, we state the instrument configuration file, directory, filename, investigator, purpose, DUT, burn hours, how many times was a lamp set operated, and the time difference between starting the thermal control and the first lamp set. The filenames are linked to a SQM daily web page described below. Not shown in Fig. SS7, the SQM time series page has a link to a web page that compares all the SQM housekeeping data and a table displaying the contents of the SQM event log Excel workbook.

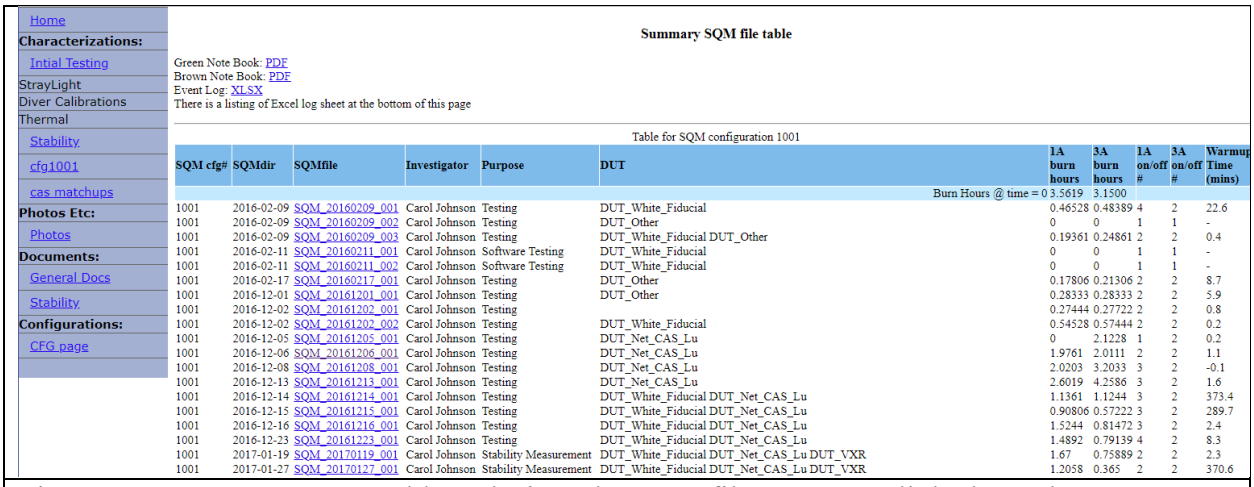

Home
Characterizations:
Intial Testing
StrayLight
Diver Calibrations
Thermal
Stability
cfg1001
cas matchups
Photos Etc:
Photos
Documents:
General Docs
Stability
Configurations:
CFG page

Summary SQM file table

Green Note Book: PDF
Brown Note Book: PDF
Event Log: XLSX
There is a listing of Excel log sheet at the bottom of this page

Table for SQM configuration 1001

SQM cfg#	SQMdir	SQMfile	Investigator	Purpose	DUT	1A burn hours	3A burn hours	1A on/off #	3A on/off #	Warmup Time (mins)
					Burn Hours @ time = 0	3.5619	3.1500			
1001	2016-02-09	SQM_20160209_001	Carol Johnson	Testing	DUT_White_Fiducial	0.46528	0.48389	4	2	22.6
1001	2016-02-09	SQM_20160209_002	Carol Johnson	Testing	DUT_Other	0	0	1	1	-
1001	2016-02-09	SQM_20160209_003	Carol Johnson	Testing	DUT_White_Fiducial DUT_Other	0.19361	0.24861	2	2	0.4
1001	2016-02-11	SQM_20160211_001	Carol Johnson	Software Testing	DUT_White_Fiducial	0	0	1	1	-
1001	2016-02-11	SQM_20160211_002	Carol Johnson	Software Testing	DUT_White_Fiducial	0	0	1	1	-
1001	2016-02-17	SQM_20160217_001	Carol Johnson	Testing	DUT_Other	0.17806	0.21306	2	2	8.7
1001	2016-12-01	SQM_20161201_001	Carol Johnson	Testing	DUT_Other	0.28333	0.28333	2	2	5.9
1001	2016-12-02	SQM_20161202_001	Carol Johnson	Testing		0.27444	0.27722	2	2	0.8
1001	2016-12-02	SQM_20161202_002	Carol Johnson	Testing	DUT_White_Fiducial	0.54528	0.57444	2	2	0.2
1001	2016-12-05	SQM_20161205_001	Carol Johnson	Testing	DUT_Net_CAS_Lu	0	2.1228	1	2	0.2
1001	2016-12-06	SQM_20161206_001	Carol Johnson	Testing	DUT_Net_CAS_Lu	1.9761	2.0111	2	2	1.1
1001	2016-12-08	SQM_20161208_001	Carol Johnson	Testing	DUT_Net_CAS_Lu	2.0203	3.2033	3	2	-0.1
1001	2016-12-13	SQM_20161213_001	Carol Johnson	Testing	DUT_Net_CAS_Lu	2.6019	4.2586	3	2	1.6
1001	2016-12-14	SQM_20161214_001	Carol Johnson	Testing	DUT_White_Fiducial DUT_Net_CAS_Lu	1.1361	1.1244	3	2	373.4
1001	2016-12-15	SQM_20161215_001	Carol Johnson	Testing	DUT_White_Fiducial DUT_Net_CAS_Lu	0.90806	0.57222	3	2	289.7
1001	2016-12-16	SQM_20161216_001	Carol Johnson	Testing	DUT_White_Fiducial DUT_Net_CAS_Lu	1.5244	0.81472	3	2	2.4
1001	2016-12-23	SQM_20161223_001	Carol Johnson	Testing	DUT_White_Fiducial DUT_Net_CAS_Lu	1.4892	0.79139	4	2	8.3
1001	2017-01-19	SQM_20170119_001	Carol Johnson	Stability Measurement	DUT_White_Fiducial DUT_Net_CAS_Lu DUT_VXR	1.67	0.75889	2	2	2.3
1001	2017-01-27	SQM_20170127_001	Carol Johnson	Stability Measurement	DUT_White_Fiducial DUT_Net_CAS_Lu DUT_VXR	1.2058	0.365	2	2	370.6

Figure SS7. SQM summary table web site. The SQM file names are linked to a data page summarizing all the housekeeping data for that particular data set.

Figure SS8 illustrates the top portion of the individual SQM file web page. All the metadata are summarized, the comments from the header are displayed, and results of parameter evaluations are tabulated. The automated processing selects when the two lamp sets are fully on or off, calculates the mean and standard deviation for the "on" times, checks for saturation in the monitor photodiodes, and records the total time the lamps were on. Graphical results follow this summary section of the web page (not shown in Fig. SS8). There is also a summary graph of all the SQM housekeeping data; individual graphs for the lamp currents, photodiode signals, SQM temperatures; a graph showing when each DUT was used in relation to the lamp currents and how "fully on" was determined; and graphs of the lamp currents during the "fully on" and "fully off" intervals. The housekeeping results are presented graphically to help diagnose any observed anomalies in the Stability System time series.

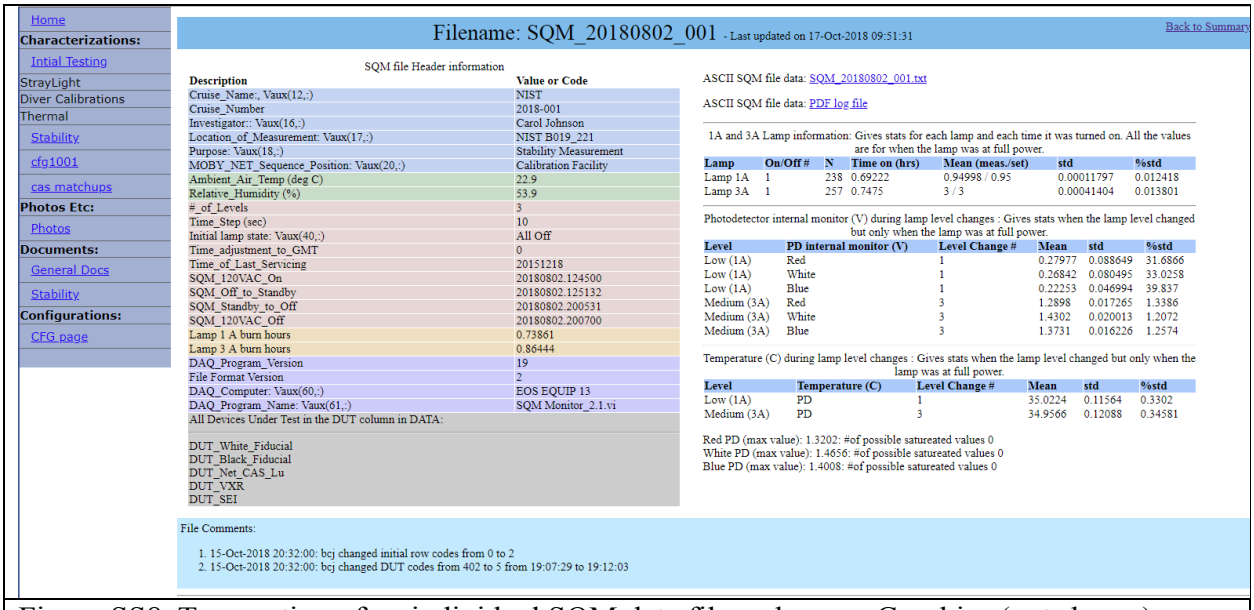

Home
Characterizations:
Intial Testing
StrayLight
Diver Calibrations
Thermal
Stability
cfg1001
cas matchups
Photos Etc:
Photos
Documents:
General Docs
Stability
Configurations:
CFG page

Filename: SQM_20180802_001 - Last updated on 17-Oct-2018 09:51:31

Back to Summary

SQM file Header information

Description	Value or Code
Cruise_Name:, Vaux(12,:)	NIST
Cruise_Number	2018-001
Investigator:: Vaux(16,:)	Carol Johnson
Location_of_Measurement: Vaux(17,:)	NIST B019_221
Purpose: Vaux(18,:)	Stability Measurement
MOBY_NET_Sequence_Position: Vaux(20,:)	Calibration Facility
Ambient_Air_Temp (deg C)	22.9
Relative_Humidity (%)	53.9
#_of_Levels	3
Time_Step (sec)	10
Initial lamp state: Vaux(40,:)	All Off
Time_adjustment_to_GMT	0
Time_of_Last_Servicing	20151218
SQM_120VAC_On	20180802.124500
SQM_Off_to_Standby	20180802.125132
SQM_Standby_to_Off	20180802.200531
SQM_120VAC_Off	20180802.200700
Lamp 1 A burn hours	0.73861
Lamp 3 A burn hours	0.86444
DAQ_Program_Version	19
File Format Version	2
DAQ_Computer: Vaux(60,:)	EOS EQUIP 13
DAQ_Program_Name: Vaux(61,:)	SQM Monitor_2.1.vi
All Devices Under Test in the DUT column in DATA:	
DUT_White_Fiducial DUT_Black_Fiducial DUT_Net_CAS_Lu DUT_VXR DUT_SEI	

ASCII SQM file data: SQM_20180802_001.txt

ASCII SQM file data: PDF log file

1A and 3A Lamp information: Gives stats for each lamp and each time it was turned on. All the values are for when the lamp was at full power.

Lamp	On/Off #	N	Time on (hrs)	Mean (meas./set)	std	%std
Lamp 1A	1	238	0.69222	0.94998 / 0.95	0.00011797	0.012418
Lamp 3A	1	257	0.7475	3 / 3	0.00041404	0.013801

Photodetector internal monitor (V) during lamp level changes : Gives stats when the lamp level changed but only when the lamp was at full power.

Level	PD internal monitor (V)	Level Change #	Mean	std	%std
Low (1A)	Red	1	0.27977	0.088649	31.6866
Low (1A)	White	1	0.26842	0.080495	33.0258
Low (1A)	Blue	1	0.22253	0.046994	39.837
Medium (3A)	Red	3	1.2898	0.017265	1.3386
Medium (3A)	White	3	1.4302	0.020013	1.2072
Medium (3A)	Blue	3	1.3731	0.016226	1.2574

Temperature (C) during lamp level changes : Gives stats when the lamp level changed but only when the lamp was at full power.

Level	Temperature (C)	Level Change #	Mean	std	%std
Low (1A)	PD	1	35.0224	0.11564	0.3302
Medium (3A)	PD	3	34.9566	0.12088	0.34581

Red PD (max value): 1.3202: #of possible satureated values 0
White PD (max value): 1.4656: #of possible satureated values 0
Blue PD (max value): 1.4008: #of possible satureated values 0

File Comments:

1. 15-Oct-2018 20:32:00: bcj changed initial row codes from 0 to 2
2. 15-Oct-2018 20:32:00: bcj changed DUT codes from 402 to 5 from 19:07:29 to 19:12:03

Figure SS8. Top portion of an individual SQM data file web page. Graphics (not shown) follow.

The web page summarizing all the SQM data is generated using automated processing and information in the SQM data file. For example, when the lamp sets are off, the dark signals from the photodiodes are compared. Time series of photodiode signals for SQM on LO and the White Fiducial in place, or the SQM on MED or HI and the Black Fiducial in place are generated. Time series are also made for lamp currents. We also wanted to examine the SQM monitor photodiodes when the MOBY CAS was viewing the SQM. This required a method to inform the SQM processing codes the CAS observing times. The CAS DAQ program (see below) generates a filename corresponding to the file closure time. The time the file started is in the header. Typically, three consecutive CAS files correspond to one CAS measurement of the SQM. The filenames, header information, source type, and distance between the CAS and the SQM (zero means it was inserted in the SQM) for the first and last CAS file are concatenated in an Excel workbook, and transferred to MLML for generating SQM photodiode matchups. The details and results are on a CAS matchup web page. The filename link goes to a section of the web page with graphics relating the CAS matchup times to the SQM housekeeping data.

The purpose of this web page is to look at the SQM data that are matched with the CAS start and stop times in the Excel file supplied by Carol. The Excel file contains rows of CAS file information. Each two rows makes a pair. I have added a Pair Number column to make it clear which pairs go together. For each Pair I find the SQM file (a data rows) that were collected betweem the "Start Time" of the first CAS file in the pair and the "End Time" in the second CAS file in the pair. The first 7 graphs show the SQM data means and standard deviations (std) for each CAS pair. The CAS pair number is the x-axis for these data sets.

XLSfile: CAS XLS Matchup file

CAS Data Type meanings in the table below
10 = means this was a transition, e.g. the SQM current was changing between levels while the CAS was taking data
15 = means the SQM was at full current but perhaps had not stabilized fully, and the CAS was taking data
20 = means I thought the SQM was fully stabilized and expect these CAS data, and the SQM photodiode data, to be repeatable.
Data Type 10 is not plotted in the group plots.

CAS Positions meanings in the table below
There are other parameters we could denote. An interesting one is if the CAS was in the SQM or on the table.
"on the table" = 20 for distance of about 20cm and "mounted in the CAS" = 0 (zero). In the plots the "on the table" are diamonds and the "mounted in the CAS" data are circles.

Top of table

Pair#	SQMfile	CAS Start-End	CAS Total Minutes	CAS Strt -> SQM standby Minutes	CAS Strt -> Lamp On Minutes	CAS Data Type	CAS Position	Lamp Level	Red PD Mean	Red PD %std	White PD Mean	White PD %std	Blue PD Mean	Blue P %std
1	SQM_20161208_001	08-Dec-2016 19:00:46 -> 20:31:38	90.9	8.6	7.0	15	on the table	4.0	1.557	0.125	1.690	0.191	1.598	0.167
2	SQM_20161208_001	08-Dec-2016 20:35:46 -> 20:46:38	10.9	103.6	102.1	20	on the table	4.0	1.557	0.083	1.691	0.087	1.598	0.128
3	SQM_20161208_001	08-Dec-2016 20:55:46 -> 21:36:38	40.9	123.6	2.8	15	on the table	2.0	1.352	0.089	1.490	0.112	1.443	0.124
4	SQM_20161208_001	08-Dec-2016 21:40:46 -> 21:51:39	10.9	168.6	47.8	20	on the table	2.0	1.351	0.105	1.491	0.126	1.442	0.147
5	SQM_20161213_001	13-Dec-2016 14:41:47 -> 15:52:39	70.9	14.3	13.0	15	on the table	1.0	0.208	0.257	0.202	0.284	0.188	0.814
6	SQM_20161213_001	13-Dec-2016 15:52:46 -> 15:55:38	2.9	85.3	83.9	20	on the table	1.0	0.208	0.146	0.202	0.037	0.190	0.316
7	SQM_20161213_001	13-Dec-2016 16:08:46 -> 18:55:38	166.9	101.3	12.3	15	on the table	2.0	1.352	0.093	1.491	0.171	1.444	0.125
8	SQM_20161213_001	13-Dec-2016 18:55:46 -> 18:58:38	2.9	268.3	179.2	20	on the table	2.0	1.352	0.101	1.491	0.100	1.444	0.126
9	SQM_20161213_001	13-Dec-2016 19:10:46 -> 20:01:38	50.9	283.3	10.0	15	on the table	4.0	1.558	0.089	1.691	0.117	1.600	0.127

Figure SS9. Top portion of an individual SQM data file web page. Graphics (not shown) follow.

SQM Modifications

We decided to keep the existing SQM adaptor plate with its 10.48 cm diameter opening and locating pins for kinematic mounting. Dimensions were taken of the adaptor plate, the White Fiducial, the acrylic diffuser, and the lamp fixtures. A Black Fiducial was made from black Delrin because the SQM monitor photodiodes saturated with the White Fiducial; it mounts to the adaptor plate kinematically. A radiance foreoptic for the CAS was designed to mount kinematically to the adaptor plate; the foreoptics design is described below.

The SQM was delivered without any spare lamps, and none were available from YES. If one lamp in a lamp set fails, the lamp set becomes inoperable. The manual did not give the lamp identification but indicated this part of the hardware was like the SeaWiFS Quality Monitor. We followed the procedure in the manual for changing lamps to get the dimensions of the lamp fixtures and confirm lamp type, which involved partial dis-assembly. In the process, we had to machine the outer cover as it was nearly impossible to remove because of a flat area at the weld, where the cover bound to the internal supports.

The 1A lamps in the NIST SeaWiFS Quality Monitor were Gilway M/N 187 at 1.05 A and 4.2 V and Welch-Allyn M/N 01160 at 3.45 A and 5 V. We purchased 16 M/N 187 from International Light Technologies (they bought Gilway) but Welch-Allyn had discontinued the 01160 lamp. The replacement lamp needed to match in terms of current, voltage, design, and connector base. The closest replacement we found was the 01111-U at 3.35 A and 6 V, and we ordered 24. The compliance voltage for the 3A power supply in the SQM is unknown. Assuming it is greater than 5 V, the replacement lamp should run constant current at 3.0 A, and this will prolong lamp lifetime, which is only 100 h for the 01111-U. We did test the 01111-U at 5 V, where the current was 2.86 A, and this produced a white output, which was encouraging. If a 3A lamp fails, all the lamps in the set should be replaced to the 01111-U model. During the testing for MOBY NET, we never had a lamp failure. The total hours during the MOBY NET project are 48.85 h for the 1A set and 51.01 h for the 3A set.

The SQM lamps are potted into a lamp fixture that is held in place in bore holes using snap rings or machined clamps, see Fig. SS10. The connector base is pressed onto the mounted lamp. The SQM lamp fixtures were measured and replacements manufactured. An alignment jig was made so the lamp would be centered in the fixture with the correct amount of length of lamp lead protruding from the fixture. The NIST shops used the same potting procedures as is used for the FEL irradiance standard lamps.

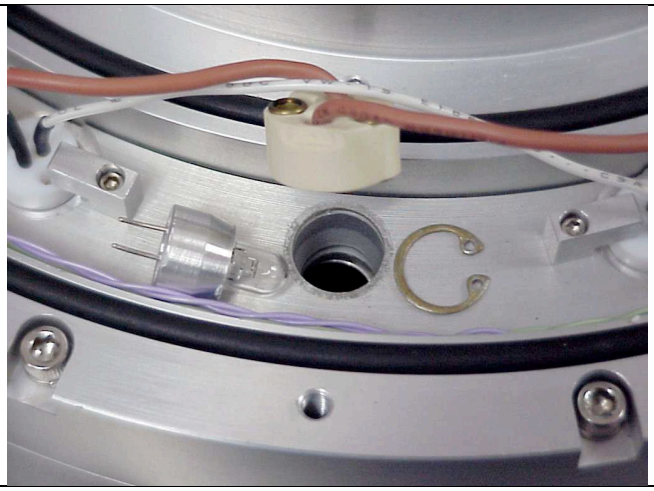

Figure SS10. Photograph of a YES SQM 3A lamp next to its connector base, bore hole, and snap ring. The lamp is inserted, the snap ring installed, and the base connected.

The SQM was delivered with a glass window and acrylic diffuser, materials that do not transmit in the UV. To quantify the loss, measurements were made with a NIST UV CAS that has spectral coverage from 200 nm to 875 nm and all scans normalized to 450 nm, see Fig. SS11. The black line (0.01 at 350 nm) is the glass window and the acrylic diffuser; the red and black lines are the glass window (0.03 at 350 nm), and the remaining data are either bare lamps or a quartz diffuser (≈0.04 at 350 nm). This established that both the YES window and diffuser needed to be replaced with quartz (e.g. fused silica) to support the goal of assessing stability at 350 nm.

We removed the YES window and diffuser, to measure and order custom fused silica parts to mate to the SQM. We procured 2 windows, 25.18 cm diameter by 9.4 mm thick, and 6 fused silica discs, 23.81 cm by 2.9 mm thick. One window is spare. Two of the discs are spares and four were used for evaluating different surface treatments to create a diffuse transmitting disc. The four diffusers were tested in the SQM and evaluated by taking images with a SLR digital camera using the manufacturer's software to process the raw images. The two-sided bead-blasted method was the best, but still results in poor spatial uniformity, see Fig. SS12. The flux is a minimum at the center, and a maximum over the lamps. This would be a disaster in a calibration source, but the SQM is a stability source, and as long as the radiometer head is aligned kinematically to view the same area and its FOV fixed, the signals should remain stable.

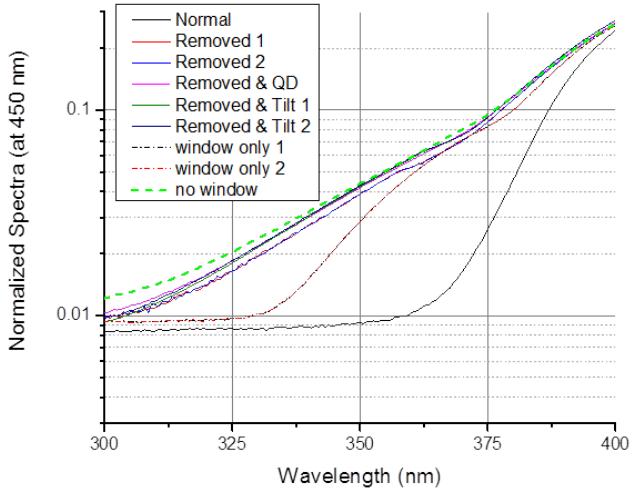

Figure SS11. Relative measurements of the output of the SQM using a NIST UV CAS normalized to 450 nm.

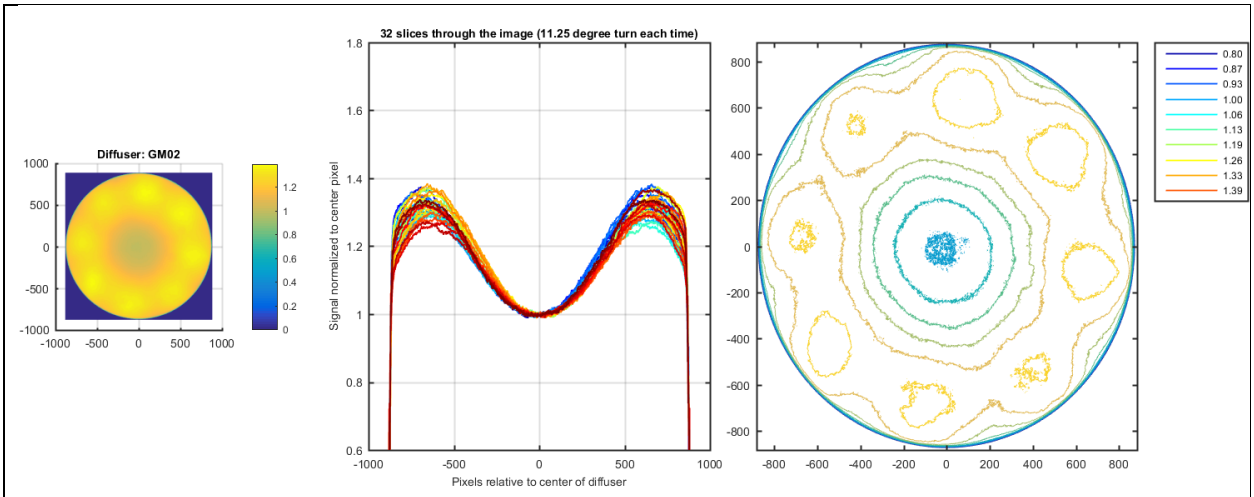

Figure SS12. Images of the SQM at the HI level using a SLR digital camera.

CAS

The CAS140 is a commercial spectroradiometer. NIST had experience with this system with repeat trips to Mt. Hopkins that indicated the irradiance responsivity was stable with transport and field use at the ±0.5% level from 350 nm to 1050 nm. One run was an outlier with up to 1% difference from the mean, but this was attributed to improper registration of the fiber bundle with the spectrometer. NIST had developed custom DAQ software using the device drivers from the vendor. Based on these experiences, we chose a CAS140CT-156 for the Stability System.

The MOBY CAS specifications are:

- Crossed Czerny-Turner spectrograph;
- Spectral coverage, 300 nm to 1100 nm;
- 3.7 nm spectral resolution using 100 μm slits;
- 0.8 nm/pixel data point interval;
- Built in shutter and order sorting filter;
- Built in set of neutral density filters;
- 15 bit A/D converter;
- 1024x128 back-illuminated CCD detector;
- LabVIEW driver software;
- USB interface with triggering options;
- 19.2 cm x 33.0 cm x 34.8 cm (H x W x D);
- Ambient operating temperatures 15°C to 35°C;
- Ambient operating relative humidity 0% to 70%, non-condensing;
- Weight 10 kg;
- 2 m long quartz fiber bundle, focusing lens at spectrometer side, bare fiber at input side, 190 nm to 1350 nm; and
- 2 m long quartz fiber bundle, focusing lens at spectrometer side, irradiance optic at input side, 190 nm to 3200 nm.

The interface to the fiber bundle and the spectrograph is the fiber plug adaptor or PLG, and the spectrometer side of the fiber bundle is terminated with a PLG optimized for the f-number of the spectrograph using a UV lens to collimate the output of the fiber bundle for focusing onto the entrance slit. A locking pin and knurled locking nut form a repeatable connection.

CAS Software

The SQM requirements and protocols also apply to the CAS. The elements include a master bound lab notebook, an event log Excel workbook, LabVIEW 2017 data acquisition (DAQ) software, and MATLAB codes for manual processing of the data. There are no CAS logsheets because that information is captured on the SQM logsheets. Although we planned to implement a coordinated CAS DAQ file structure for MLdbase analysis, this was not accomplished. Unlike the SQM, LabVIEW DAQ software already existed for the CAS from prior NIST work, and manual processing was implemented to investigate these data given the requirement to assess performance. Once the data files started coming in, priority was given on investigating results

rather than developing an automated processing system. The level of NIST expertise in the MLdbase environment was also a contributing factor.

- The master bound lab notebook is an index to all CAS operations, filename, date, location, source, bench, fiber, foreoptic, integration time, number of scans in each file, number of accumulations on the CCD, neutral density filter identification, datatype, max DN observed, and notes.
- The event log workbook is a history of every CAS type activity, taking note of on and off times, foreoptic changes at the PLG connector, shipments, source measured, and so forth. It should be updated frequently.
- The LabVIEW DAQ software gives the operator control over the path of the CAS initialization files, the path for the data file, input on very limited set of metadata, and setting of CAS scan parameters. There is a choice to not save the data file and information provided on the CCD temperature and maximum DN. Typically three sequential files are taken one with the lens cap on ("Background") and another with the lens cap off ("Signal"). When viewing an integrating sphere source or the SQM from a distance, an on-axis disc is inserted in the optical path and the third file "Ambient" data are acquired. Figure SS13 illustrates the front panel of the CAS DAQ software, and Fig. SS14 is a portion of a typical data file.
- The manual analysis is written in MATLAB. Files with the same datatype in one measurement sequence, e.g. the three sequential signal data files, are combined into one *_raw.mat file that has variables for the CAS output (wavelength and DN/ms) as well as variables from the limited header information. The filename of the *_raw.mat file indicates the data type (signal, background, or ambient). The three filenames that correspond to one measurement are stored in three columns in an Excel spreadsheet to establish the correct pairing of which background or ambient file to subtract from the signal file. A flag is set if the operator wants to process this grouping to a *_net.mat file. Then, the net files can be compared graphically or used to derive the CAS radiance or irradiance responsivity given a source calibration file.

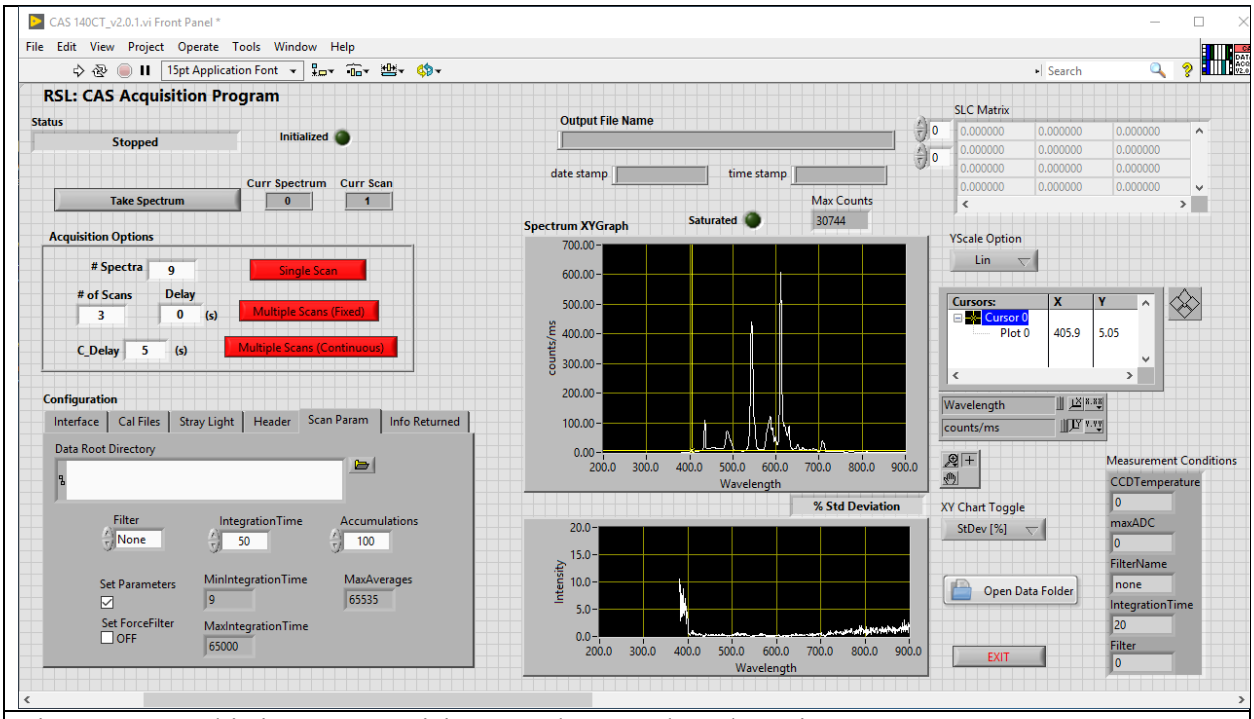

Figure SS13. This is Tom's revision, not the Woodward version…

CAS ID	664014214											
Date:	7/25/2018											
Time:	19:22:47											
Operator:	bcj											
Experiment:	RSL time series											
Source	OL455-12											
Location:	RSL											
Fore-optic:	Other											
Stray light correction	Identity											
Comment												
Filter:	2											
Integration time:	50											
Accumulation:	100											
WL	Run 1	Run 2	Run 3	Run 4	Run 5	Run 6	Run 7	Run 8	Run 9	Mean	% STD	Corrected Spectrun
297.494	-1.62E-03	-2.43E-03	-4.26E-03	6.08E-04	1.42E-03	2.03E-03	8.11E-04	2.03E-04	-2.23E-03	-6.08E-04	-3.46E+02	-6.08E-04
298.3183	-6.08E-03	-1.01E-03	-6.08E-03	-6.49E-03	-8.72E-03	-6.08E-03	-4.06E-03	-4.66E-03	-7.10E-03	-5.59E-03	-3.89E+01	-5.59E-03
299.1425	-7.30E-03	-1.82E-03	-2.64E-03	-1.82E-03	-4.06E-03	-3.45E-03	-5.68E-03	-3.04E-03	-2.43E-03	-3.58E-03	-5.14E+01	-3.58E-03
299.9667	-3.24E-03	-2.03E-03	-1.22E-03	-1.82E-03	6.08E-04	4.06E-04	-1.01E-03	-1.62E-03	-1.42E-03	-1.26E-03	-9.43E+01	-1.26E-03
300.7909	-6.49E-03	-2.64E-03	-3.45E-03	-2.64E-03	-5.27E-03	-3.24E-03	-3.45E-03	-2.64E-03	-6.08E-03	-3.99E-03	-3.86E+01	-3.99E-03
301.6151	-5.88E-03	-2.03E-04	2.03E-04	1.62E-03	-1.22E-03	2.43E-03	2.03E-03	2.23E-03	-4.06E-03	-3.15E-04	-9.33E+02	-3.15E-04

Figure SS14. Sample CAS ascii data file. The filename convention in the DAQ program is "CAS_YYMMDD_HHMMSS.xls" although it is an ascii file, not an Excel file; this file is CAS_180725_192340.xls.

CAS Foreoptics

The irradiance head is the EOP-146 from Instrument Systems with a spectral range of 190 nm to 2500 nm. The specifications state the cosine response is within 5% of ideal for angles up to 32° off axis. In this design, the fiber bundle is located behind a transmitting diffuser that is 15 mm in diameter. We used the irradiance head with FEL standard irradiance lamps as part of the stability time series, see below.

The radiance head for MOBY CAS is custom. The equivalent COTS Instrument Systems part is a complex system containing an alignment camera, increasing the price. Also, it would have been difficult to mate the TOP 200 to the SQM. Our design images onto the end of the radiance fiber bundle using a UV fused silica plano convex lens, Thorlabs P/N LA4052-A-ML, where "A" refers to a broadband antireflective coating for the 350 nm to 700 nm spectral region. A protective fused silica window, also AR coated, proceeds the window. An adjustable iris is in front of the fiber tip; it was added to block reflections from the metal surrounding the optical fiber bundle. During testing we found its setting was difficult to maintain, and we fixed it fully open. The components are mounted in Thorlabs lens tubes and threaded into a mounting plate that mounts kinematically to the SQM. The fiber bundle is also mounted kinematically to this mounting plate. Figure SS15 is the layout and photograph of the MOBY CAS Lu head. The lens is 25.4 cm in diameter with a focal length of 35 mm. The fiber bundle diameter is 1.5 mm, setting the full angle FOV to 2.5°. The radiance head and the White and Black Fiducials are held in the SQM using locking cams. A custom shipping container was procured that maintains the fiber bend radius at 46 cm or greater and does not require the operator to disconnect the Lu fiber bundle from the CAS spectrograph.

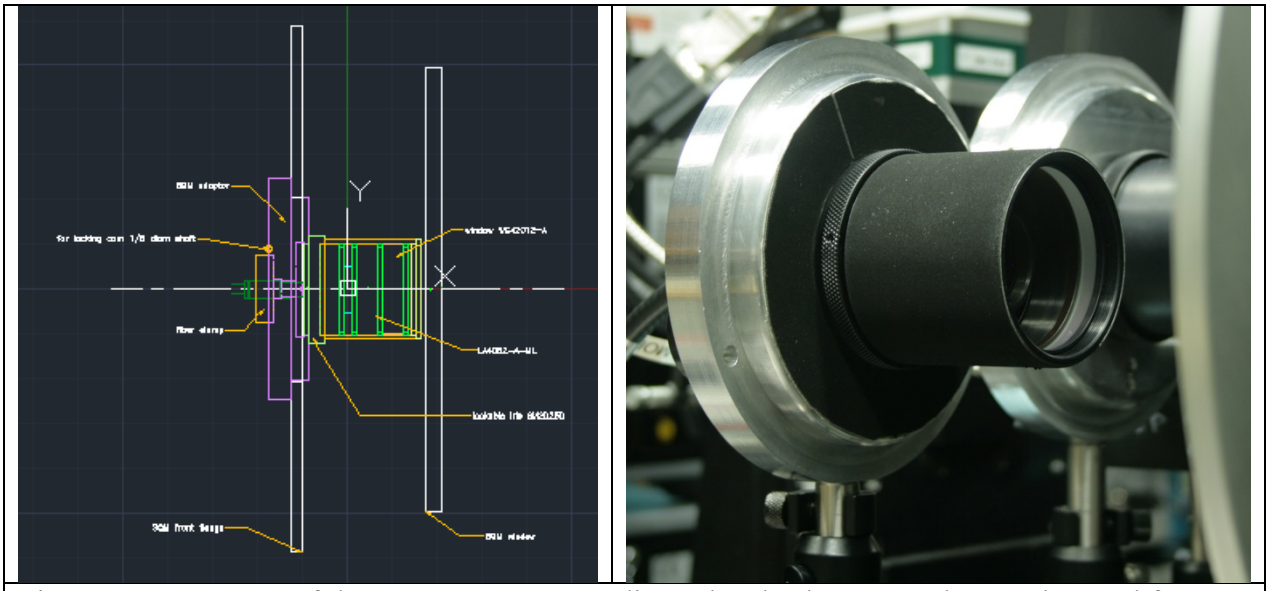

Figure SS15. Layout of the MOBY CAS Lu radiance head. The SQM adaptor plate and front window are indicated. When inserted, the Lu head is very close to the SQM window.

Stability System Test Results

In March 2016 we began testing the CAS with its irradiance head (fiber bundle E055 and EOP146) in a laboratory at NIST dedicated to stability testing of spectroradiometers. Other CAS's and an instrument from Spectral Evolution, Inc. were used. An FEL standard irradiance lamp, located 16.4 cm behind a partition with a 7.62 cm diameter aperture, was aligned to the optical axis defined by the "Z" axis of an X, Z motorized stage using a laser. The Z direction is along the optical axis and the X axis translates the fiber coupled irradiance heads horizontally. The setup is stable, resulting in conditions of repeatability. The only perturbations were turning the FEL lamp on and off, power cycling the spectroradiometers, and flexing the optical fibers as the X stage moved. A photograph of the irradiance heads is in Fig. SS16. We began with S195 but it drifted, so we changed to lamp S194. Data were taken from 15-Apr-2016 to 20-Jun-2016

under the repeatability conditions, then the CAS was moved to the Remote Sensing Laboratory (RSL). On occasion, the CAS was used in the irradiance laboratory, but in between these measurements the CAS had been moved, the foreoptics replaced at the PLG port to use the Lu head, or the CAS had been shipped (once to Miami and once to Honolulu). We term this the reproducibility test; it terminated 17-Jan-2018. The results are shown in Figs. SS17 and SS18.

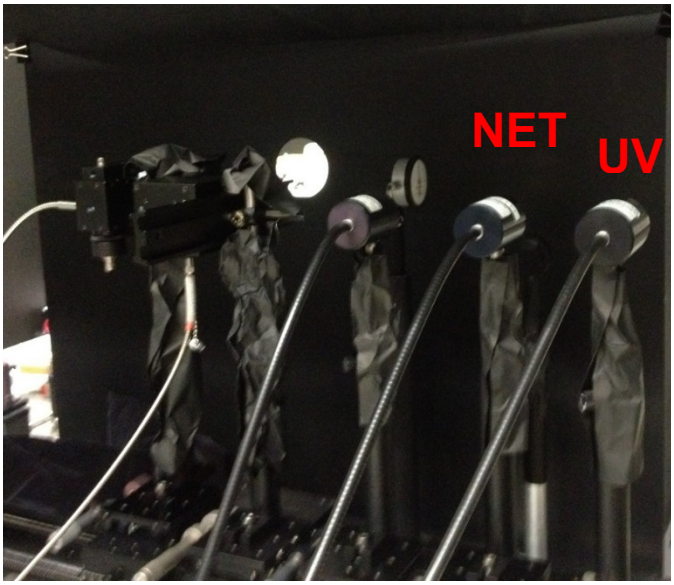

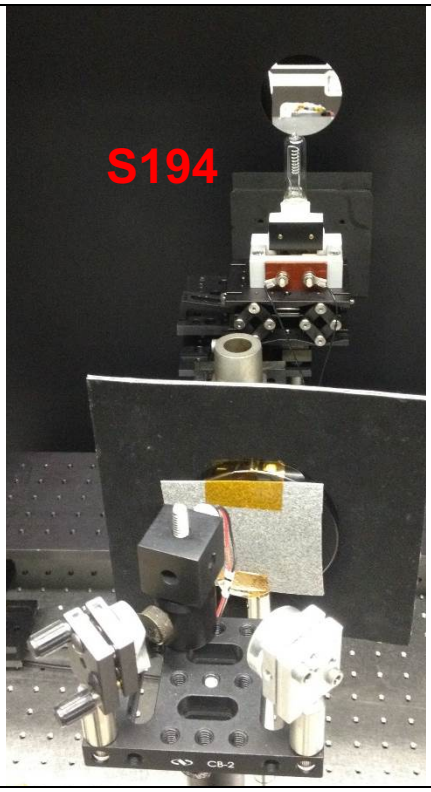

Figure SS16. Left – irradiance heads used in the study; right – view from behind the FEL lamp looking towards the radiometers.

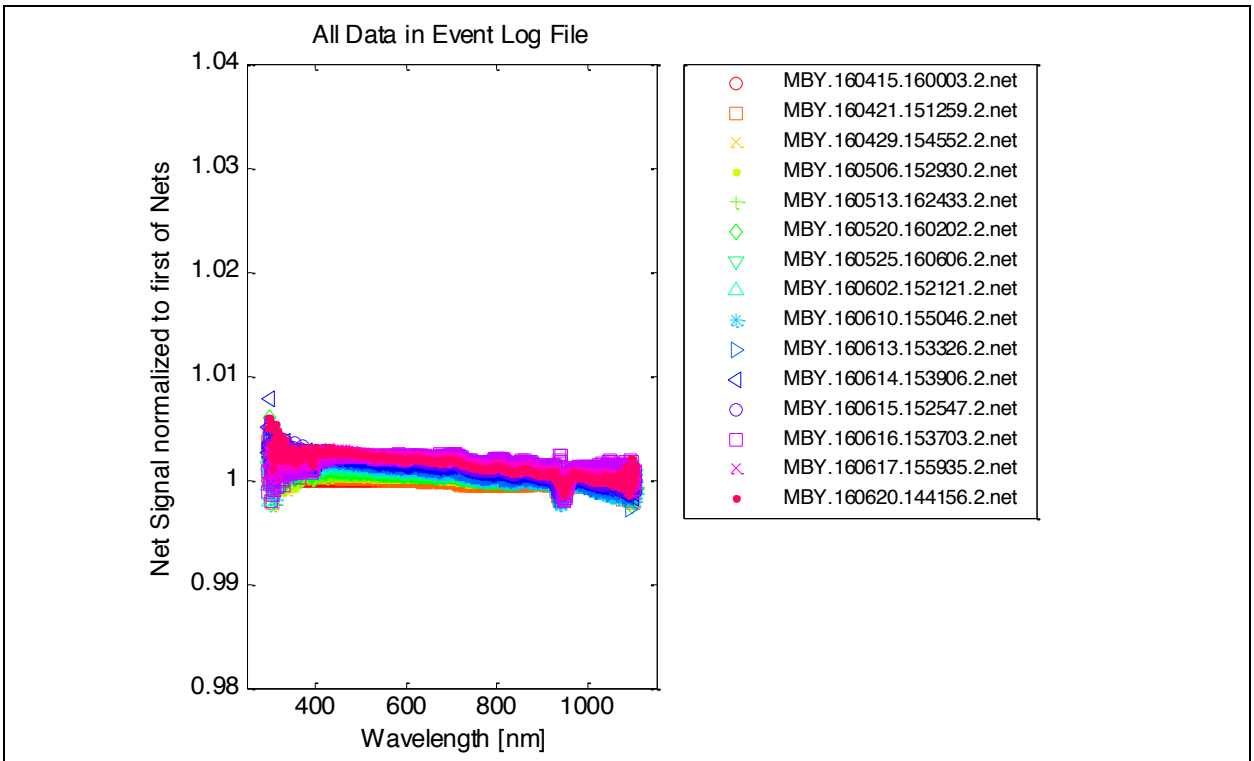

Figure SS17. Irradiance repeatability. The CAS net output has been normalized to the first file in the set.

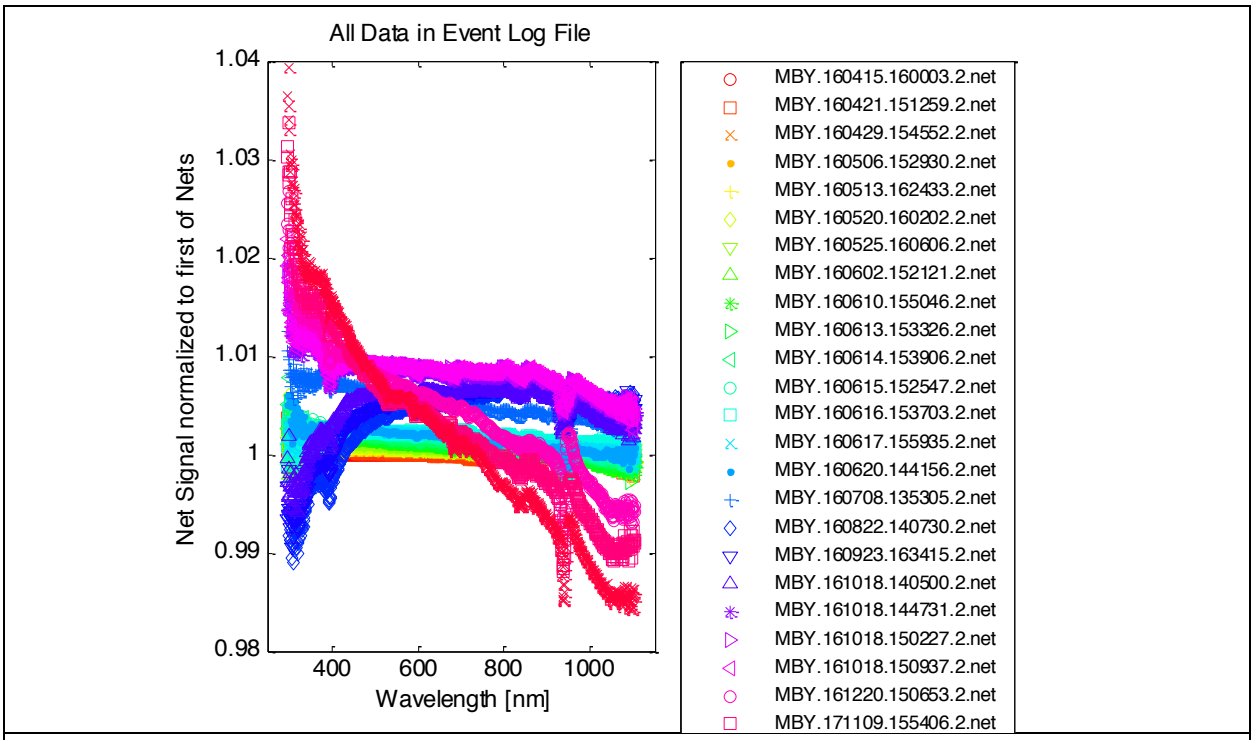

Figure SS18. Irradiance reproducibility. The CAS net output has been normalized to the first file in the set.

In December 2016 we began testing the CAS in radiance mode with the Lu head. These tests were done in the RSL in combination with three other sources and six other radiometers. The sources were all integrating sphere sources, two of the other radiometers were ASD FieldSpecs, two were CAS', one was the Visible Transfer Radiometer (VXR), and one was a Spectral Evolution, Inc. (SEI) model 4500. The two other CAS' were used intermittently, the ASDs could view the sphere sources but not the SQM, and the VXR, SEI, and MOBY CAS viewed all three integrating spheres and the SQM. Two of the spheres had the same overall design, the difference is one is dedicated to field deployments (the NIST Portable Radiance source, or NPR) and the other stays in RSL (NPR-Jr). These are 30 cm diameter Spectralon spheres from Labsphere with 10 cm exit apertures and four internal 30 W lamps. The third sphere was a model OL455-12 from Optronic Laboratories (affiliate of Solar Light Company, Inc.) with a 7.62 cm exit aperture and a single, external lamp. The sources are on a fixed table and the radiometers on a moving table. The VXR is on a vertical stage and the fiber coupled heads to all the spectrometers are on a small X, Y, stage that is mounted on the large moving table. A source laser on the fixed table and a detector laser on the large moving table are used to align the radiometers to the sources, with individual X, Y coordinates for each position. The positioning is under computer control. Figure SS19 is a photograph of the moving table from the vantage point of above the SQM on the source table, and Fig. SS20 is a photograph of the fixed source table.

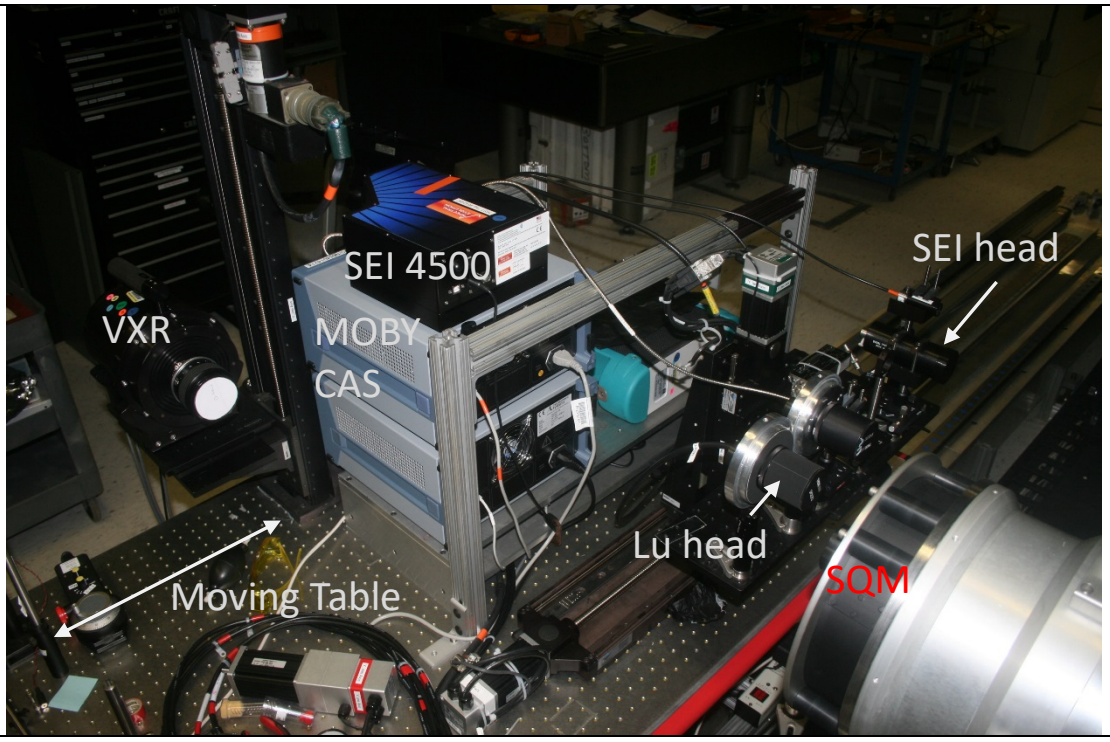

Figure SS19. Setup in RSL for the radiance time series showing the radiometers on the large moving table.

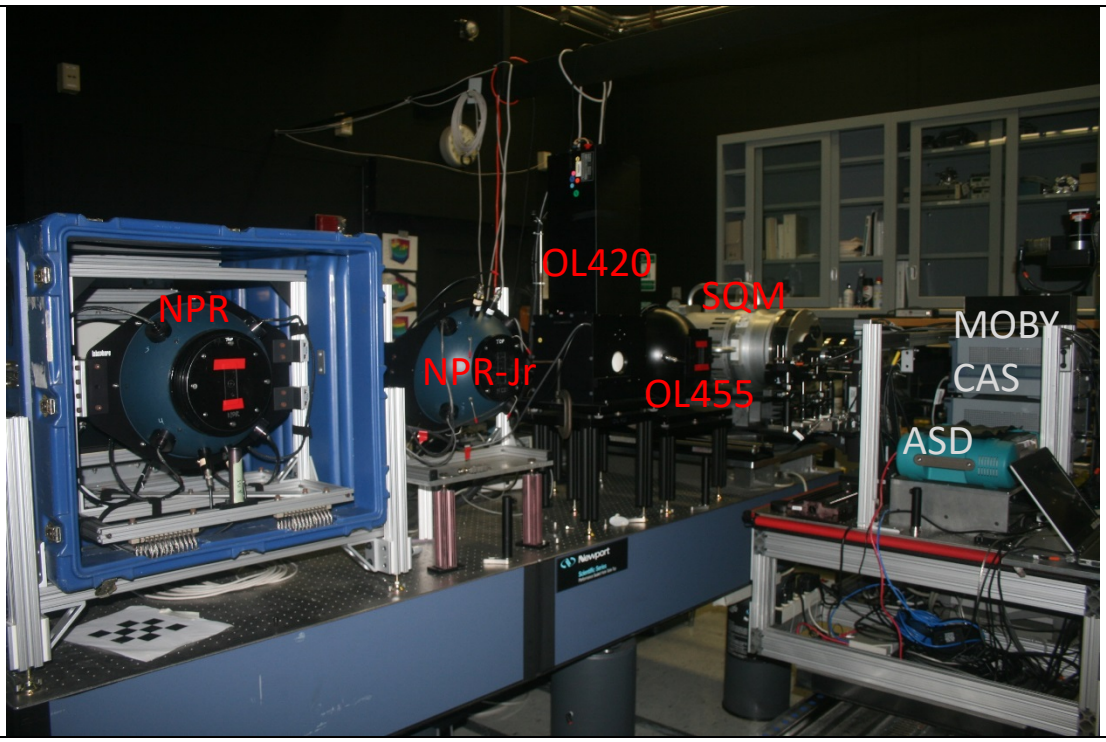

Figure SS20. Setup in RSL for the radiance time series showing the sources on the fixed table.

As with the irradiance time series, we can investigate repeatability and reproducibility. For repeatability, the sources and the CAS were turned off and on, the optical fibers flexed during motion of the small X, Y stage. The CAS Lu head was removed from its mount to fix to the adaptor plate of the SQM. Upon replacement to the small X, Y stage, the height was constrained but the rotation about the vertical axis required adjustment using the source laser. The conditions of reproducibility included shipment to Miami, operation outdoors, operation in different labs at NIST, and switching from irradiance to radiance foreoptics. Figure SS21 illustrates the repeatability results with the CAS and the NPR, SQM MED, and SQM LO. For the SQM results, the Lu head was mounted to the SQM.

The VXR is a six channel filter radiometer dating from the mid 1990's. The bandpasses are approximately 10 nm and the filters centered at 411 nm, 441 nm, 548 nm, 661 nm, 775 nm, and 870 nm. The time series of the VXR measurements of NPR are shown in Fig. SS23. The channels 1 to 6 correspond to the UV to NIR channels, and the time series is from Jan 2017 to Jul 2018. Channel 1 at 411 nm has the greatest variability, up to 1.5% peak to peak, but the other channels, in particular the 870 nm channel, vary within ±0.5%. Figure SS24 is a similar time series, from April 2017 to Aug 2018, of the VXR measuring the SQM MED level from 1.05 m. The outlier in Dec 2017 was in Miami, where the alignment of the VXR to SQM was less accurate. Given the spatial non uniformity of the SQM, we attribute the outlier to alignment error. If this point is removed, the results are very similar to the VXR and NPR time series.

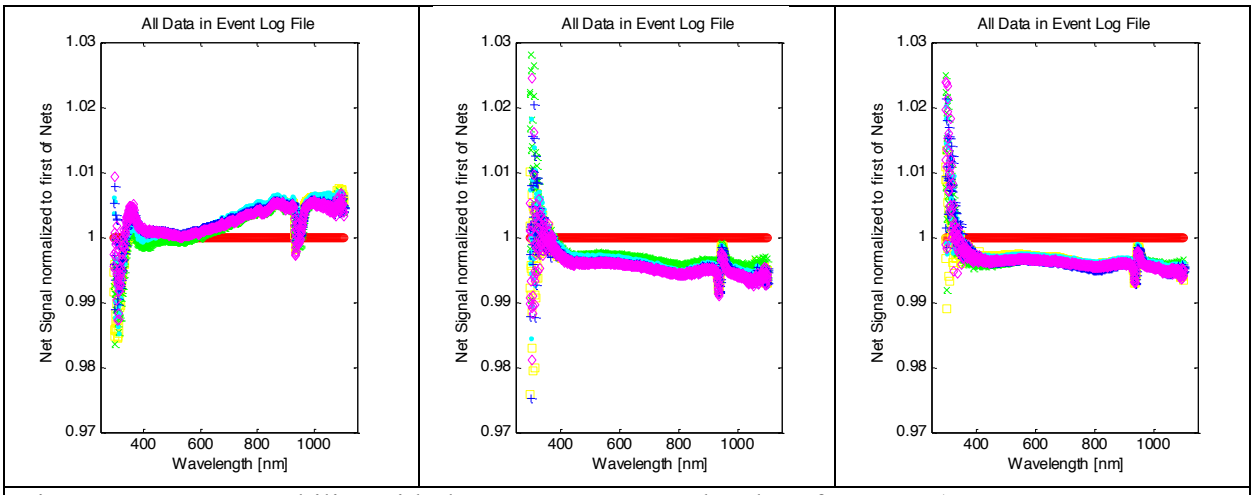

Figure SS21. Repeatability with the MOBY CAS Lu head. Left – NPR (01-May-2018 to 27-Jul-2018), middle – SQM MED, right – SQM LO (both 29-May-2018 to 02-Aug-2018).

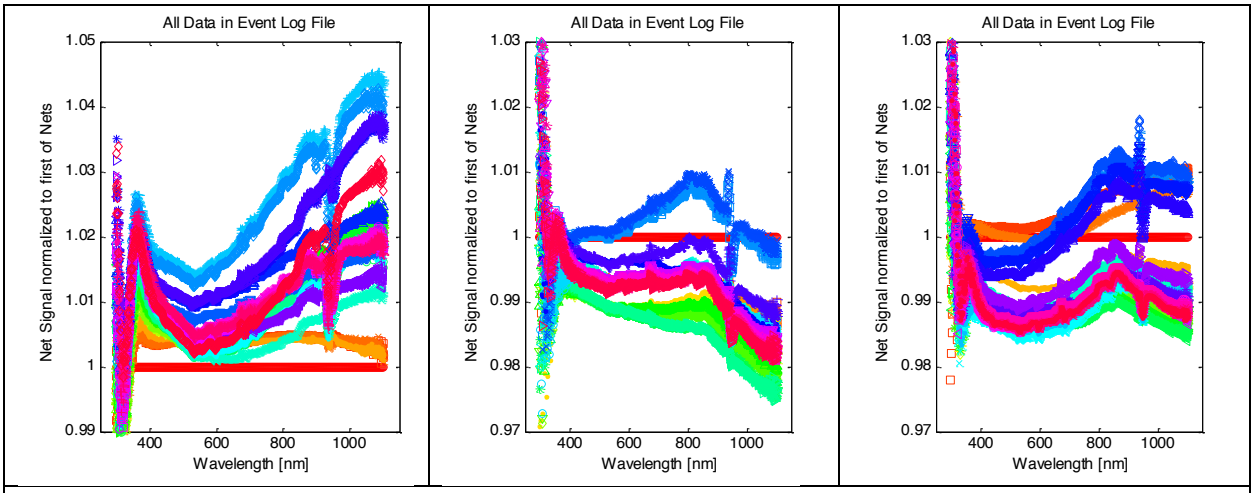

Figure SS22. Reproducibility with the MOBY CAS Lu head. Left – NPR (08-Dec-2016 to 26-Jul-2018), middle – SQM MED (08-May-2017 to 02-Aug-2018) , right – SQM LO (07-Apr-2017 to 02-Aug-2018).

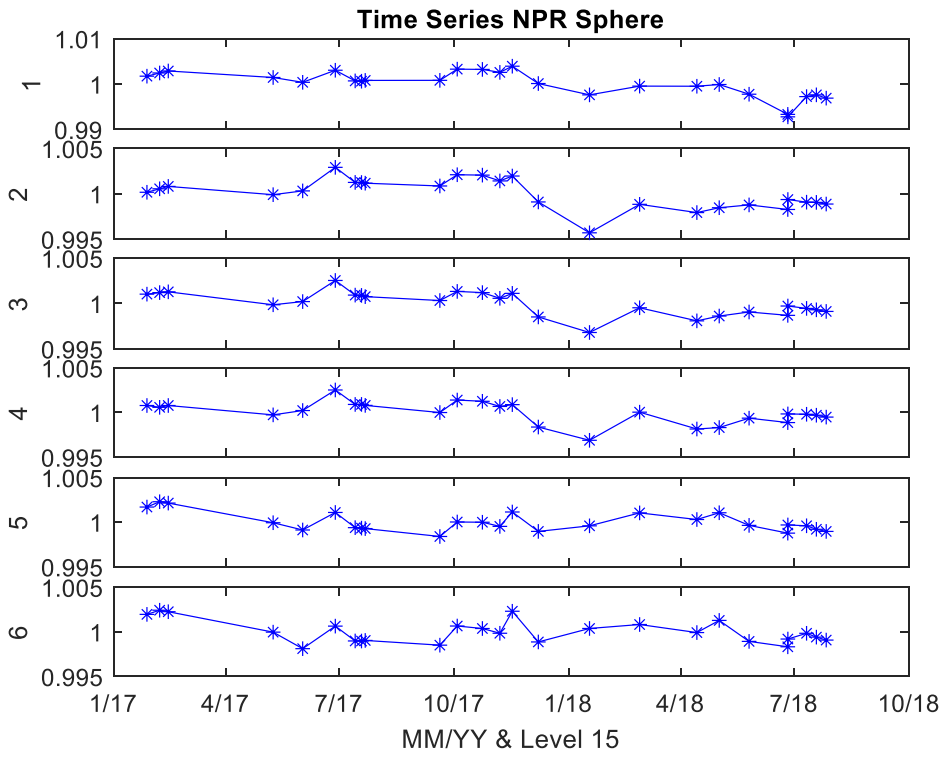

Figure SS23. Time series of the NPR using the VXR.

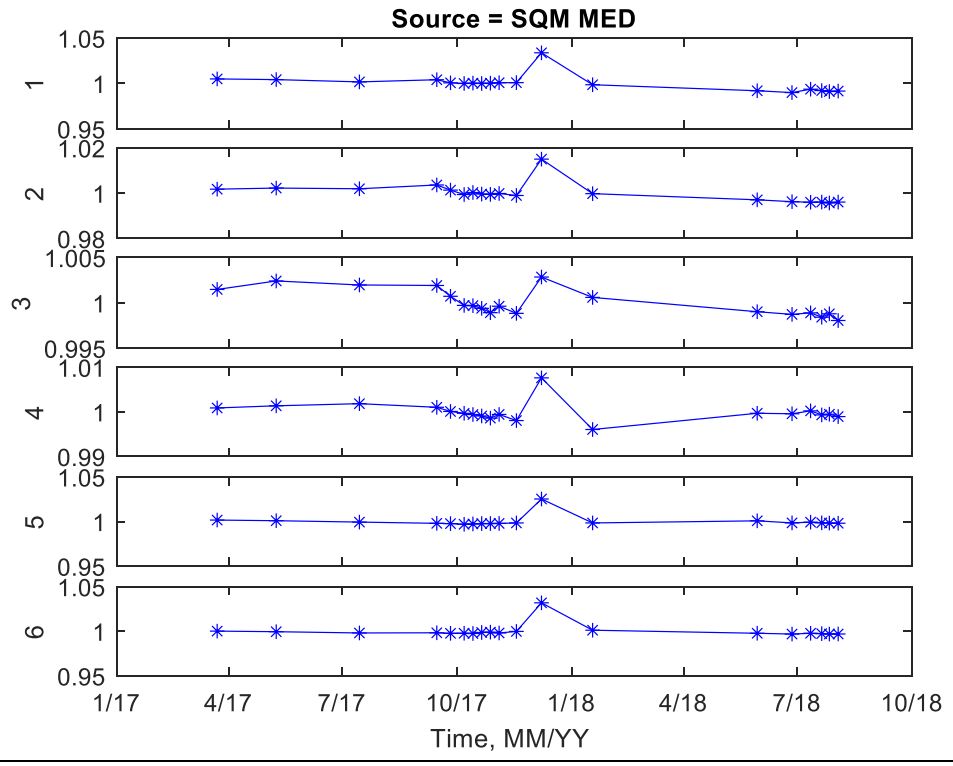

Figure SS24. Time series of SQM MED using the VXR.

The SQM stability was assessed using the internal monitor detectors when the White Fiducial, Black Fiducial, or the Lu CAS head was used. Figure SS25 illustrates the White Fiducial time series with the LO level, Fig. SS26 the Black Fiducial with the MED level, and Fig. SS27 during all Lu CAS measurements. Note the slight difference in the monitor photodiode signals depending on the location of the Lu CAS head.

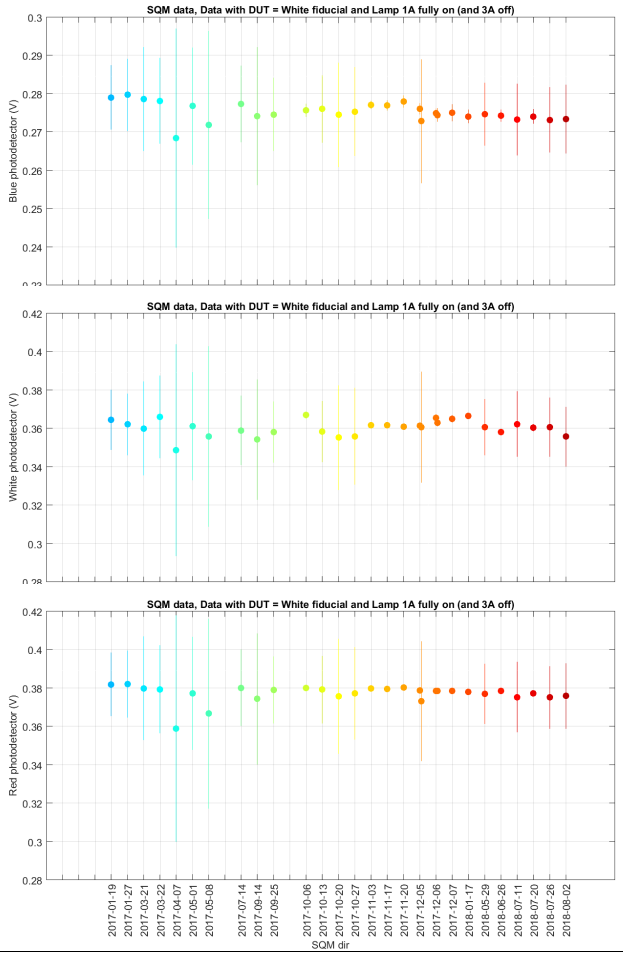

Figure SS25. White Fiducial time series, SQM LO level, for the interval from 19-Oct-2017 to 02-Aug-2018. The top panel is the Blue photodiode, the middle panel is the unfiltered photodiode, and the bottom panel is the Red photodiode.

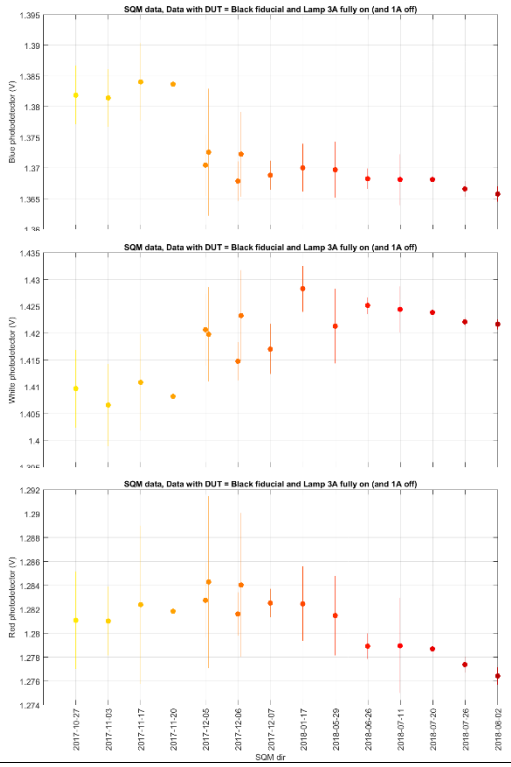

Figure SS26. Black Fiducial time series, SQM MED level from 27-Oct-2017 to 02-Aug-2018. The top panel is the Blue photodiode, the middle panel is the unfiltered (White) photodiode, and the bottom panel is the Red photodiode.

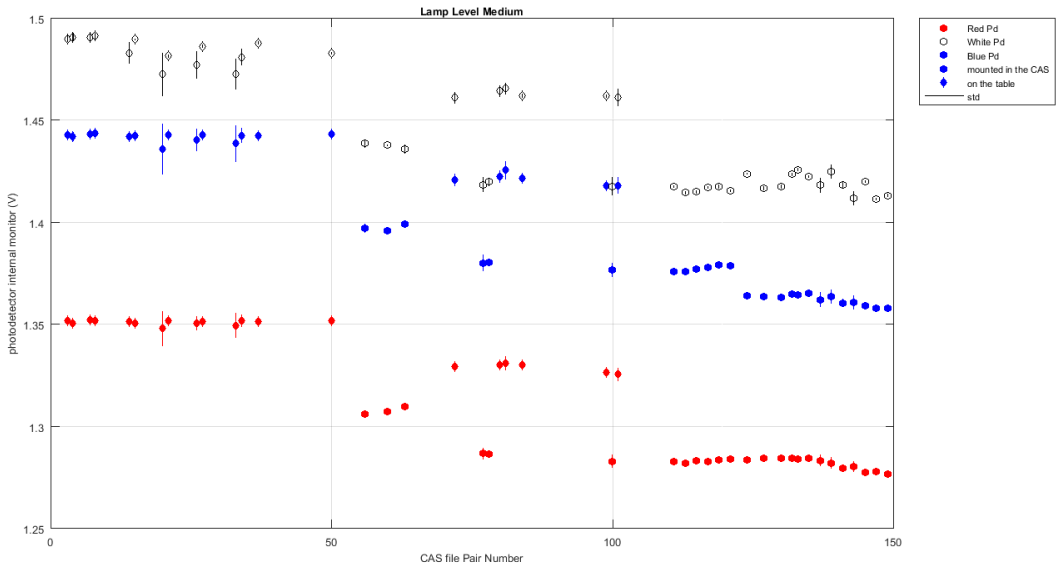

Figure SS27. Lu CAS time series, SQM MED level. Triangle symbols are the CAS Lu 20 cm from the SQM adaptor plate, and circle symbols are with the Lu head mounted to the adaptor plate. The colors correspond to which photodidode (White, Blue, Red).

The relative coefficient of variation (COV) was used to assess the time series results. For the CAS data, four 10 nm wide spectral bands were defined, centered at 400 nm, 550 nm, 600 nm, and 700 nm. Within each band the COV was determined at each wavelength, and the resulting COVs averaged. In addition to the repeatability and reproducibility tests, we evaluated the short term repeatability – the 36 scans in the three sequential files taken over about 2 min. For the SQM fiducials, the COV corresponds to the time series. Tables SS1 and SS2 presents the results for the CAS and SQM monitor photodiodes.

Table SS1. COV values in percent for the CAS Lu head viewing the NPR, SQM MED, and SQM LO. The SQM results are with the Lu head in the SQM adaptor plate.

Component	**COV %**	**400 nm**	**550 nm**	**600 nm**	**700 nm**
CAS COV, Lu head, 36 scans	NPR SQM MED SQM LO	0.060 0.099 0.097	0.020 0.046 0.042	0.018 0.044 0.036	0.016 0.039 0.031
CAS Lu Repeatability, same setup	NPR SQM MED SQM LO	0.098 0.105 0.138	0.097 0.123 0.135	0.098 0.131 0.135	0.104 0.142 0.140
CAS Es Repeatability, same setup	S194	0.080	0.080	0.078	0.078
CAS Lu Reproducibility, all data w/ final Lu head	NPR SQM MED SQM LO	0.420 0.260 0.389	0.389 0.325 0.453	0.389 0.361 0.485	0.418 0.403 0.518
CAS Es Reproducibility, all data	S194	0.461	0.386	0.350	0.337

Table SS2. COV for the SQM monitor photodiodes with the two fiducials.

Component	**COV %**	**Blue**	**Red**	**White**
SQM Reproducibility	White Fiducial, LO Black Fiducial, MED	0.87 1.53	1.22 1.58	1.14 1.37

The short term repeatability is comparable to the repeatable over several months, and the values are comparable for the two foreoptic configuration. This is very encouraging. The NPR is a bright and stable source and we get comparable COV values for the repeatability of the SQM as with the NPR, which indicates the SQM is stable and the CAS has adequate SNR for the SQM LO level. The COV values for the reproducibility conditions are about four times greater than the repeatability and also comparable for the two optical configurations; these changes are spectral. The COV values are preliminary, however. Note the grouping of reproducibility results, indicating the distribution is not normal. The different groupings are not uniformly represented in terms of sample number. Finally, the SQM internal photodiodes are not as stable as the CAS. We have not performed thorough quality control on the White and Black Fiducial data, and this may improve the results.

Future Activities

The non-uniformity of the bead blasted quartz diffuser for the SQM was noted, and we investigated a new technology using high purity synthetic fused silica made opaque by infusion of high density gas bubbles that act as scattering centers. A study was carried out on these materials, see (Lemaillet, Patrick et al. 2016). We ordered a 19.5 cm diameter by 2.9 mm thick S 500 Diffusil disk and made an adaptor for the SQM. We did not use it to allow completion of our continuous time series. It is recommended to change the bead blasted diffuser to the opaque quartz before continuing with the SQM.

The CAS has an internal shutter, which closes for a dark reading at the start of every file. These values are subtracted internally from the readings, and differences are saved in the file. Based on the "max count" reading, there is apparently an offset of about 300 DN but tests of reading the dark using the Instrument Systems drivers indicate this is subtracted out. The concern is we can't access the readings of the CCD dark counts, which may inform on detector temperature or dark count drift. We will pursue this with the Instrument Systems engineering staff. The newer CAS 140D allows for manual dark current adjustment.

The reason for the larger reproducibility COV values compared to the repeatability COV values is not understood. We list possible factors and conclusions in Table SS3. Note that the same internal neutral density filter and integration time were used on each source.

Table SS3. Factors that may affect the reproducibility of the CAS.

Description	**Mechanism**	**Likely?**	**Plan**
Linearity with flux	Drift in correction (largest for large DN, e.g. middle of CCD)	No, doesn't fit observations	N/A
Integration time	Drift / change in shutter delay may expose different regions of CCD	No, doesn't fit observations	N/A
Fiber to spectrograph coupling	PLG mount does not repeat	No, we checked this	N/A
Wavelength shift or throughput change	Mechanical changes of optical imaging or throughput	Perhaps	Analyze wavelength calibrations
Wavelength shift	Thermally induced shift of image on CCD	Perhaps	Characterize in thermal chamber
Neutral density filters	Drift / change in neutral density filter transmittance	No, doesn't fit observations	N/A
Neutral density filters	Non uniformity combined with lack of repeat positioning	Unlikely	Cycle filters
Order sorting filter	Thermally induced change in transmittance and/or position of edge	Possible	Characterize in thermal chamber

It is recommended to continue with the CAS software development. The LabVIEW DAQ software needs to be updated to read additional housekeeping data such as CCD temperature, to

change the measurement sequence to record darks, and to write a header file that is compatible with the MLdbase structure. The steps to implement the MLdbase structure include defining all the quantities, fields, choices, and the organizational structure. For example, the separate "signal", "background", and "ambient" files should be stored in one *_raw.mat file. Different types of ambient, say with different size occulting disk, need to be in the same file, as well as any data taken with the doped glass wavelength filters. The code that performs this task must keep track of the files that were used with accommodation for reprocessing while keeping manual steps to a minimum. Quality control would be done at this step.

The CAS requires two ascii files to operate, an *.ini file and an *.isc file. The *.ini file gives details about the instrument hardware configuration such as number of active pixels, number of total pixels, wavelength calibration, linearity correction values, and type and blaze of grating, etc. The *.isc file gives calibration information, both for the spectral transmittance of the internal neutral density filters as well as optional radiometric calibration data. We operated with a generic *.isc file that treats both the neutral density and calibration data as unity. Otherwise the values saved have been automatically corrected and it is difficult to assess how close one was to saturation. Because the MOBY CAS will acquire data using any CAS 140CT's *.ini or *.isc file, it was possible to acquire incorrect data. The automated processing will include correcting these bad files for pixel assignment in wavelength and linearity, which is possible because we know the *.ini file used. These corrections primarily impact other studies we did with the MOBY CAS, such as when we used it to validate the MOBY irradiance scale in Hawaii.

Another advantage of automated processing is it allows us to exercise full control, including reprocessing, over the wavelength calibration, linearity corrections, stray light corrections, thermal corrections, and any other CAS corrections.

9) How did well did we do towards our goals?

Target	Achieved
Spectral range 350-900 nm	350-900 nm
3nm resolution	Predicted and achieved 1nm FWHM, 0.3-0.4 nm spectral spacing
Radiometric uncertainty <4% blue, 5% red	Not yet, good comparisons with MOBY at 5-10% but other problems
Stability 1% per deployment	Not yet
Capability of Autonomous field operation	Yes, controller has been working for many years.
Capable of maintaining calibration through 3-5 year period	Planned on 6-12 month redeployments, never 3-5 years
Built for sustainability and field maintained	As modular as possible. System rugged with some redundancy and features to limit damage
Laboratory and field characterized with NIST	Have been dong this consistently
Fully autonomously deliver data to NASA	Never thought this was correct. Should be delivered with short latency (days) to allow QC.

10) TRL Table

Portion of project	TRL in	TRL goal	TRL achieved	Explanation
Control system	2	7	7	Controllers operating in field for several years
MOBY Hull	2	7	5-7	2 hulls have been built, they have not been operated in the field
Optical System	2	7	5-7	The systems have been operated in the field. We still have issues to resolve
Stability System	5	6	6	The systems have been operated in the field, but not with MOBY-Net optics

9) The Future

Here are the points that we think are important for a follow-on project.

11a) Improve the radiometric stability.

We have several ideas on where the instabilities are at this time. Our tests have indicated that the fundamental spectrometers are very stable, so the instabilities must come in the steps between the collectors (which have MOBY heritage, thus have been proven to be stable) and the spectrometers. Also, as shown in section 6c-3, our stability during the deployment is actually very good. The major problem seems to be stability or consistency between pre/post calibration and in-field measurements. There are several collimators in the link, the stability results we showed earlier were before a beam splitter was in the system, so that cannot be the source of the problems. We think that the problem maybe with these collimators and some alignment instability or sensitivity. Also, with the small apertures we are using to stop down the system, there may be a large dependence on alignment or fiber mode structure which are causing the problems. In any case this is a problem that we are currently working on and really have to solve in the very near future, hopefully by the next MOBY deployment in February.

11b) Improvements to collection optics

During this work we have maintained the same collection optics as MOBY-Heritage. There is room for improvement, particularly with the surface irradiance collector's cosine response. Additionally there are some new diffuser materials available, such as the Diffusil mentioned earlier in connection to the SQM that could allow both hardened surfaces in the collectors and better cosine response. This would require some iteration, as these can only reliably be characterized experimentally at this time.

11c) Developing a more modern stability source with enhanced UV output.

As we say above, the stability source we evaluated was the SQM, from the SeaWiFS/SIMBIOS era. It is not even clear, if we wanted to order another one from YES, whether they would be interested in supplying them. Their initial development, during SIMBIOS, expected that many would be ordered for the community and that did not come to pass. While the SQM came close to our goals, and with improvements would meet our goals, newer commercial sources for the PACE era stability source need to be investigated, with a goal of increasing the output into the UV and making a more compact, lighter instrument.

Note in respect to 11b and 11c, an immediate path forward would be to help develop an SBIR solicitations on these subjects. We would be willing to help on this if that is appropriate.

11d) CAS Stability monitor.

Recommendation on the CAS line of instruments is dependent on the outcome of the thermal testing (which will be done in Nov 2018), but consideration of other vendors must be accompanied by solid data showing long term reproducibility. It may be necessary to operate the CAS with additional control of the ambient temperature.

11e) Further software development for stability system.

It is strongly recommended for both the source and radiometer that full control over the operation is possible, and that the DAQ software be designed for compatibility with the

MLdbase organization structure. Implementation of the stability system should be as user-friendly as possible, simple and efficient, and meet the goal of 1% reproducibility.

11f) Experiment on shipping system and testing MOBY-Net concept.

Once the system is stable in Hawaii, we need to do an experiment where we calibrate the system in Hawaii, ship it to Miami and/or NIST, install the system on a "mock" buoy (some sort of structure) and take data of some sort, then take the system off and send it back to Hawaii for recalibration, running the stability system along the path. In the first round of this experiment, there is no real reason to ship a buoy, so the experiment can be done totally in one lab or the other (or outside).

11g) deploy full mooring in another site in Hawaii (?)

A next step, before the step described below, could be to deploy a full system in Hawaii, possibly near the current MOBY system. The advantage of this is that we would be able to estimate the costs involved with such a deployment reliably, would prove the system reliability, and would be relatively easier from the logistics point of view. The negative is that it would not give us the experience of installation in another site and all the logistical problems that this would probably entail. Whether the cost of this is justified maybe questionable, as our current plan is to do a cross-over experiment between MOBY-Heritage and the new optical system starting soon

11h) Work with a group to start an installation in another site.

The final experiment would be to work with another group to install a mooring and deploy the buoy in another site. This would take finding another suitable site with the correct environmental conditions and logistical support. Some possible examples could be:

Puerto Rico if the infrastructure was there and we could find suitable collaborators and a suitable "secure" site. Shipping would be relatively easy and customs free.

Western Australia, David Antoine has experience in these types of programs and wrote a letter of support for the original MOBY-Net proposal.

European site? Eumetsat currently has two groups working on developing plans for a vicarious calibration site. One is the Boussole group, which has proposed reworking the Boussole site with a new optical system built by CIMEL. We are working with the other group on using a MOBY-Net system. A possible location for this system is Lampedusa, but at least two other possible European sites will be investigated as part of their effort.

Where ever the site is located, it will probably require a different mooring configuration then our current system. There is also the issue of data communication, as we are currently dependent, and take advantage of, broadband cellphone coverage. Switching to a more remote site, with communication through a satellite will require development time, hardware costs, and some software redevelopment.

References

Hooker, S. B. and J. Aiken (1998). "Calibration Evaluation and Radiometric Testing of Field Radiometers with the SeaWIFS Quality Monitor (SQM)." J. Oceanic and Atmosp. Tech. **15**: 995 - 1007.

Johnson, B. C., P.-S. Shaw, S. B. Hooker and D. Lynch (1998). "Radiometric and engineering performance of the SeaWiFS Quality Monitor (SQM): A portable light source for field radiometers." Journal of Atmospheric and Oceanic Technology **15**: 1008-1022.

Lemaillet, P., H. Patrick, T. A. Germer, L. M. Hanssen, B. C. Johnson and G. T. Georgiev (2016). "Goniometric and hemispherical reflectance and transmittance measurements of fused silica diffusers." Proc. SPIE **9961**: 996109-996101 - 996109-996112.

Meister, G., G. S. Fargion and C. McClain (2009). "Long-term monitoring of radiometer sensitivity for radiometric comparisons among optical laboratories." Proc. SPIE **7452**: 74521A-74521 74521A-74512.

Publications/presentations during project related to this project (and to previous NASA grants, but published during this period):

Papers

G. Zibordi, M. Talone, K. J. Voss, B. C. Johnson, "Impact of spectral resolution of in situ ocean color radiometric data in satellite matchups analysis", Opt. Exp., 25, A798-A812 (2017), DOI: 10.1364/OE.25.00A798.

K. J. Voss, H. R. Gordon, S. Flora, B. C. Johnson, M. Yarbrough, M. Feinholz, T. Houlihan, "A method to extrapolate the diffuse upwelling radiance attenuation coefficient to the surface as applied to the Marine Optical Buoy (MOBY)", J. Atm. and Ocean. Tech., 34, 1423-1432 (2017), DOI: 10.1175/JTECH-D-16-0235.1.

M. Feinholz, B. C. Johnson, K. Voss, M. Yarbrough, and S. Flora, "Immersion Coefficient for the Marine Optical Buoy (MOBY) Radiance Collectors", J. Res. N.I.S.T., **122**, 1-9 (2017), DOI:10.6028/jres.122.031.

K. J. Voss and S. Flora, "Spectral Dependence of the seawater-air radiance transmission coefficient", J. Atm. Ocean. Techn., **34**, 1203-1205 (2017), DOI: 10.1175/JTECH-D-17-0040.1.

A. Tonizzo, M. Twardowski, S. McLean, K. Voss, M. Lewis, C. Trees, "Closure and uncertainty assessment for ocean color reflectance using measured volume scattering functions and reflective tube absorption coefficients with novel correction for scattering", Applied Optics, **56**, 130-146 (2017).

K. J. Voss and L. Belmar Da Costa, "Polarization properties of FEL lamps as applied to radiometric calibration", Applied Optics, 55, 8829-8832 (2016).

G. Zibordi, F. Melin, K. Voss, B. C. Johnson, B. Franz, E. Kwiatkowska; J-P. Huot, M. Wang, D. Antoine, "System Vicarious Calibration for Ocean Color Climate Change Applications: Requirements for In Situ Data", Remote Sensing of the Environment, 159,361-369 (2015).

Talks:

"MOBY: Past, Present, and Future", International Ocean Color Science Meeting, San Francisco, June, **Plenary talk.**

Invited talks at Chinese University for Geosciences and at Wuhan University: K. Voss, "Ocean Color Vicarious Calibration, the role of MOBY, April, 2017.

– FRM4SOC, ESA/ESRIN, Frascati, Italy, 2/21-23/17. Series of 4 talks plus one additional talk

- An overview of the Marine Optical Buoy: Past, present and future(given by K. Voss)
- Radiometric Calibration of MOBY & Associated uncertainties (given by B. C. Johnson)
- MOBY: QA/QC and environmental uncertainties in the final MOBY product (given by K.Voss)
- MOBY: time series, lessons learned and status of MOBY-Refresh/MOBY-Net. (given by K.Voss)
- Radiometric Metrology for Ocean Color (given by B. C. Johnson).

"The Marine Optical Buoy (MOBY) protocols and use in Satellite System Vicarious Calibration (SVC)", Invited talk at the AMT4SFRM in Plymouth Marine Laboratory: K. Voss, , 2018.

Posters:

"Experimental nLw and Lw products from the Marine Optical Buoy (MOBY)", K. Voss, D. Clark, M. Feinholz, S. Flora, H. Gordon, B. C. Johnson, J. Mueller, M. Yarbrough, Ocean Optics XXII, Portland, Me., October, 2014.

"MOBY Uncertainties", C. Johnson, D. Clark, M. Feinholz, S. Flora, H. Gordon, J. Mueller, A. Parr, K. Voss, M, Yarbrough, Ocean Optics XXII, Portland, Me., October, 2014.

"MOBY-NET, an ocean color vicarious calibration system", Earth Science Technology Forum, CalTech, Los Angeles, June, 2015.

"Progress on MOBY-Net", Ocean Color Research Team Meeting, Silver Springs, Maryland, May.

"Progress on MOBY-Net and MOBY-Refresh" K. Voss, B. C. Johnson, M. Yarbrough, A. Gleason, S. Flora, M. Feinholz, Ocean Optics XXIII, Victoria, Canada., October, 2016.

"The Marine Optical BuoY (MOBY) technology Refresh and Time Series", K. Voss, A.Gleason, B. C. Johnson, M. Yarbrough, M. Feinholz, and S. Flora, , AGU Fall meeting, San Francisco, December, 2016.